Reports of the Department of Geodetic Science and Surveying

Report No. 331

IMPROVED GLOBAL PREDICTION OF 300-NAUTICAL-MILE MEAN FREE-AIR ANOMALIES

by

Jaime Y. Cruz

Prepared for

National Aeronautics and Space Administration
Goddard Space Flight Center
Greenbelt, Maryland 20770

Grant No. NGR 36-008-161
OSURF Project 783210

The Ohio State University
Department of Geodetic Science and Surveying
1958 Neil Avenue
Columbus, Ohio 43210

May, 1982

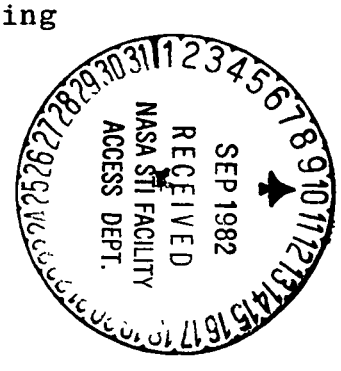

Abstract

Current procedures being used for the global prediction of 300nm mean anomalies starting from known values of 1°x 1° mean anomalies yield unreasonable prediction results when applied to 300nm blocks which have a rapidly varying gravity anomaly field and which contain relatively few observed 60nm blocks. Improvements to this situation are studied.

Improvement of overall 300nm anomaly prediction is first achieved by using area-weighted as opposed to unweighted averaging of the 25 generated 60nm mean anomalies inside the 300nm block. Then, improvement of prediction over rough 300nm blocks is realized through the use of fully known 1°x 1° mean elevations, taking advantage of the correlation that locally exists between 60nm mean anomalies and 60nm mean elevations inside the 300nm block. An improved prediction model which adapts itself to the roughness of the local anomaly field is found to be the model of Least Squares Collocation with systematic parameters, the systematic parameter being the slope b which is a type of Bouguer slope expressing the correlation that locally exists between 60nm mean anomalies and 60nm mean elevations.

Foreword

This report was prepared by Mr. Jaime Y. Cruz, Graduate Research Associate, the Department of Geodetic Science and Surveying, The Ohio State University under NASA Grant NGR36-008-161, The Ohio State University Research Foundation Project No. 783210. The grant covering this research is administered through the NASA Goddard Space Flight Center, Greenbelt, Maryland, 20771, Mr. Jean Welker, Technical Officer.

This report was also submitted to the Graduate School of the Ohio State University in partial fulfillment of the requirements for the degree of Master of Science.

Acknowledgment

I wish to thank Dr. Richard H. Rapp for providing valuable guidance during the course of this study. Thanks are also due to Dr. Urho A. Uotila for serving on the reading committee, and to Miss Susan Carroll for her excellent typing of the manuscript. My wife Edna provides continuing support and encouragement.

Table of Contents

1. Introduction

Kaula (1966) described and implemented procedures for the prediction of mean gravity anomaly inside 300nm blocks (nm = nautical mile, see section 3). The procedures involved linear regression from known 60nm mean anomalies inside the individual 300nm blocks. Rapp (1972) introduced two additions to the procedures and computer programs used by Kaula. The first addition was the consideration of data noise by the introduction of a noise matrix into the prediction equations. The second addition was the estimation of accuracies of predicted 300nm anomalies. The techniques of Rapp actually involved the method of Least Squares Collocation with no systematic parameters.

The procedures and computer programs used by Kaula, together with the subsequent enhancements by Rapp, constitute the current procedures being used to predict 300nm mean anomalies from 1°x 1° mean anomalies. The purpose of this report is to study improvements to these current 300nm anomaly prediction procedures.

First, background information which will be useful in subsequent discussions will be covered in Sections 2 to 8. Then, in Section 9, it will be shown that current 300nm anomaly prediction procedures need to be improved over 300nm blocks which have a rough anomaly field and which contain relatively few observed 60nm blocks. In Section 10, current procedures will be modified not necessarily to improve predictions over rough areas but to improve predictions through the use of more rigorous prediction formulas.

To develop improvements to current prediction procedures as far as rough areas are concerned, three possibilities will be considered:

1. the use of a local as opposed to a global covariance function in order that the local roughness of the anomaly field may be properly expressed in the prediction equations. This will be covered in Section 11.

2. the removal of gross local trend between 60nm anomalies and elevations in accordance with the model 'Least Squares Collocation with systematic parameters.' This will be covered in Sections 13, 14, 15, 16, and 17.

3. the use of elevations as observed quantities, in addition to the observed anomalies, in a least squares collocation prediction involving an anomaly autocovariance function, an elevation autocovariance function, and an anomaly-elevation crosscovariance function. This will be covered in Section 18.

2. Least Squares Collocation Equations

Moritz (1972) gives a detailed presentation of Least Squares Collocation. Relevant equations are collected here for easy reference.

Notations

x	:	vector of observations
A	:	a known rectangular matrix
X	:	vector of systematic parameters
AX	:	systematic part of observations
s'	:	signal part of observations
n	:	noise part of observations
E_{XX}	:	error covariance of estimated parameters
$C_{s's'}$	:	covariance of signals of observation points
C_{nn}	:	covariance of noise of observations
s	:	vector of signals at prediction points
$C_{ss'}$	:	covariance between the signals being predicted and the signals at observation points
t	:	vector of "complete signals" at computation points, defined through equation (6)
B	:	a known rectangular matrix
BX	:	effect of the systematic parameters on the "complete signals"
C_{ss}	:	covariance of the signals at computation points
E_{tt}	:	error covariance of the predicted "complete signals"
E_{ss}	:	error covariance of the predicted signals

Formulas

The vector of observations is modeled as:

$$x = AX + s' + n \qquad (1)$$

The parameters are estimated from:

$$X = (A^T(C_{s's'} + C_{nn})^{-1}A)^{-1}\ A^T(C_{s's'} + C_{nn})^{-1}\ x\ . \qquad (2)$$

The error covariance of estimated parameters is:

$$E_{xx} = (A^T(C_{s's'} + C_{nn})^{-1}\ A)^{-1}\ . \qquad (3)$$

The vector of signals at computation points is predicted as:

$$s = C_{ss'}\,Q \qquad (4)$$

where Q depends only on observation points and not on computation points. Q is given by:

$$Q = (C_{s's'} + C_{nn})^{-1}\ (x - AX). \qquad (5)$$

The vector of "complete signals" at computation points is defined as:

$$t = BX + s \quad . \tag{6}$$

The error covariance of predicted "complete signals" is:

$$E_{tt} = C_{ss} - C_{ss'}(C_{s's'} + C_{nn})^{-1} C_{ss'}^{T} + (HA - B)\, E_{XX}(A^{T}H^{T} - B^{T}) \tag{7}$$

where

$$H = C_{ss'}(C_{s's'} + C_{nn})^{-1} \quad . \tag{8}$$

If it is assumed that the observation vector does not contain a systematic part, then the equations are:

$$x = s' + n \tag{9}$$

$$t = s = C_{ss'}(C_{s's'} + C_{nn})^{-1} x \tag{10}$$

$$E_{tt} = E_{ss} = C_{ss} - C_{ss'}(C_{s's'} + C_{nn})^{-1} C_{ss'}^{T} \tag{11}$$

3. 300nm Block Subdivision Scheme

The global 300nm block subdivision scheme employed by Kaula (1966) and retained in Rapp (1972) and in all predictions considered in this report is described in this section. The world is divided along parallels of latitude into 36 zones, each zone with a latitude extent of 5°. Individual latitude zones are then further separately divided along meridians such that near equal area blocks are obtained, with area as nearly equal as possible to the area of a 5°x 5° block at the equator. The longitude extents of individual near equal area blocks are forced to be an integral number of degrees of longitude. Since an angular distance of 5° at the equator corresponds to a linear distance of 300 nautical miles, the near equal area blocks formed as described are called 300nm blocks.

The specific algorithm used to generate the boundaries of 300nm blocks is obtained after putting θ equal to 5° in the equations found in Hajela (1975), pp. 2-3. Under this scheme longitude extents of 300nm blocks become 300nm ± 30nm. Longitude extents of 300nm blocks vary from 5° of longitude at the equator to 120° of longitude at the poles. Figure 1 shows the appearance of boundaries of 300nm blocks in the Northern Hemisphere on an equal area projection. The boundaries in the Southern Hemisphere are symmetrically the same. For identification purposes the 300nm blocks of the world are uniquely numbered according to a wrap-around scheme, starting from the North Pole at 0°-longitude, proceeding eastward and southward as shown in Figure 1, until the last 300nm block at the South Pole is reached. The complete numbered set totalling 1654 blocks is shown in Figure 2.

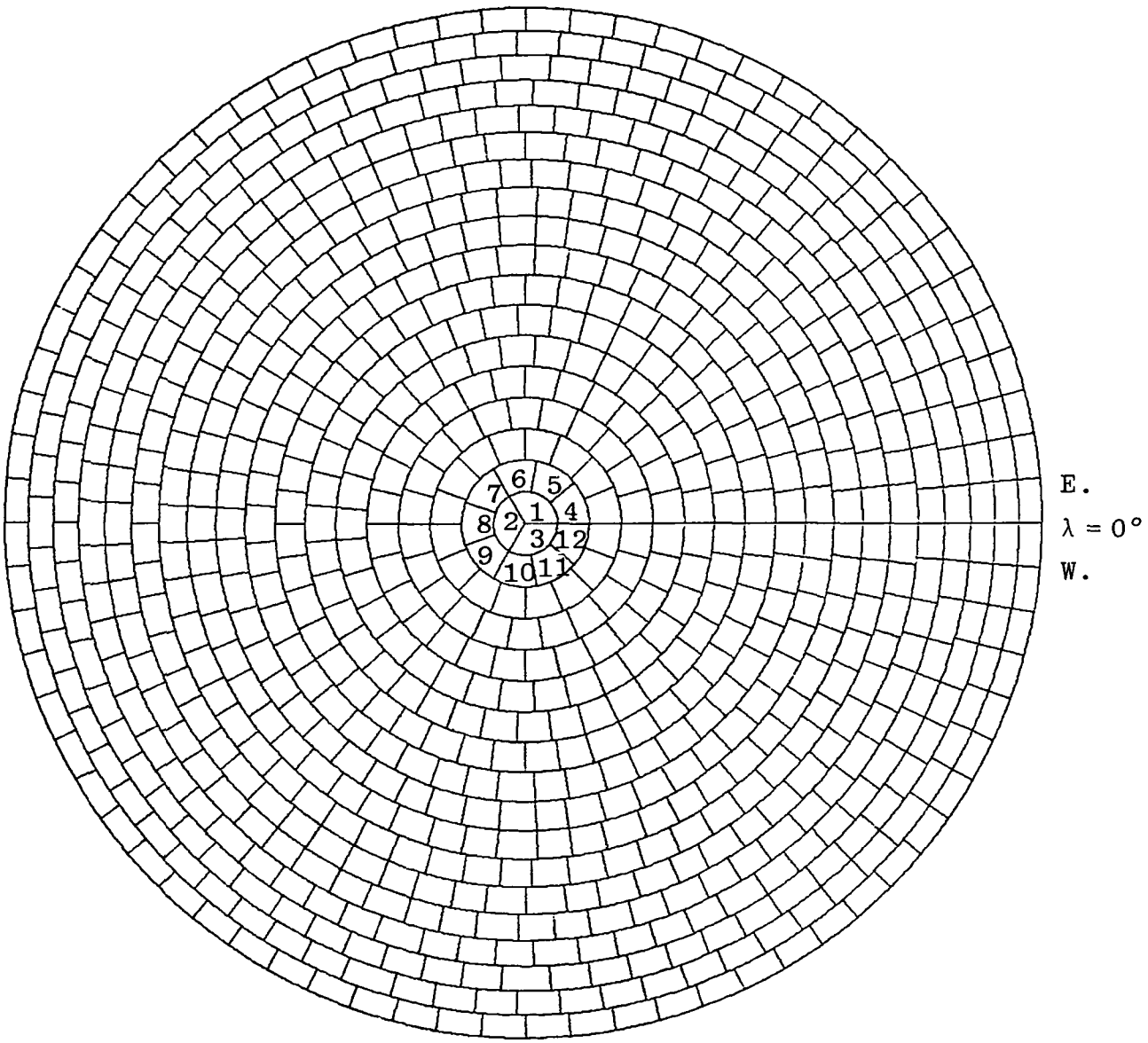

Figure 1 300nm Block Boundaries and Numbering Scheme

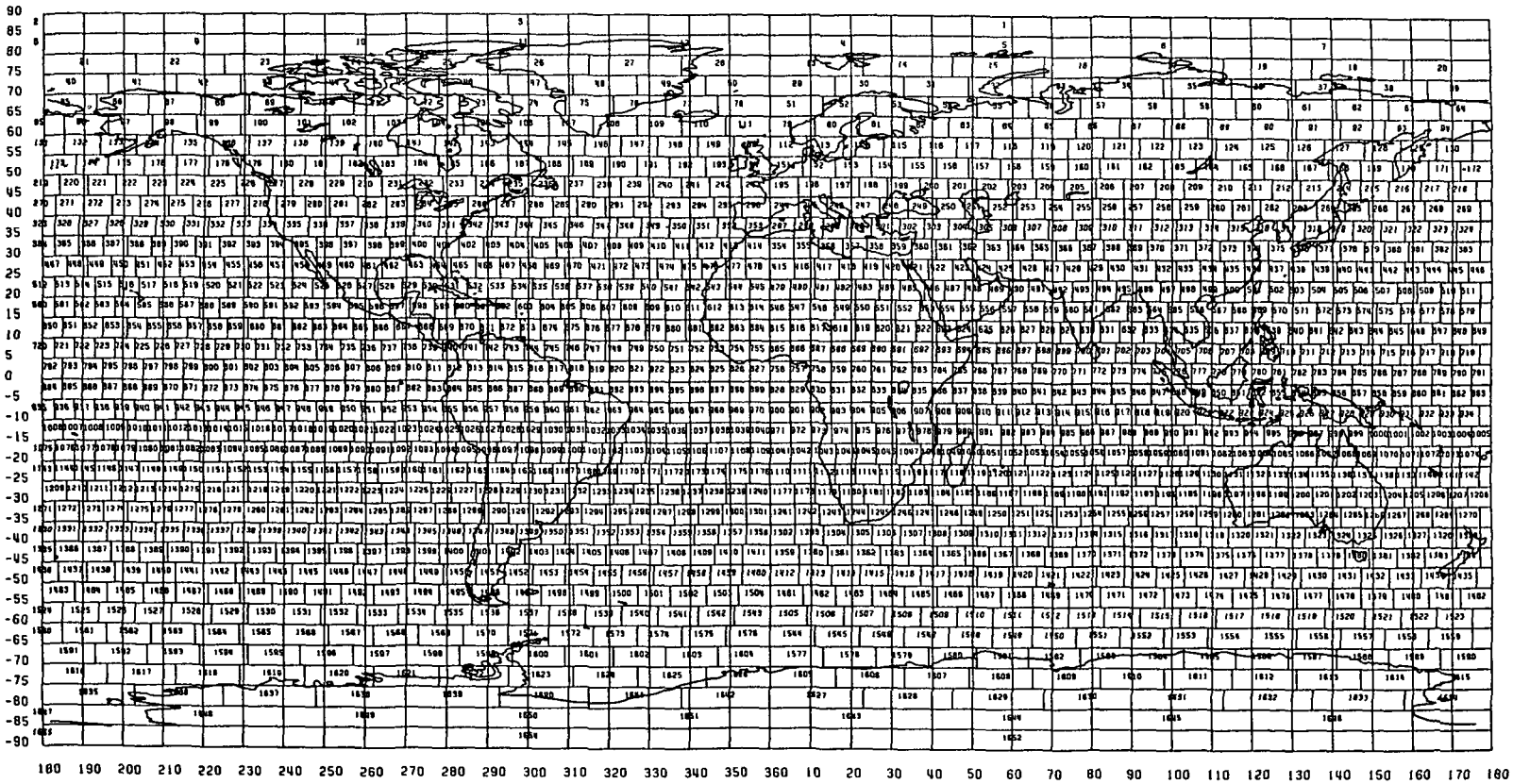

Figure 2 Total Set of Numbered 300nm Blocks

Each 300nm block is further conceptually divided into 25 near equal area blocks. The 300nm block is first divided into 5 1°-latitude zones. Each 1°-latitude zone is then further divided along meridians into 5 near equal area blocks, called 60nm blocks, which have an integral number of degrees of longitude in longitude extent (see Hajela (1975), Table 4). Under this scheme the longitude extents of 60nm blocks are 60nm ±30nm. Longitude extents of 60nm blocks vary from one degree of longitude near the equator to 24 degrees of longitude near the poles. Within any 300nm block, the difference between two 60nm areas can reach, but never exceed, a factor of two (Hajela (1975) Table 4).

4. Data Structure Inside the 300nm Block

Procedures considered in this report predict a 300nm mean anomaly starting from known values of 1°x 1° mean anomalies and 1°x 1° mean elevations inside the 300nm block. Under the 300nm block subdivision scheme, there are considerably more 1°x 1° blocks inside 300nm blocks near the poles than those near the equator. The number of 1°x 1° blocks inside a 300nm blocks increases with increasing latitude of the 300nm blocks. For example, an equatorial 300nm block has 5x5=25 1°x 1° blocks inside it. A polar 300nm block has 5x120=600 1°x 1° blocks inside it. Therefore, there are potentially much more 1°x 1° data values inside 300nm blocks towards the poles than those towards the equator.

To make the data distribution more uniform it is natural to average 1°x 1° anomalies falling inside a particular 60nm block to obtain a single value to be considered the "observed" 60nm anomaly for that 60nm block. In the same way 1°x 1° elevations inside the 60nm block may be averaged to form the 60nm elevation. Since the component 1°x 1° blocks of any 60nm block all lie in a common 1°-latitude zone, it follows that the areas of 1°x 1° blocks inside a 60nm block are all equal; this makes it sufficient to straight average the 1°x 1° values to form the 60nm value. The standard errors of the original 1°x 1° values are propagated into the 60nm value according to the usual covariance propagation formula. The data structure is thus transformed such that the unit data blocks are near equal area 60nm blocks instead of 1°x 1° blocks. The use of such a data structure is reasonable and greatly simplifies prediction computations.

Therefore, during predictions the working data structure inside the 300nm block is as follows. There are exactly 25 60nm blocks arranged in a 5x5 array and numbered as shown in Figure 3. There are 25 60nm mean anomalies, some or all of which may be known, with each known 60nm anomaly having a standard error associated with it. There are 25 60nm mean elevations with corresponding standard errors, all of which are always known for any 300nm block since 1°x 1° elevations are fully known in the world. Finally, the exact areas of the individual 60nm blocks, useful for weighting purposes, are also known from the algorithm that generates 60nm block boundaries.

Anomaly predictions considered in this report will involve the prediction of unknown 60nm mean anomalies inside the 300nm block (or, also possible, the direct prediction of the 300nm anomaly) using as known values, either just the known 60nm mean anomalies and their accuracies, or both the known 60nm anomalies and 60nm elevations and their accuracies.

1	2	3	4	5
6	7	8	9	10
11	12	13	14	15
16	17	18	19	20
21	22	23	24	25

Figure 3

25 60nm blocks inside a 300nm block

5. Covariance Matrices

The computation of covariance matrices that enter the prediction equations considered in this report is described in this section. A numerical covariance function is first computed using global averaging procedures as described in Section 5.1. From this numerical covariance function the 25x25 covariance matrix of the 60nm blocks shown in Figure 3 can be formed as described in Section 5.2. This 25x25 covariance matrix becomes a basic covariance matrix from which the other covariance matrices needed in prediction equations are derived through covariance matrix propagation as discussed in Section 5.3.

5.1 Computation of a 60nm Numerical Covariance Function

Kaula (1966) and Rapp (1977) discuss a practical set of procedures for the computation of an isotropic, homogeneous numerical covariance function for mean values.

Let

Δg_j, Δg_k : mean anomalies at two arbitrary blocks j and k

A_j , A_k : areas of blocks j and k

ψ_{jk} : angular distance between the centers of blocks i and j

ψ_i : an angular distance.

Numerical mean anomaly covariances can be computed as follows:

$$\mathrm{cov}(\Delta g,\Delta g) = C(\psi_i) = \frac{\Sigma\, A_j\, A_k\, \Delta g_j\, \Delta g_k}{\Sigma\, A_j\, A_k} \qquad (12)$$

$$\psi_i = \frac{\Sigma\, A_j\, A_k\, \psi_{jk}}{\Sigma\, A_j\, A_k} \qquad (13)$$

where the summation is taken over all blocks j and k satisfying:

$$\begin{aligned} \psi_{jk} &= 0 && \text{for } i=0 \\ 0 < \psi_{jk} &< \Delta\psi && \text{for } i=1 \\ (i-1)\cdot\Delta\psi \le \psi_{jk} &< i\cdot\Delta\psi && \text{for } i=2,3,\ldots \end{aligned} \qquad (14)$$

$\Delta\psi$ is some angular distance that is considered appropriate for use in the computations, considering the sizes of the blocks of interest.

For 60nm blocks, $\Delta\psi$ is chosen to be

$$\Delta\psi = 1^\circ \qquad (15)$$

As explained in Rapp (1977), virtually identical covariances, out to ψ approximately equal to 6°, are obtained even if the following simplifying condition is added to conditions (14):

the 60nm blocks j and k fall inside a common 300nm block. (16)

Using equations (12) and (13) along with conditions (14) (15) and (16), a 60nm numerical covariance function was computed, with the results shown in Table 1. The data set used was the OSU combined altimeter/terrestrial data set of October 1979 (Rapp, 1979, 1980). The anomalies of the data set were referred to the gravity formula of the Geodetic Reference System 1967. Also shown in Table 1 is the number of terms used in the summations occuring in equations (12) and (13). As can be seen, there is an ample amount of data for the determination of each $C(\psi_i)$.

Given two 60nm blocks with angular distance between centers equal to ψ , the 60nm anomaly covariance between the two blocks can be interpolated from Table 1. In the procedures included in this report, linear interpolation is used; this corresponds to using a piecewise linear approximation to the covariance function (see Sunkel (1981a) for a discussion of implications of various interpolation methods).

Table 1

$cov(\Delta g,\Delta g) = C(\psi_i)$, computed from the combined altimeter/terrestrial data set

i	ψ_i DEG	ψ_i RAD	$cov(\Delta g,\Delta g)=C(\psi_i)$ ($mgal^2$)	No.of Product Pairs Used
0	0.0000	0.0000	625	37790
1	0.9796	0.0171	382	50057
2	1.6201	0.0283	275	92763
3	2.5081	0.0438	207	127132
4	3.4661	0.0605	185	101042
5	4.3769	0.0764	176	61813
6	5.3623	0.0936	141	8657
7	6.2280	0.1087	109	283

5.2 Formation of Covariance Matrices

From the $C(\psi_i)$ discussed in Section 5.1 the 25x25 matrix containing the covariances among the 60nm blocks inside a 300nm block can be formed. This matrix will be denoted by $C_{\Delta g\Delta g}$. Strictly, different 300nm blocks will have different $C_{\Delta g\Delta g}$'s simply because the set of ψ-values for the component 60nm blocks will in general be different for different 300nm blocks. A possible approach is therefore to take each 300nm block of the world, compute the ψ-values referred to the centers of the component 60nm blocks, and interpolate from the numerical covariance function for the covariances that will make up the $C_{\Delta g\Delta g}$ for the particular 300nm block. However, this may take more computational effort than necessary.

A simplifying assumption will instead be made that any 300nm block of the world is conceptually mapped into a common 300nm block shown in Figure 3; this common 300nm block has the properties that it is planar and that the angular distance ψ between any two adjacent 60nm blocks is considered to be equal to 1° along any row or column. Obviously, an equatorial 300nm block is distorted least in this kind of mapping while a polar 300nm block is distorted most. The distortions in positions translate into distortions of ψ-values which in turn translate into distortions of the covariances interpolated from the numerical covariance function using the distorted ψ-values. However, considering the well-known fact that the actual covariance values used do not critically affect the results of predictions (Rapp, 1977), coupled with the fact that 300nm blocks of greatest interest are hardly very near the poles, then the assumed mapping seems satisfactory. The advantage of such a simplifying assumption is in the great reduction of effort in the computation of covariances.

Referring to Figure 3, let

$\text{cov}(\Delta g_i, \Delta g_j)$: anomaly covariance between 60nm blocks i and j

M_i , N_i : row, column of block i

M_j , N_j : row, column of block j .

The distance between any two blocks i and j can now be computed in planar approximation as:

$$\psi = \sqrt{(M_i - M_j)^2 + (N_i - N_j)^2} \quad \text{(degrees)} . \tag{17}$$

The covariance $\text{cov}(\Delta g_i , \Delta g_j)$ corresponding to this ψ-value can be linearly interpolated from the numerical covariance function such as the one in Table 1. The 25x25 covariance matrix is then formed as:

$$C_{\Delta g \Delta g} = [\text{cov}(\Delta g_i , \Delta g_j)] \tag{18}$$

where i, j = 1,2,..., 25; and $\text{cov}(\Delta g_i , \Delta g_j)$ is the element of $C_{\Delta g \Delta g}$ in the ith row and jth column.

5.3 Propagation of Covariance Matrices

Let P and Q be two random vectors, by which will be meant two vectors which do not have any systematic part (M{P}=0, M{Q}=0). The covariance matrix between P and Q may be defined as:

$$C_{PQ} = M\{PQ^T\} \tag{19}$$

where M is some averaging operator.

Consider another random vector R which is related to P through the linear transformation:

$$R = L_{RP} P \tag{20}$$

where L_{RP} is the linear transformation matrix which transforms P to R . The covariance matrix between R and Q is:

$$\begin{aligned} C_{RQ} &= M\{RQ^T\} \\ &= M\{L_{RP} P Q^T\} \\ &= L_{RP} M\{P Q^T\} \\ &= L_{RP} C_{PQ} . \end{aligned} \tag{21}$$

Again consider another random vector S which is related to Q through the linear transformation:

$$S = L_{SQ} Q \tag{22}$$

where L_{SQ} is the linear transformation matrix which transforms Q to S . The covariance matrix between P and S is:

$$C_{PS} = M\{PS^T\}$$
$$= M\{PQ^T L_{SQ}^T\}$$
$$= M\{PQ^T\} L_{SQ}^T$$
$$C_{PS} = C_{PQ} L_{SQ}^T . \quad (23)$$

The covariance matrix between R and S is:

$$C_{RS} = M\{RS^T\}$$
$$= M\{L_{RP} P Q^T L_{SQ}^T\}$$
$$= L_{RP} M\{PQ^T\} L_{SQ}^T$$
$$C_{RS} = L_{RP} C_{PQ} L_{SQ}^T . \quad (24)$$

Equations (19), (20), (21), (22), (23), and (24) define how a covariance matrix C_{PQ} propagates through linear transformations of the random vectors P and Q .

Now let t and u be two non-random vectors, that is, vectors which contain both a systematic part and a random part ($M\{t\}\neq 0$, $M\{u\}\neq 0$):

$$t = \bar{t} + T \quad (25)$$

$$u = \bar{u} + U . \quad (26)$$

Here, an overbar denotes the systematic part, and a capital letter denotes the random part of a non-random vector. The covariance matrix between t and u is defined as:

$$C_{tu} = M\{(t-\bar{t})(u-\bar{u})^T\} \quad (27)$$

$$= M\{TU^T\}$$
$$C_{tu} = C_{TU} \quad (28)$$

Equation (28) says that the covariance matrix between two non-random vectors is equal to the covariance matrix between their random parts.

Consider two non-random vectors v and w :

$$v = \bar{v} + V$$

$$w = \bar{w} + W$$

Let v and w be related to each other through the linear transformation:

$$v = Lw . \quad (29)$$

Then,

$$v = L(\bar{w} + W)$$
$$= L\bar{w} + LW$$

so that

$$\bar{v} = L\bar{w} \quad (30)$$

$$V = LW , \quad (31)$$

that is, if two non-random vectors are related to each other through some linear transformation matrix L, then their systematic and random parts are related through L.

Using equations (28) and (31) it is now easy to extend covariance matrix propagation formulas to the case of non-random vectors. Let p, q, r, s be non-random vectors such that

$$r = L_{RP}\, p \quad \text{and} \quad s = L_{SQ}\, q .$$

Then, by equation (31):

$$R = L_{RP}\, P \quad \text{and} \quad S = L_{SQ}\, Q .$$

The covariance matrix between r and s becomes:

$$\begin{aligned} C_{rs} &= C_{RS} && \text{by equation (28)} \\ &= L_{RP}\, C_{PQ}\, L_{SQ}^T && \text{by propagation formula (24)} \\ &= L_{RP}\, C_{pq}\, L_{SQ}^T && \text{by equation (28).} \end{aligned}$$

Therefore,

$$C_{rs} = L_{RP}\, C_{pq}\, L_{SQ}^T . \qquad (32)$$

Equation (32), analogous to equation (24), defines how a covariance matrix C_{pq} propagates through linear transformations of the non-random vectors p and q.

From the basic covariance matrix $C_{\Delta g \Delta g}$ discussed in Section 5.1, other covariances can now be derived through covariance matrix propagation. Let

$\bar{\Delta g}$: the 300nm anomaly
Δg : vector with elements the 25 60nm anomalies inside the 300nm block (Conceptually, there are always 25 60nm anomalies, though some of them may be unknown.)
$C_{\bar{\Delta g} \Delta g}$: covariance between the 300nm anomaly and the 25 60nm anomalies
$C_{\bar{\Delta g} \bar{\Delta g}}$: variance of the 300nm anomaly.

For the rest of this report a key assumption will be made as follows:

> If all the 25 60nm anomalies inside a 300nm block are known, then it is completely satisfactory to obtain the 300nm anomaly as the area-weighted average of those 25 60nm anomalies (60nm anomalies are obtained by straight averaging from 1°x 1° anomalies as explained in Section 4).

This assumption seems reasonable in practice; theoretical consequences may be pursued based on ideas contained in a recent report by Sünkel (1981b), but this will not be attempted at this time.

A direct consequence of the above assumption is that the 300nm anomaly $\bar{\Delta g}$ will be related to the vector Δg containing the 25 conceptual 60nm anomalies through the linear transformation:

$$\bar{\Delta g} = L_{\bar{\Delta g}\Delta g}\, \Delta g, \qquad (33)$$

where, specifically, $L_{\bar{\Delta g}\Delta g}$ is the area-weighted averaging operator:

$$L_{\bar{\Delta g}\Delta g} = \frac{1}{\sum_{i=1}^{25} A_i} (A_1\ A_2 \ldots A_{25}) \qquad (34)$$

with A_i, the area of the 60nm block i, being known from the algorithm that generates 60nm block boundaries. Equation (34) is a generalization from current prediction procedures. Current prediction procedures assume that all the A_i's in equation (34) are equal, leading to a straight averaging in equation (33).

Given equation (33) and applying covariance matrix propagation formula (21),

$$C_{\bar{\Delta g}\Delta g} = L_{\bar{\Delta g}\Delta g}\, C_{\Delta g \Delta g} \qquad (35)$$

That is, $C_{\bar{\Delta g}\Delta g}$ is computable by area-weighted averaging elements of $C_{\Delta g \Delta g}$ along columns (or along rows, because of the symmetry of $C_{\Delta g \Delta g}$).

Again considering equation (33) and applying propagation formula (23),

$$C_{\bar{\Delta g}\bar{\Delta g}} = C_{\bar{\Delta g}\Delta g}\, L_{\bar{\Delta g}\Delta g}^{T}, \qquad (36)$$

that is, the area-weighted average of the elements of $C_{\bar{\Delta g}\Delta g}$. Or, applying propagation formula (24),

$$C_{\bar{\Delta g}\bar{\Delta g}} = L_{\bar{\Delta g}\Delta g}\, C_{\Delta g \Delta g}\, L_{\bar{\Delta g}\Delta g}^{T} \qquad (37)$$

that is, the area-weighted average of all elements of $C_{\Delta g \Delta g}$.

To provide a feeling for the elements of $C_{\bar{\Delta g}\Delta g}$ and $C_{\bar{\Delta g}\bar{\Delta g}}$, the basic matrix $C_{\Delta g \Delta g}$ was first formed as described in Section 5.1 and using numerical values from Table 1. Then, $C_{\bar{\Delta g}\Delta g}$ and $C_{\bar{\Delta g}\bar{\Delta g}}$ were computed using equations (35) and (36) and assuming equal areas in equation (34). The results are shown in Table 2. The values contained in $C_{\Delta g \Delta g}$ itself are not shown, these values being easily seen from equations (17) and (18) and Table 1.

Table 2

Anomaly Covariance Between the 300nm Block and an Individual 60nm Block (i.e., $\text{cov}(\Delta g, \Delta g_j)$), Assuming Equal Areas for the 60nm Blocks. Units: mgal^2 .

226	245	250	245	226
245	267	273	267	245
250	273	279	273	250
245	267	273	267	245
226	245	250	245	226

Variance of 300nm Block (i.e., $\text{cov}(\overline{\Delta g}, \overline{\Delta g})$), Assuming Equal Areas for the 60nm Blocks: 252 mgal^2 .

6. Equivalence of Indirect and Direct Predictions

Let a vector t of "complete signals" be predicted from an observation vector x using the equations of Section 2. Now let another vector $\bar{t}$ be a vector of "complete signals":

$$\bar{t} = \bar{B}X + \bar{s} \tag{38}$$

where

$\bar{B}X$: systematic part of $\bar{t}$

$\bar{s}$: signal part of $\bar{t}$.

Let $\bar{t}$ be related to t through the linear transformation:

$$\bar{t} = Lt \tag{39}$$

where L is the linear transformation matrix which transforms t to $\bar{t}$. On substituting equation (6) into equation (39),

$$\begin{aligned} \bar{t} &= L(BX + s) \\ &= LBX + Ls. \end{aligned} \tag{40}$$

The systematic part of $\bar{t}$ becomes, on comparing equations (38) and (40):

$$\bar{B}X \equiv LBX . \tag{41}$$

The signal part of $\bar{t}$ becomes:

$$\bar{s} \equiv Ls . \tag{42}$$

Equations (38), (41), and (42) constitute an indirect prediction of $\bar{t}$ because in equation (42) the signal part of $\bar{t}$ is not predicted from observations directly but rather from a transformation of the predicted signal part of t.

Substituting equation (4) into equation (42):

$$\bar{s} = L\, C_{ss'}\, Q \,. \tag{43}$$

Considering the transformation equation (42) as being analogous to equation (20), and applying the covariance matrix propagation formula (21):

$$C_{\bar{s}s'} = L\, C_{ss'} \,. \tag{44}$$

Therefore, equation (43) may be written as:

$$\bar{s} = C_{\bar{s}s'}\, Q \,. \tag{45}$$

Equation (45) is analogous to equation (4). Equations (38), (41), and (45) constitute a direct prediction of $\bar{t}$ because in equation (45) the signal part of $\bar{t}$ is predicted directly from observations.

The error covariance of the predicted "complete signals" in $\bar{t}$ is, using equation (7):

$$E_{\bar{t}\bar{t}} = C_{\bar{s}\bar{s}} - C_{\bar{s}s'}(C_{s's'} + C_{nn})^{-1}\, C_{\bar{s}s'}^{T} + \\ + (\bar{H}A - \bar{B})\, E_{XX}(A^{T}\bar{H}^{T} - \bar{B}^{T}) \tag{46}$$

where

$$\bar{H} = C_{\bar{s}s'}(C_{s's'} + C_{nn})^{-1} \tag{47}$$

From the covariance matrix propagation formula (23):

$$C_{\bar{s}\bar{s}} = L\, C_{ss}\, L^{T} \,. \tag{48}$$

Since equation (41) is an identity for all X, then

$$\bar{B} = LB \,. \tag{49}$$

Substituting equations (44), (48), and (49) into (46):

$$E_{\bar{t}\bar{t}} = LC_{ss}L^{T} - LC_{ss'}(C_{s's'} + C_{nn})^{-1}\, C_{ss'}^{T}\, L^{T} + \\ + L(HA - B)E_{XX}(A^{T}H^{T} - B^{T})\, L^{T} \\ = L(C_{ss} - C_{ss'}(C_{s's'} + C_{nn})^{-1}\, C_{ss'}^{T} + \\ + (HA - B)\, E_{XX}\, (A^{T}\, H^{T} - B^{T}))\, L^{T} \,.$$

Substituting equation (7) into the last equation, finally:

$$E_{\bar{t}\bar{t}} = L\, E_{tt}\, L^{T} \,, \tag{50}$$

which also follows directly from equation (39) by covariance propagation.

Therefore, the error covariance of the predicted "complete signals" contained in $\bar{t}$ may be computed using the direct method expressed by equation (46) or the indirect method expressed by equation (50).

The predictions included in this report use a combination of the indirect and direct methods described above. The indirect prediction is used to predict the 300nm anomaly; the $\bar{t}$ in equation (39) is the 300nm anomaly, and the t is the vector containing the 25 60nm anomalies inside the 300nm block. On the other hand, the direct method expressed by equation (46) is used to compute the variance of the predicted 300nm anomaly.

7. Current Prediction Procedures

Current prediction procedures to be examined in this report are those which predict a 300nm anomaly as the unweighted average of a completed set of 25 60nm anomalies inside the 300nm block (Kaula (1966), Rapp (1977)). The set of 25 60nm anomalies is completed by predicting any unknown 60nm anomalies from the known 60nm anomalies inside the 30nm block using equations to be explained in Section 7.1. If there are no known 60nm anomalies inside the 300nm block, the 300nm anomaly can still be predicted, using separate techniques which will not be examined in this report but which the reader can find in Rapp (1977).

As part of current 300nm anomaly prediction procedures, a prior global analysis of the data set being used is done to generate a numerical covariance function. An example of a generated global numerical covariance function is given in Table 1 (Section 5.1). The numerical covariance function is used as explained in Section 5.1 to form $C_{\Delta g \Delta g}$, the covariance matrix which is basic to the computation of the covariance matrices needed in the prediction equations.

7.1 Prediction of 60nm Anomaly

To predict an unknown 60nm anomaly from known 60nm anomalies inside the 300nm block, Least Squares Collocation with no systematic parameters is employed by the current procedures. This means that an "observed" 60nm anomaly is simply modeled as being composed of a signal part and a noise part as in equation (9). The prediction equation when no systematic parameters are being modeled is equation (10), which with upgraded notations becomes:

$$\Delta g_i = C_{\Delta g_i \Delta g^*}(C_{\Delta g^* \Delta g^*} + D_{\Delta g^* \Delta g^*})^{-1} \Delta g^* \qquad (51)$$

where:

Δg_i : predicted 60nm anomaly

Δg^* : nx1 vector of known 60nm anomalies

$C_{\Delta g_i \Delta g^*}$: covariance between the 60nm anomaly being predicted and the 60nm anomalies at observed 60nm blocks; 1xn submatrix of the $C_{\Delta g \Delta g}$ discussed in Section 5.1

$C_{\Delta g^* \Delta g^*}$: covariance between the 60nm anomalies at observed 60nm blocks; nxn submatrix of the $C_{\Delta g \Delta g}$ discussed in Section 5.1

$D_{\Delta g^* \Delta g^*}$: covariance of noise of known 60nm anomalies; diagonal matrix, with elements the square of the standard errors of the known 60nm anomaly values.

7.2 Prediction of 300nm Anomaly

Once the set of 25 60nm anomalies have been completed by predicting any unknown 60nm anomalies inside the 300nm block using equation (51), current procedures predict the 300nm anomaly as the straight average:

$$\bar{\Delta g} = \frac{1}{25} \sum_{i=1}^{25} \Delta g_i \ . \qquad (52)$$

Comparing equation (52) with equations (33) and (34) it is seen that current procedures assume that all the 60nm areas A_i are equal. The effect of this assumption will be examined in Section 10.

Also, equation (52) is analogous to equation (42) so that current procedures use an indirect prediction of 300nm anomaly. However, for exact equivalence of equations (52) and (42) all 25 Δg_i values in equation (52) and not just the unknown Δg_i 's must have been predicted by the methods of Section 7.1. Predicting the already known 60nm anomalies has the effect of filtering out the observational noise from those 60nm anomalies. The numerical effect of not filtering the known anomalies is mentioned in Section 10.

The error variance of predicted $\bar{\Delta g}$ is computed by the direct method (Section 6) using equation (11), which with changed notations becomes:

$$m_{\bar{\Delta g}}^2 = C_{\bar{\Delta g}\bar{\Delta g}} - C_{\bar{\Delta g}\Delta g^*} \left(C_{\Delta g^* \Delta g^*} + D_{\Delta g^* \Delta g^*}\right)^{-1} C_{\bar{\Delta g}\Delta g^*}^T \qquad (53)$$

where

$C_{\bar{\Delta g}\Delta g^*}$: covariance between the 300nm anomaly and the 60 nm anomalies at observed 60nm blocks; 1xn subvector of the $C_{\Delta g \Delta g}$ given in equation (35)

$C_{\bar{\Delta g}\bar{\Delta g}}$: variance of the 300nm anomaly, given by equation (36) and (37).

Under the assumption of the current procedures that all the A_i in equation (34) are equal,

$C_{\bar{\Delta g}\bar{\Delta g}*}$: 1xn subvector of $C_{\bar{\Delta g}\Delta g}$ obtained by straight averaging columns of $C_{\Delta g\Delta g}$. See Table 2 for sample numerical values.

$C_{\bar{\Delta g}\bar{\Delta g}}$: straight average of all elements of $C_{\bar{\Delta g}\Delta g}$ or of $C_{\Delta g\Delta g}$. See Table 2 for sample numerical value.

8. The Test Area

For numerical studies conducted in this report, use was made of 24 300nm test blocks covering the Tonga Trench area. The location of the 24 test blocks is shown in Figure 4. The numbers used to identify the 300nm blocks follow the numbering scheme described in Section 3. The values shown inside the 300nm blocks are 1°x 1° mean free air anomalies as contained in the OSU combined altimeter/terrestrial data set of October 1979 (the same data set used in Section 5.1). The axis of the Tonga lies along the highly negative anomaly values through blocks 1076, 1144, 1209, 1271, and 1272.

For immediate comparison, Figure 5 shows 1°x 1° mean free air anomalies for the test area as contained in the OSU terrestrial data set of October 1979 (Rapp, 1980). Where no value is indicated, there is no October 1979 terrestrial data for that particular 1°x 1° block. As can be seen from Figures 4 and 5, the altimeter/terrestrial data set is much more complete than the terrestrial data set. This is true not only in the test area but in the whole world, as can be seen from maps found in Rapp (1980) showing the global coverage of each of the two data sets.

The test area is characterized by a wide range of roughness of 300nm anomaly field, from smooth to very rough. The specific character of each 300nm block regarding anomaly and elevation magnitude and roughness is given in Table 3. The definitions of descriptors used in Table 3 are given in Table 4, which uses the following abbreviations:

ANOM : 300nm anomaly, computed by straight averaging known 60nm anomalies inside the 300nm block

RMSCA : RMS centered anomaly, i.e., the root mean square of 60nm anomalies inside the 300nm block after the value ANOM has been subtracted from each 60nm anomaly

ELEV : 300nm elevation, computed by straight averaging 60nm elevations inside the 300nm block.

RMSCE : RMS centered elevation, i.e., the root mean square of 60nm elevations inside the 300nm block after the value ELEV has been subtracted from each 60nm elevation.

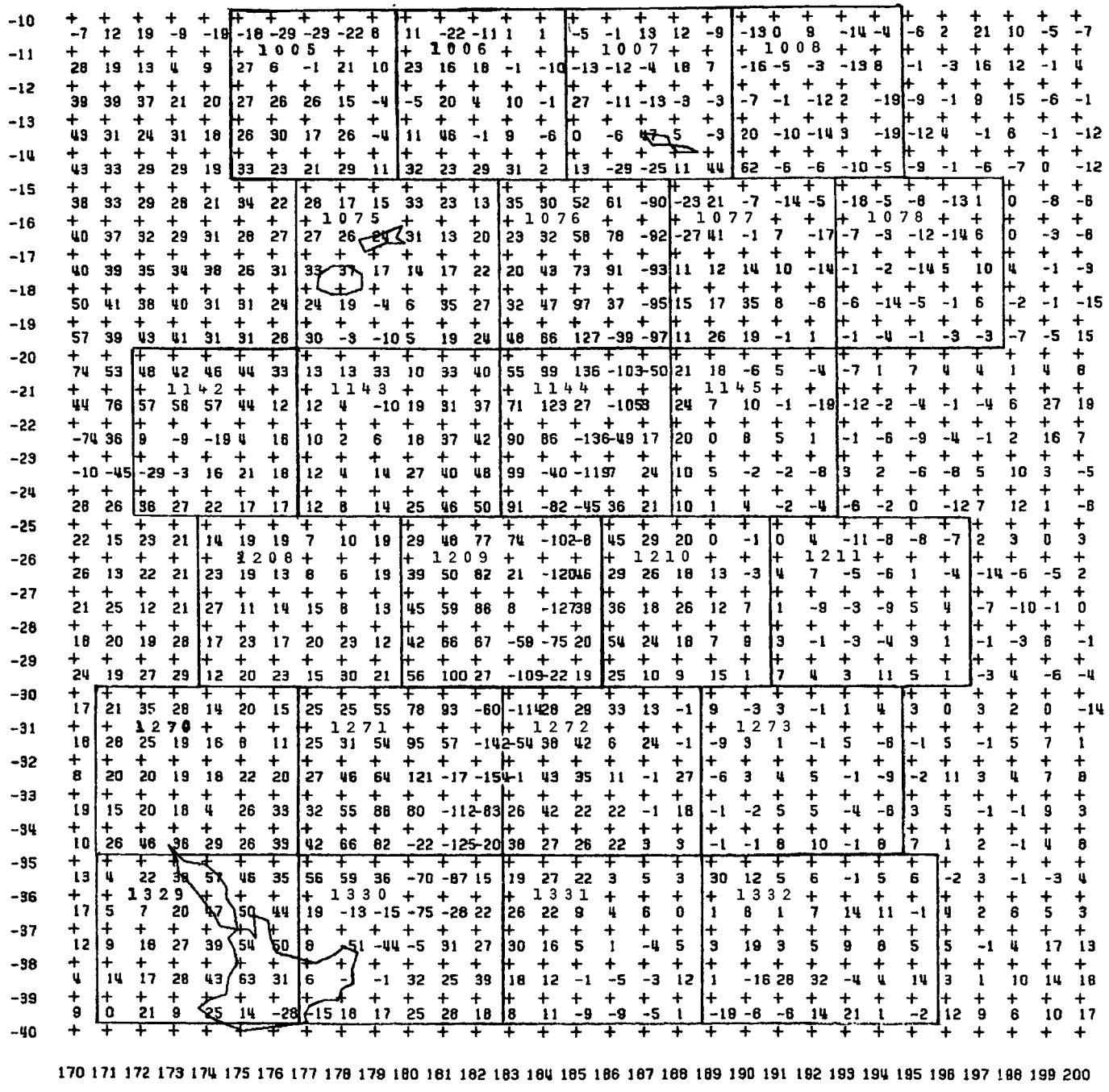

Figure 4: October 1979 1°x 1° Altimeter/Terrestrial Anomaly Coverage (mgals) and Location of 300nm Test Blocks Over the Tonga Trench Area.

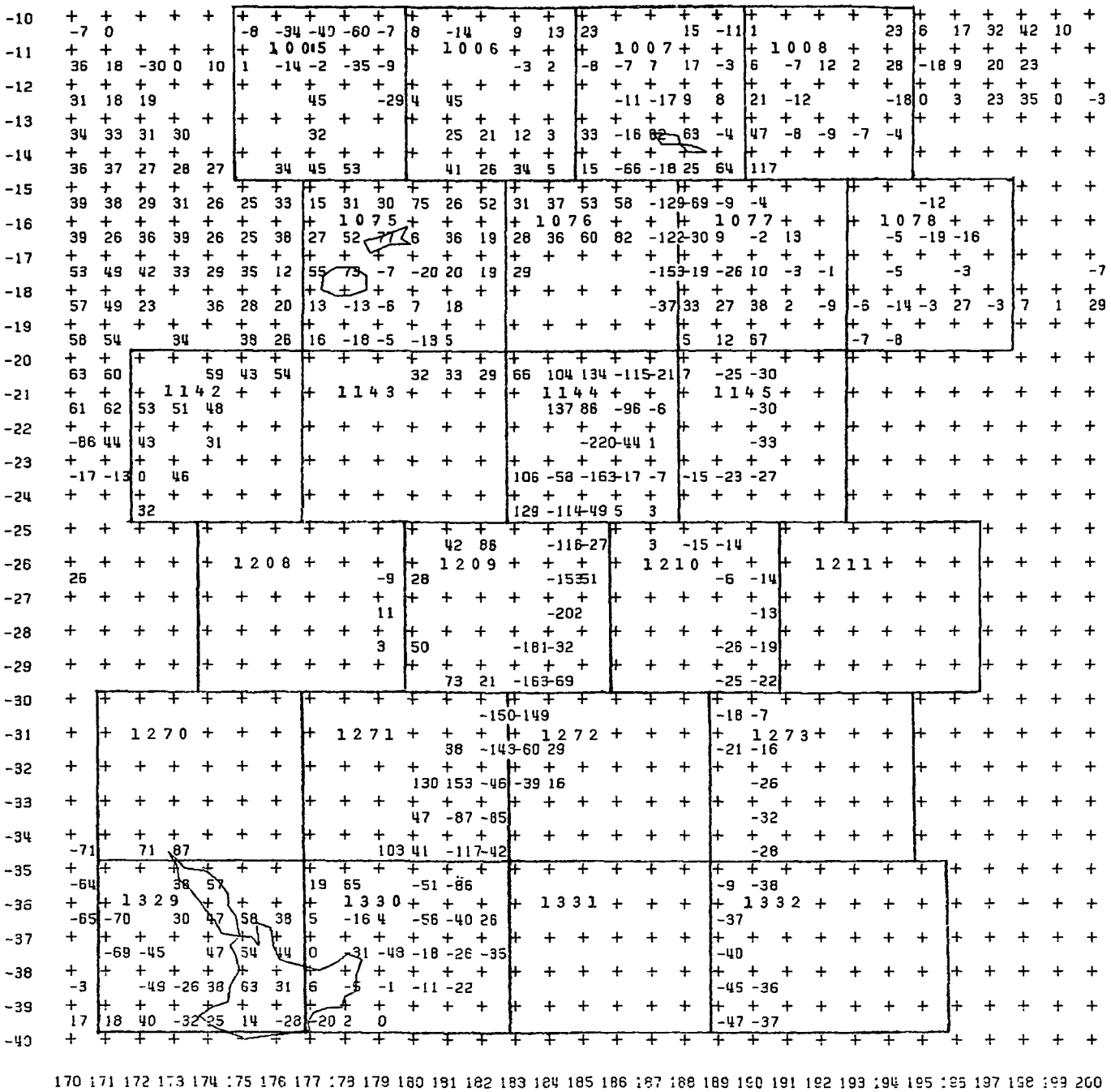

Figure 5: October 1979 1°x 1° Terrestrial Anomaly Coverage (mgals) and Location of 300nm Test Blocks Over the Tonga Trench Area

Table 3

Characterization of the 24 300nm Test Blocks Covering the Tonga Trench Area, Regarding Anomaly and Elevation Magnitude and Roughness

	Anomaly		Elevation	
Block	Magnitude	Roughness	Magnitude	Roughness
1005	MED HIGH	MILD	MED LOW	SMOOTH
1006	MEDIUM	MILD	LOW	MED RGH
1007	MEDIUM	MILD	LOW	MED RGH
1008	MEDIUM	MILD	LOW	MED RGH
1075	MED HIGH	SMOOTH	MED LOW	MED RGH
1076*	MED HIGH	VRY RGH	LOW	VRY RGH
1077	MEDIUM	MILD	VRY LOW	SMOOTH
1078	MEDIUM	SMOOTH	LOW	SMOOTH
1142	MED HIGH	MILD	LOW	MED RGH
1143	MED HIGH	MILD	MED LOW	MED RGH
1144*	MEDIUM	VRY RGH	LOW	VRY RGH
1145	MEDIUM	SMOOTH	VRY LOW	SMOOTH
1208	MED HIGH	SMOOTH	LOW	MED RGH
1209*	MED HIGH	VRY RGH	LOW	VRY RGH
1210	MED HIGH	MILD	VRY LOW	SMOOTH
1211	MEDIUM	SMOOTH	VRY LOW	SMOOTH
1270	MED HIGH	SMOOTH	MED LOW	RGH
1271*	MEDIUM	VRY RGH	LOW	RGH
1272*	MED HIGH	RGH	VRY LOW	SMOOTH
1273	MEDIUM	SMOOTH	VRY LOW	SMOOTH
1329	MED HIGH	MILD	MED LOW	MED RGH
1330*	MEDIUM	RGH	LOW	RGH
1331	MEDIUM	SMOOTH	VRY LOW	SMOOTH
1332	MEDIUM	SMOOTH	VRY LOW	SMOOTH

*rough to very rough 300nm blocks, critical to the studies in this report.

Table 4

Definitions of Descriptors for 300nm Blocks

Descriptor	Range of Values	% Out of Total[1]
A. Anomaly Magnitude.	ANOM ≡ Anomaly	
LOW	ANOM < -30 mgals	4
MED LOW	-30 ≤ ANOM < -10	20
MEDIUM	-10 ≤ ANOM < 10	51
MED HIGH	10 ≤ ANOM < 30	21
HIGH	30 ≤ ANOM	4
B. Anomaly Roughness.	RMSCA ≡ RMS Centered Anomaly.	
SMOOTH	0 ≤ RMSCA < 10 mgals	42
MILD	10 ≤ RMSCA < 25	43
RGH*	25 ≤ RMSCA < 45	11
VRY RGH*	45 ≤ RMSCA	4
C. Elevation Magnitude.	ELEV ≡ Elevation.	
VRY LOW	ELEV < -5200 m	6
LOW	-5200 ≤ ELEV < -3000	46
MED LOW	-3000 ≤ ELEV < 0	19
MEDIUM	0 ≤ ELEV < 500	17
HIGH	500 ≤ ELEV < 1200	8
VRY HIGH	1200 ≤ ELEV	4
D. Elevation Roughness.	RMSCA ≡ RMS Centered Elevation.	
SMOOTH	RMSCA < 500 m	62
MED RGH	500 ≤ RMSCA < 1000	20
RGH	1000 ≤ RMSCA < 1700	13
VRY RGH	1700 ≤ RMSCA	5

[1]Total number of 300nm blocks considered: 1611

*critical categories for the purpose of this report.

Table 4 was established from an analysis of the combined altimeter/terrestrial data set. Since this data set had adequate 1°x 1° mean anomaly coverage (Rapp, 1980) and since 1°x 1° mean elevations are fully known, the computations of the quantities ANOM, RMSCA, ELEV, and RMSCE for the 300nm blocks were generally meaningful. Each 300nm block of the world was taken, and values of ANOM, RMSCA, ELEV, and RMSCE computed for the block. These values then fell within corresponding ranges given in Table 4. A frequency count was kept of the number of 300nm blocks falling within the various ranges, and the percentages out of the total number of blocks considered were computed and given in the last column of Table 4. For example, Table 4 says that 300nm blocks which have RMSCA $\geq$ 45 constitute only 4% of the total number of observed 300nm blocks; as such, blocks with RMSCA $\geq$ 45 may be regarded as having very rough anomaly fields. Similary, 300nm blocks with 25 $\leq$ RMSCA $<$ 45 are seen to constitute about 11% of the total number of 300nm blocks considered, and these may be regarded as blocks with rough anomaly fields. It will be seen in Section 9 that 300nm blocks with rough to very rough anomaly fields are the blocks where current 300nm anomaly prediction procedures need to be improved.

In Table 3, the blocks marked with asterisks are critical blocks for studies conducted in this report (see Section 9). These blocks fall in the categories of blocks with rough to very rough anomaly fields, the categories marked also with asterisks in Table 4. It should be noted from Table 3 that the blocks categorized as having rough to very rough anomaly fields are the same blocks which are categorized as having rough to very rough terrain, a consequence of anomaly-elevation correlation that will be more fully covered in Section 12.

9. Problem With Current Procedures

To examine the performance of current prediction procedures under a variety of cases of anomaly field roughness and number of known 60nm blocks, the procedures were used to predict 300nm anomalies for the 24 test blocks in the Tonga Trench area. Since all the test blocks have their 25 60nm anomalies known in the altimeter/terrestrial data set, "true" values of the 300nm anomalies were obtained by area-weighted averaging the 25 known 60nm anomalies inside the individual 300nm blocks, in accordance with equation (33).

Then, to simulate lack of data during prediction, only those 1°x 1° altimeter/terrestrial anomalies for which there was a corresponding known 1°x 1° anomaly in the terrestrial data set were used to predict 300nm anomalies. Therefore, the data configuration was that shown in Figure 5, although

the actual data values used came from the altimeter/terrestrial data set shown in Figure 4. Predictions were done using current procedures (Section 7) and the global numerical covariance function given in Table 1. The results are shown in Table 5.

Column 1 of Table 5 gives the standard block sequence number. Column 2 gives N , the number of known 60nm anomalies used in the prediction. Column 2 also gives the character of the anomaly field as to roughness, obtained from Table 3. Column 3 gives "true" values. Column 4 gives the predicted 300nm anomaly. Column 5 gives the error of prediction (predicted value minus "true" value) and the standard error of prediction.

The immediate conclusion from Table 5 is that current prediction procedures yield satisfactory results for smooth to mild 300nm anomaly fields, start to have problems with rough 300nm anomaly fields, and definitely yield unreasonable results for very rough 300nm anomaly fields. As Table 4 shows, rough 300nm blocks ($25 \leq RMSCA < 45$) constitute about 10% and very rough blocks ($RMSCA \geq 45$) about 5% of all the 300nm blocks of the world, so that roughly 15% of all 300nm blocks are problematic blocks similar to blocks 1076, 1144, 1209, 1271, 1272, and 1330 shown in Table 5. Other tests would indicate that the problem is particularly pronounced for rough to very rough 300nm blocks which contain relatively few known 60nm blocks, say less than 15, and is rather insignificant when the number of known 60nm blocks is close to the maximum number 25, say greater than 20.

10. Prediction With Area-Weighted Averaging

A 300nm anomaly prediction procedure which is more rigorous than the current procedrues may immediately be obtained by using area-weighted averaging expressed by equations (33) and (34) instead of the straight averaging expressed by equation (52). Also, pursuing the second comment under equation (52) all 25 60nm anomalies inside the 300nm block, unknown or known, must be predicted prior to area-weighted averaging the 25 60nm anomalies.

Therefore, prediction of the 300nm test block anomalies was done with what will be called Method A. The data set used was the October 1979 terrestrial data set. The covariance function used was that given in Table 1, which was a covariance function based on the altimeter/terrestrial data set. Strictly, a new covariance function should have been computed based on the terrestrial data set, but this would not have made any difference for the purpose of this section.

Table 5

Prediction Using Current Procedures With
Global Anomaly Covariance Function,
Illustrating Prediction Problems
Over Rough 300nm Blocks

Block	N/CHAR	"True" Anom (mgal)	Anomaly (mgal) Current Proc Alt/Ter Subset	Error/$m_{\Delta g}$ (mgal) Current Proc Alt/Ter Subset
1005	16/MLD	11.1	8.8	-2.3/3.5
1006	16/MLD	9.2	6.3	-2.9/3.2
1007	22/MLD	2.4	0.5	-1.9/2.0
1008	16/MLD	-2.9	-2.1	0.8/3.1
1075	23/SMTH	19.4	20.4	1.0/1.8
1076*	13/VRY RGH	21.7	-3.7	-25.4/5.6
1077	20/MLD	5.3	7.1	1.8/2.5
1078	13/SMTH	-4.3	-3.9	0.4/3.9
1142	11/MLD	23.4	21.4	-2.0/5.5
1143	3/MLD	21.6	13.8	-7.8/11.0
1144*	22/VRY RGH	10.3	5.5	-4.8/2.0
1145	8/SMTH	4.1	6.0	1.9/6.1
1208	3/SMTH	16.5	8.4	-8.1/10.8
1209*	13/VRY RGH	16.0	-8.8	-24.8/3.6
1210	10/MLD	17.9	10.0	-7.9/6.3
1211	#	-0.5	#	#
1270	2/SMTH	22.2	19.0	-3.2/11.8
1271*	13/VRY RGH	17.0	-3.6	-20.6/5.9
1272*	5/RGH	13.4	-4.5	-17.9/9.4
1273	7/SMTH	0.7	-0.2	-0.9/7.7
1329	19/MLD	27.1	26.5	-0.6/3.0
1330*	21/RGH	2.4	-0.7	-3.1/2.4
1331	#	7.7	#	#
1332	8/SMTH	6.2	0.0	-6.2/7.9

#No October 1979 terrestrial data exists.

*blocks showing prediction problems
(rough and very rough blocks)

Method A used previous equations summarized as follows. First, the 25 60nm anomalies were predicted using an extension of equation (51):

$$\Delta g = C_{\Delta g \Delta g^*} \left(C_{\Delta g^* \Delta g^*} + D_{\Delta g^* \Delta g^*}\right)^{-1} \Delta g^* \ , \qquad (54)$$

where now Δg is a 25 x 1 vector containing the 25 predicted 60nm anomalies. Then, using the area-weighted averaging operator given by equation (34):

$$L_{\Delta \bar{g} \Delta g} = \frac{1}{\sum_{i=1}^{25} A_i} \left(A_1 \ A_2 \ . \ . \ . \ A_{25}\right)$$

the 300nm anomaly was indirectly predicted (Section 6) using equation (33):

$$\Delta \bar{g} = L_{\Delta \bar{g} \Delta g} \ \Delta g \ .$$

Finally, the variance of the predicted 300nm anomaly was computed using equation (53):

$$m_{\Delta \bar{g}}^2 = C_{\Delta \bar{g} \Delta \bar{g}} - C_{\Delta \bar{g} \Delta g^*} \left(C_{\Delta g^* \Delta g^*} + D_{\Delta g^* \Delta g^*}\right)^{-1} C_{\Delta \bar{g} \Delta g^*}^T$$

where $C_{\Delta \bar{g} \Delta g^*}$ and $C_{\Delta \bar{g} \Delta \bar{g}}$ were computed by area-weighted averaging from the basic covariance matrix $C_{\Delta g \Delta g}$. The prediction results and the square root of $m_{\Delta \bar{g}}^2$ are shown in Table 6, column 3.

A direct prediction procedure which is exactly equivalent to the indirect procedure used by Method A may be done as follows, if desired. Equation (54) when substituted into equation (33) results in:

$$\Delta \bar{g} = L_{\Delta \bar{g} \Delta g} \ C_{\Delta g \Delta g^*} \left(C_{\Delta g^* \Delta g^*} + D_{\Delta g^* \Delta g^*}\right)^{-1} \Delta g^* \ .$$

Applying covariance matrix propagation, the last equation may be written in the form of the direct prediction:

$$\Delta g = C_{\Delta \bar{g} \Delta g^*} \left(C_{\Delta g^* \Delta g^*} + D_{\Delta g^* \Delta g^*}\right)^{-1} \Delta g^* \ . \qquad (55)$$

The variance of predicted $\Delta \bar{g}$ is again given by equation (53).

For the evaluation of Method A, current prediction procedures were applied to the same terrestrial data set used by Method A. The covariance function used was again the one given in Table 1. The results of predictions are shown in Table 6, column 2. The difference between Method A and the current

Table 6

Predictions Using Method A With Global Anomaly Covariance Function, Illustrating the Effect of Area-Weighted Averaging and Prediction of all 25 60nm Anomalies.

Block	Anom/$m_{\Delta g}$ (mgal) Current Proc Oct79 Terr Set	Anom/$m_{\Delta g}$ (mgal) Method A Oct79 Terr Set	Anom Difference (mgal) Method A - Current Proc
1005	3.4/5.5	4.8/5.5	1.4
1006	13.0/5.3	12.3/5.3	-0.7
1007	7.9/3.8	8.3/3.8	0.4
1008	8.9/5.3	5.5/5.3	-3.4
1075	21.8/3.8	18.6/3.7	-3.2
1076*	3.7/7.5	11.8/7.5	8.1
1077	2.4/4.5	3.7/4.5	1.3
1078	-4.9/5.6	-4.6/5.6	0.3
1142	34.8/7.4	32.4/7.4	-2.4
1143	14.1/12.3	13.5/12.4	-0.6
1144*	-1.3/4.5	1.6/4.5	2.9
1145	-15.9/8.5	-14.1/8.5	1.8
1208	0.6/12.4	0.5/12.8	-0.1
1209*	-20.3/7.6	-6.6/7.8	13.7
1210	-11.1/8.0	-10.1/8.0	1.0
1211	#	#	#
1270	25.7/13.2	23.5/13.4	-2.2
1271*	-3.2/7.6	0.4/7.5	3.6
1272*	-17.1/11.1	-13.5/11.4	3.6
1273	-16.0/8.7	-15.4/9.0	0.6
1329	15.3/5.4	27.4/5.1	12.1
1330*	-13.2/5.0	-15.1/4.8	-1.9
1331	#	#	#
1332	-23.8/10.5	-20.9/10.7	2.9

#No October 1979 terrestrial data exists.

*rough and very rough blocks.

procedures is indicated in Table 6, column 4. It is seen from Table 6 that there tend to be cases of considerable difference[1] between the two methods in their predicted 300nm anomalies, although the two methods yield practically the same predicted accuracies. Since Method A is more rigorous than current procedures, Method A has to be the preferable method.

To study the numerical effect of not predicting the already known 60nm anomalies, area-weighted averaging (Method A) was again applied, but this time without predicting the known 60nm anomalies inside the 300nm block. The same data set and covariance function as used before were utilized. The method is called Method A' and the results are shown in Table 7, column 3. The difference between Method A' and Method A is shown in Table 7, column 4. It is seen that there tend to be cases of considerable difference between the two methods. It was decided that it would be worth the effort to predict all 25 60nm anomalies in an improved method for the prediction of 300nm anomaly.

As a further test of Method A, the method was applied to a subset of the altimeter/terrestrial data set obtained by considering only those 1°x 1° altimeter/terrestrial anomalies for which there were corresponding known 1°x 1° anomalies in the terrestrial data set. The covariance function used in the predictions was again the one given in Table 1. The results which are given in Table 8 again show that there tend to be cases of considerable difference between Method A and current procedures, this time in the case of altimeter/terrestrial data. An important case occurs for block 1271 for which Method A gave a much better 300nm anomaly prediction than current procedures judging from closeness of the predicted value to "true" value given in column 2 of Table 8. The smaller values of predicted accuracies in Table 8, column 4 as compared with the predicted accuracies in Table 6, column 3 are due to the smaller standard deviations in the altimeter/terrestrial data as compared with those in the terrestrial data.

---

[1]This report will often deal with comparison of alternative prediction methods in terms of differences in predicted results. Whether a certain difference is large or small should always be decided in the light of the magnitude of the estimated prediction error. A difference of 10mgals may be considered very large when the estimated prediction error over the 300nm block is just 3mgals, but it is certainly not that large when the estimated prediction error is 15mgals. Regarding the magnitude of the estimated prediction error, an allowance should be made for the fact that the use of a global covariance function in the prediction will tend to give a too small value for the estimated prediction error over a rough area.

Table 7

Predictions Using Method A' With Global Anomaly Covariance Function, Illustrating the Effect of Not Predicting all 25 60nm Anomalies in Method A

Block	Anom/$m_{\bar{\Delta g}}$ (mgal) Method A Terrestrial Data Set	Anomaly (mgal) Method A' Terrestrial Data Set	Anom Difference (mgal) Method A'- Method A
1005	4.8/5.5	3.3	-1.5
1006	12.3/5.3	13.0	0.7
1007	8.3/3.8	7.9	-0.4
1008	5.5/5.3	8.9	3.4
1075	18.6/3.7	20.7	2.1
1076*	11.8/7.5	3.7	-8.1
1077	3.7/4.5	2.3	-1.4
1078	-4.6/5.6	-4.9	-0.3
1142	32.4/7.4	34.9	2.5
1143	13.5/12.4	14.5	1.0
1144*	1.6/4.5	-1.1	-2.7
1145	-14.1/8.5	-15.9	-1.8
1208	0.5/12.8	0.5	0.0
1209*	-6.6/7.8	-23.3	-16.7
1210	-10.1/8.0	-11.1	-1.0
1211	#	#	#
1270	23.5/13.4	27.1	3.6
1271*	0.4/7.5	7.0	6.6
1272*	-13.5/11.4	-15.8	-2.3
1273	-15.4/9.0	-15.9	-0.5
1329	27.4/5.1	17.4	-10.0
1330*	-15.1/4.8	-15.0	0.1
1331	#	#	#
1332	-20.9/10.7	-23.8	-2.9

#No October 1979 terrestrial data exists.

*rough and very rough blocks.

Table 8

Predictions Using Method A With Global Anomaly Covariance Function, Applied to the Combined Altimeter/Terrestrial Subset

Block	"True" Anom (mgal) Alt/Ter Subset	Anom/$m_{\bar{\Delta g}}$ (mgal) Current Procedures Alt/Ter Subset	Anom/$m_{\bar{\Delta g}}$ (mgal) Method A Alt/Ter Subset	Anomaly Diff. (mgal) Method A-Current Procedures
1005	11.1	8.8/3.5	8.7/3.5	-0.1
1006	9.2	6.3/3.2	6.5/3.2	0.2
1007	2.4	0.5/2.0	0.1/2.0	-0.4
1008	-2.9	-2.1/3.1	-2.3/3.1	-0.2
1075	19.4	20.4/1.8	19.0/1.6	-1.4
1076*	21.7	-3.7/5.6	-4.1/5.5	-0.4
1077	5.3	7.1/2.5	7.0/2.5	-0.1
1078	-4.3	-3.9/3.9	-4.0/3.9	-0.1
1142	23.4	21.4/5.5	21.3/5.4	-0.1
1143	21.6	13.8/11.0	13.3/11.0	-0.5
1144*	10.3	5.5/2.0	6.0/2.0	0.5
1145	4.1	6.0/6.1	6.0/6.1	0.0
1208	16.5	8.4/10.8	8.2/11.3	-0.2
1209*	16.0	-8.8/3.6	-11.9/3.7	-3.1
1210	17.9	10.0/6.3	10.0/6.3	0.0
1211	-0.5	#	#	#
1270	22.2	19.0/11.8	19.0/11.8	0.0
1271*	17.0	-3.6/5.9	7.3/5.7	10.9
1272*	13.4	-4.5/9.4	-2.7/9.7	1.8
1273	0.7	-0.2/7.7	-0.2/8.0	0.0
1329	27.1	26.5/3.0	27.9/2.7	1.4
1330*	2.4	-0.7/2.4	-4.3/2.1	-3.6
1331	7.7	#	#	#
1332	6.2	0.0/7.9	-0.2/8.1	-0.2

#No October 1979 terrestrial data exists.

*rough and very rough blocks.

In summary, Tables 6, 7, and 8 indicate that the two ideas behind Method A are worth incorporating in an improved 300nm anomaly prediction. The two ideas are:

1. prediction of all the 25 60nm anomalies, unknown or known, inside the 300nm block. This has the effect of filtering out observational noise from the known 60nm anomalies;

2. Use of area-weighted averaging of the 25 60nm anomalies to obtain the 300nm anomaly. This will improve prediction results especially for rough 300nm blocks with greatly unequal 60nm areas inside them (as mentioned in Section 3, the difference between two 60nm areas inside a 300nm block can reach, though cannot exceed, a factor of two).

11. Prediction With Rough Covariance Function

Covariance matrices used in Least Squares Collocation equations are formed from a basic covariance function as described in Section 5.2. A covariance function such as the one given in Table 1 is a global covariance function, having been obtained by global averaging from 300nm blocks both rough and smooth. A global covariance function cannot truly represent the local anomaly behavior over rough 300nm blocks because rough 300nm blocks form a small minority (see Table 4) out of the total number of blocks used in the averaging process to obtain the global covariance function. It is therefore interesting to investigate whether 300nm anomaly predictions over rough areas can be improved through the use of a rough covariance function obtained by averaging from only those 300nm blocks with rough anomaly field.

Table 9 shows a rough numerical covariance function $cov(\Delta g, \Delta g)$. The function was computed from the combined altimeter/terrestrial data set using the same procedures ued to generate Table 1. This time, only those 300nm blocks which were classified as very rough (see Table 4, RMSCA $\geq$ 45mgals) were used in the averaging process that computed $cov(\Delta g, \Delta g)$. Note the big difference between the covariances from Tables 1 and 9; in particular, note the very much enlarged variance (the covariance at $\psi=0°$) and the shortened correlation length (the ψ-value at which the covariance falls to half the value of the variance).

Table 9

$cov(\Delta g, \Delta g)$ from the OSU Combined Altimeter/Terrestrial Data Set of October 1979, Using only Those 300nm Blocks With RMSCA > 45mgals (see Table 4)

Deg.	Rad.	$cov(\Delta g, \Delta g)$ (mgal^2)	No. of Product Pairs Used
0.0000	0.0000	4222	1470
0.9793	0.0171	1934	1986
1.6247	0.0284	769	3620
2.5074	0.0438	84	5029
3.4714	0.0606	17	4093
4.3831	0.0765	66	2495
5.3817	0.0939	-229	353
6.2559	0.1092	-1797	10

The rough covariance function from Table 9 was used as described in Section 5.2 to form covariance matrices needed in collocation equations. Subsequently, predictions were done under current procedures as described in Section 7, this time using the rough covariance matrices just formed. Prediction results are given in Table10, Column 3. For comparison, results of predictions

Table 10

Predictions Illustrating the Use of a Rough Covariance Function (Table 9) Instead of a Global Covariance Function (Table 1)

Block	Anom/$m_{\bar{\Delta g}}$(mgal) Current Procedures Global Cov. Function Terrestrial Data Set	Anom/$m_{\bar{\Delta g}}$(mgal) Current Procedures Rough Cov. Function Terrestrial Data Set	Anom/$m_{\bar{\Delta g}}$ Differences(mgal) Column 3- Column 2
1105	3.4/5.5	3.2/10.0	-0.2/4.5
1006	13.0/5.3	11.8/8.9	-1.2/3.6
1007	7.9/3.8	8.2/5.6	0.3/1.8
1008	8.9/5.3	8.8/9.0	-0.1/3.7
1075	21.8/3.8	21.6/5.4	-0.2/1.6
1076*	3.7/7.5	1.8/15.4	-1.9/7.9
1077	2.4/4.5	3.3/7.5	0.9/3.0
1078	-4.9/5.6	-3.9/10.2	1.0/-4.4
1142	34.8/7.4	28.7/14.4	-6.1/7.0
1143	14.1/12.3	7.0/22.6	-7.1/10.3
1144*	-1.3/4.3	0.0/6.8	1.3/2.3
1145	-15.9/8.3	-13.1/15.9	2.8/7.4
1208	0.6/12.4	0.1/22.2	-0.5/9.8
1209*	-20.3/7.4	-21.3/12.3	-1.0/4.7
1212	-11.1/8.0	-8.1/16.4	3.0/8.4
1211	#	#	#
1270	25.7/13.2	13.9/23.1	-11.8/9.9
1271*	-3.2/7.6	4.1/15.5	7.3/7.9
1272*	-17.1/11.1	-6.6/20.5	10.5/9.4
1273	-16.0/8.7	-10.3/18.-	5.7/9.3
1329	15.3/5.4	11.0/9.4	-4.3/4.0
1330*	-13.2/5.0	-12.5/7.9	0.7/2.9
1331	#	#	#
1332	-23.8/10.5	-16.2/19.5	7.6/9.0

No October 1979 terrestrial data exist for these blocks.

* rough and very rough blocks

using current procedures with the global covariance function from Table 1 were copied from Table 6, column 2 to Table 10, Column 2. The differences between the two sets of predictions are given in Table 10, Column 4.

It is seen that the anomaly differences given in Column 4 are all within the standard errors of prediction given in Column 2. In other words, there is no essential difference between the two sets of predicted anomalies. This result simply illustrates the conclusion already arrived at in Rapp (1977) that predicted anomalies are not critically sensitive to the covariance function used.

However, the significant effect of using different covariance functions is on the standard errors of predictions. Note the big differences in standard errors of predictions from the two sets, as given in Column 4. The much larger error of prediction associated with the use of a rough covariance function is caused by the enlarged variance and shortened correlation length for unchanged data spacing, implied by the use of the rough covariance function (see, for example, Sunkel (1981a)). Since a rough covariance function more truly represents the anomaly behavior over rough areas, it is to be expected that the standard errors of predictions given in Column 3 are more appropriate than those given in Column 2, in the case of rough blocks. For smooth blocks the standard errors of predictions should be those given in Column 2 since as already concluded in Section 9 theses values are satisfactory.

In conclusion, since the standard error of prediction is sensitive to the covariance functions used, therefore a more appropriate value for the standard error of prediction may be obtained by using a covariance function which truly represents the anomaly behavior in the area of interest. For example, in the case of current prediction procedures and even in the case of Method A discussed in Section 10, a global covariance function can be used for smooth and mild 300nm blocks which according to Table 4 comprise roughly 85% of the world, while a rough covariance function should be used for rough and very rough 300nm blocks which according to Table 4 comprise roughly 15% of the world.

It is to be noted that the use of a covariance function that is appropriate for the anomaly field being considered will only solve the problem of the better estimation of the absolute error of prediction. Whether the absolute error of prediction will be large or small is another problem. To keep the error of prediction small, steps should be taken to smooth out a rough anomaly field in some way in order to obtain an anomaly field which has a smaller variance and a larger correlation length. (Sunkel 1981a, Figure 5). This will be the subject of succeeding sections.

12. Correlation Between 60nm anomalies and Elevations

An examination of graphs of 60nm anomaly vs. elevation inside 300nm blocks shows that there is a distinct linear trend between 60nm anomalies and elevations. The linear trend is most pronounced in the case of 300nm blocks which are rough both in anomaly field and in terrain. This leads to the consideration of the possibility that 60nm elevations which happen to be fully known globally may contain enough information about 60nm anomalies that can be extracted to improve 60nm anomaly and eventually 300nm anomaly predictions.

For the remainder of this report improvements to the 300nm anomaly prediction will be investigated with regards to the use of 60nm elevation information. In this section a study of the global behavior of 60nm anomalies and elevations and the global trend that exists between them will first be presented. The OSU combined altimeter/terrestrial data set of October 1979, being the most reliable and complete data set available at the time of the investigations, was used in the study to be presented.

12.1 Global Behavior of 60nm Anomalies and Elevations

Let X take on elevation values which are multiples of 100 meters, and let Y take on anomaly values which are multiples of 5 mgals. Now define:

$Z_{XY}(X,Y)$ = number of observed 60nm blocks in the world with the properties:

$$X-50 \leq h_p < X+50 \text{ (meters)} \qquad (56)$$

$$Y-2.5 \leq \Delta g_p < Y+2.5 \text{ (mgals)} ,$$

where

h_p: 60nm elevation
Δg_p: 60nm anomaly.

To give an example involving specific values, given $X=-5500$m and $Y=-10$ mgals, then Z is about 100, using the OSU combined altimeter/terrestrial data set of October 1979. A general picture of the plot of Z_{XY} vs. X,Y is given in Figure 6, obtained from an analysis of the OSU combined altimeter/terrestrial data set of October 1979.

Now let

$Z_X(X)$ = number of observed 60nm blocks in the world with the property

$$X-50 \leq h_p < X+50 \text{ (meters)}, \qquad (57)$$

without regard to Δg_p . Z_X may be obtained form Z_{XY} as follows:

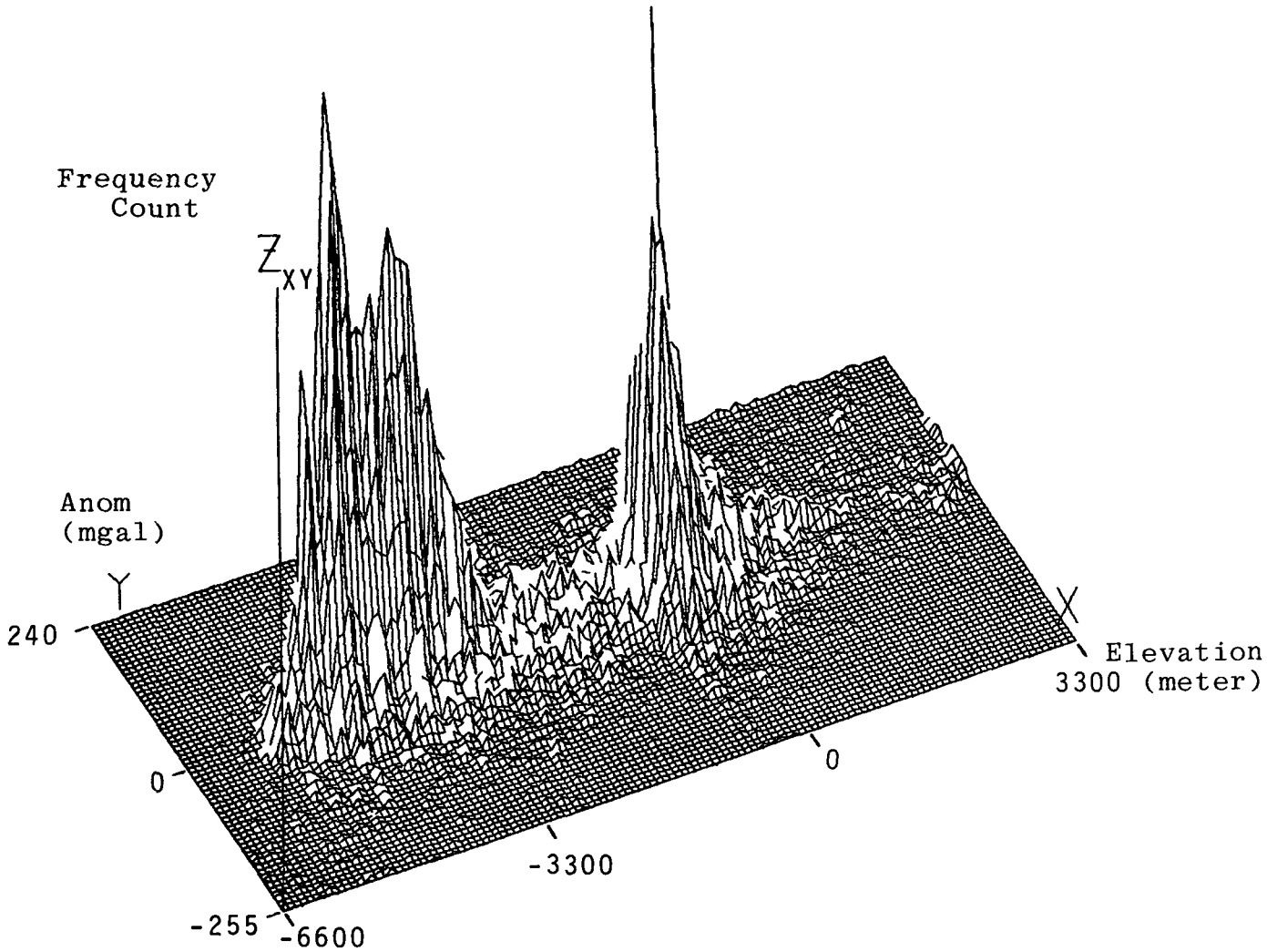

Figure 6: Histogram showing the Number of Observed 60nm Blocks in the World With 60nm Anomalies and Elevations Falling Within Specified 100-m Elevation and 5-mgal Anomaly Intervals.

$$Z_X(X) = \sum_Y Z_{XY}(X,Y) \qquad (58)$$

Figure 7 shows a plot of Z_X vs. X , obtained from the Z_{XY} shown in Figure 6. From Figure 7 it can be concluded that the 60nm elevations of the world are predominantly clustered around two elevations, one at about -4200m and the other at about +300m.

Again let

$Z_Y^+(Y)$ = number of observed 60nm blocks in the world with the properties:

$$h_p \geq -1200 \text{ (meters)} \qquad (59)$$

$$Y-2.5 \leq \Delta g_p < Y+2.5 \text{ (mgals)},$$

where -1200m is an arbitrarily selected X-value that is found in between the two major peaks in Figure 6. Z_Y^+ may be obtained from Z_{XY} as follows:

$$Z_Y^+(Y) = \sum_{X \geq -1200} Z_{XY}(X,Y) \; . \qquad (60)$$

Figure 8 shows a plot of Z_Y^+ vs. Y , obtained from the Z_{XY} shown in Figure 6. Similarly, let

$Z_Y^-(Y)$ = number of observed 60nm blocks in the world with the properties:

$$\begin{aligned} &h_p < -1200 \text{ (meters} \\ Y-2.5 \leq\ &g_p < Y+2.5 \text{ (mgals).} \end{aligned} \qquad (61)$$

Z_Y^- may be obtained from Z_{XY} as follows:

$$Z_Y^-(Y) = \sum_{X < -1200} Z_{XY}(X,Y) \qquad (62)$$

Figure 9 shows a plot of Z_Y^- vs. Y , obtained from the Z_{XY} shown in Figure 6. From Figure 8 and 9 it can be seen that as expected the 60nm anomalies of the world are clustered around zero, considering large samples (compare with Rapp (1977), Figure 2).

More detailed versions of Figures 8 and 9 may be obtained by considering

$Z_Y^\circ(X_0,Y)$ = number of observed 60nm blocks in the world with the properties:

$$\begin{aligned} &X_0-50 \leq h_p < X_0+50 \text{ (meters} \\ &Y-2.5 \leq \Delta g_p < Y+2.5 \text{ (mgals),} \end{aligned} \qquad (63)$$

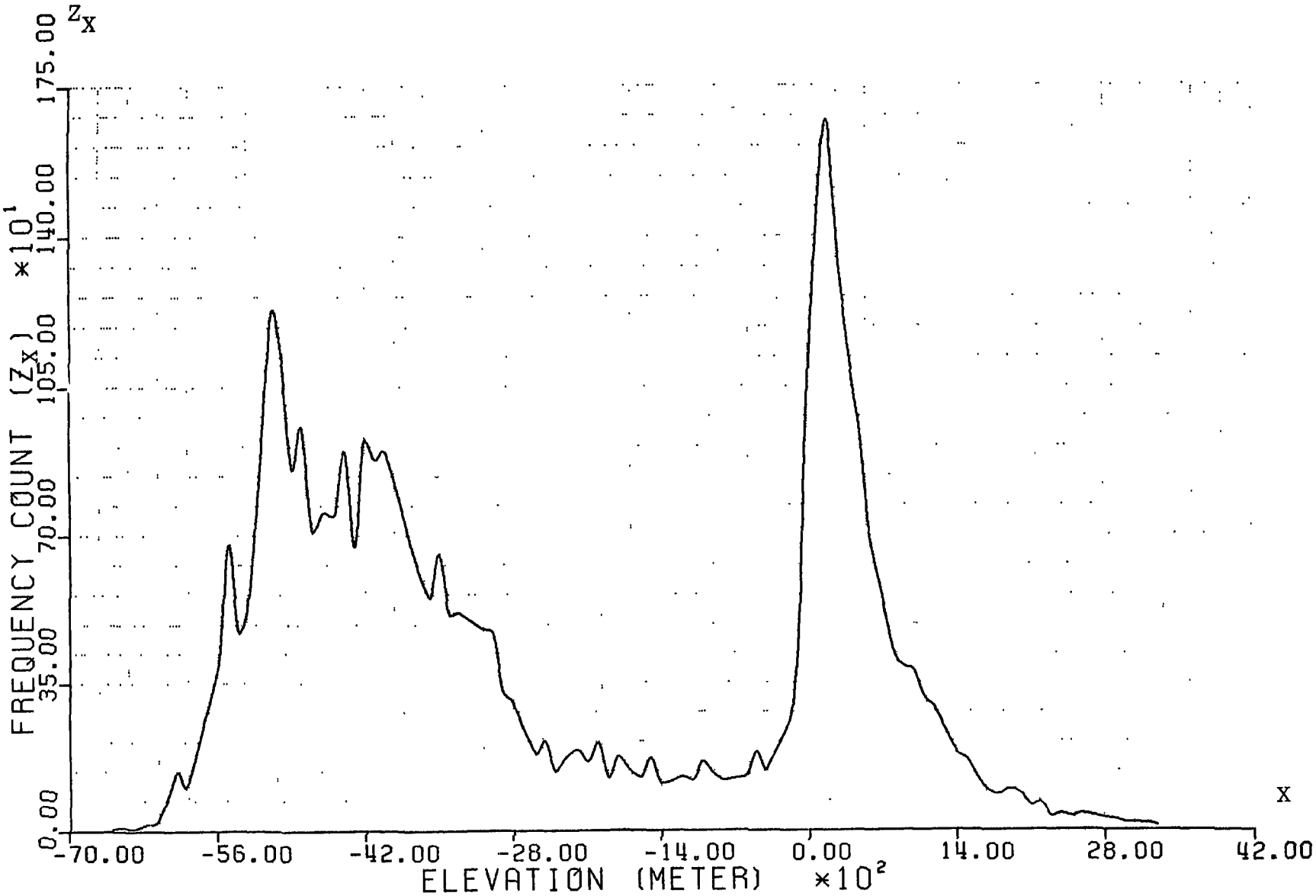

Figure 7: Number of Observed 60nm Blocks in the World With 60nm Elevations Falling Within A Specified 100-m Elevation Interval.

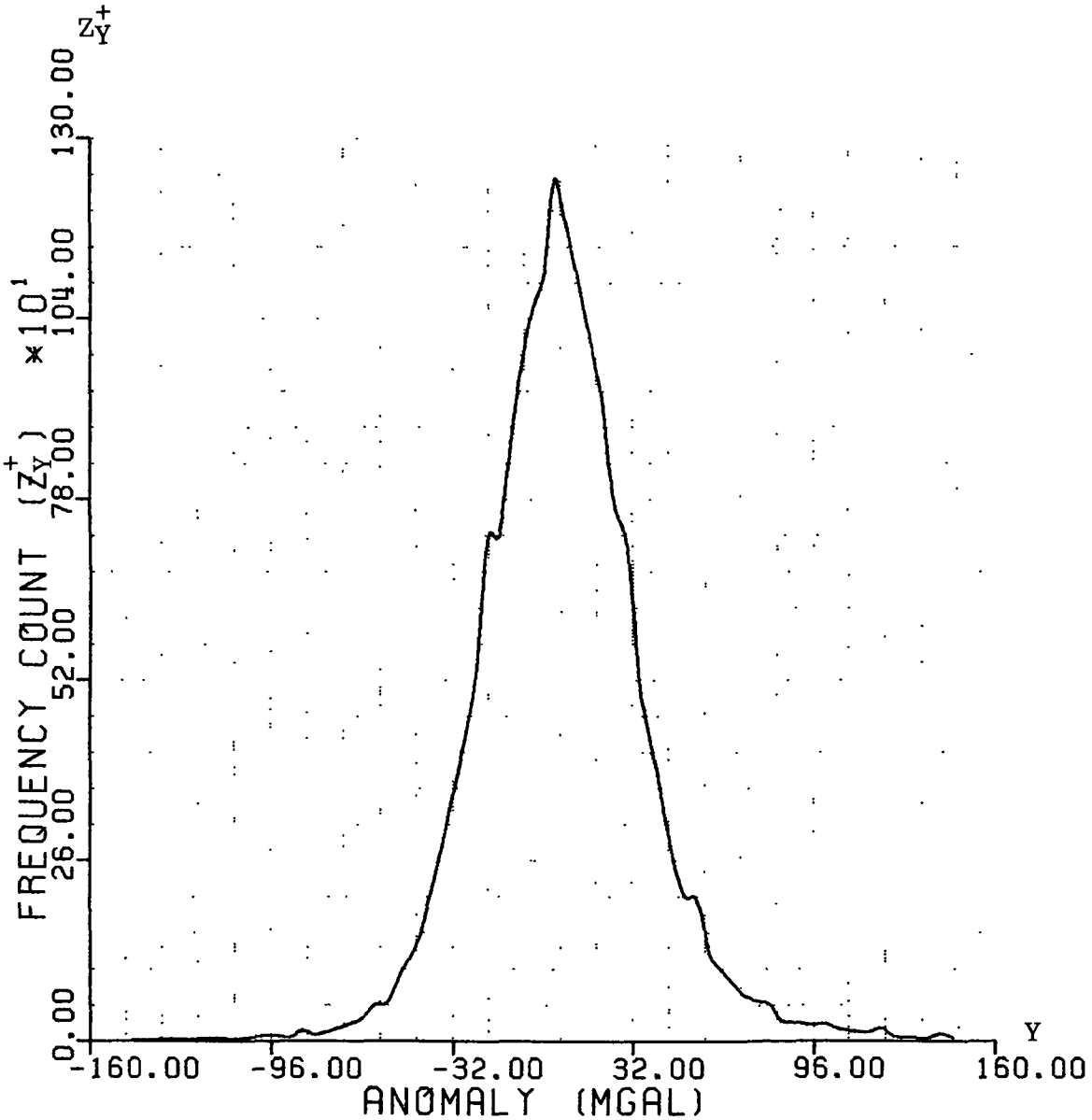

Figure 8: Number of Observed 60nm Blocks in the World with 60nm Anomalies Falling With a Specified 5-mgal interval, Considering only 60nm Blocks with 60nm Elevations Greater than or Equal to -1200m.

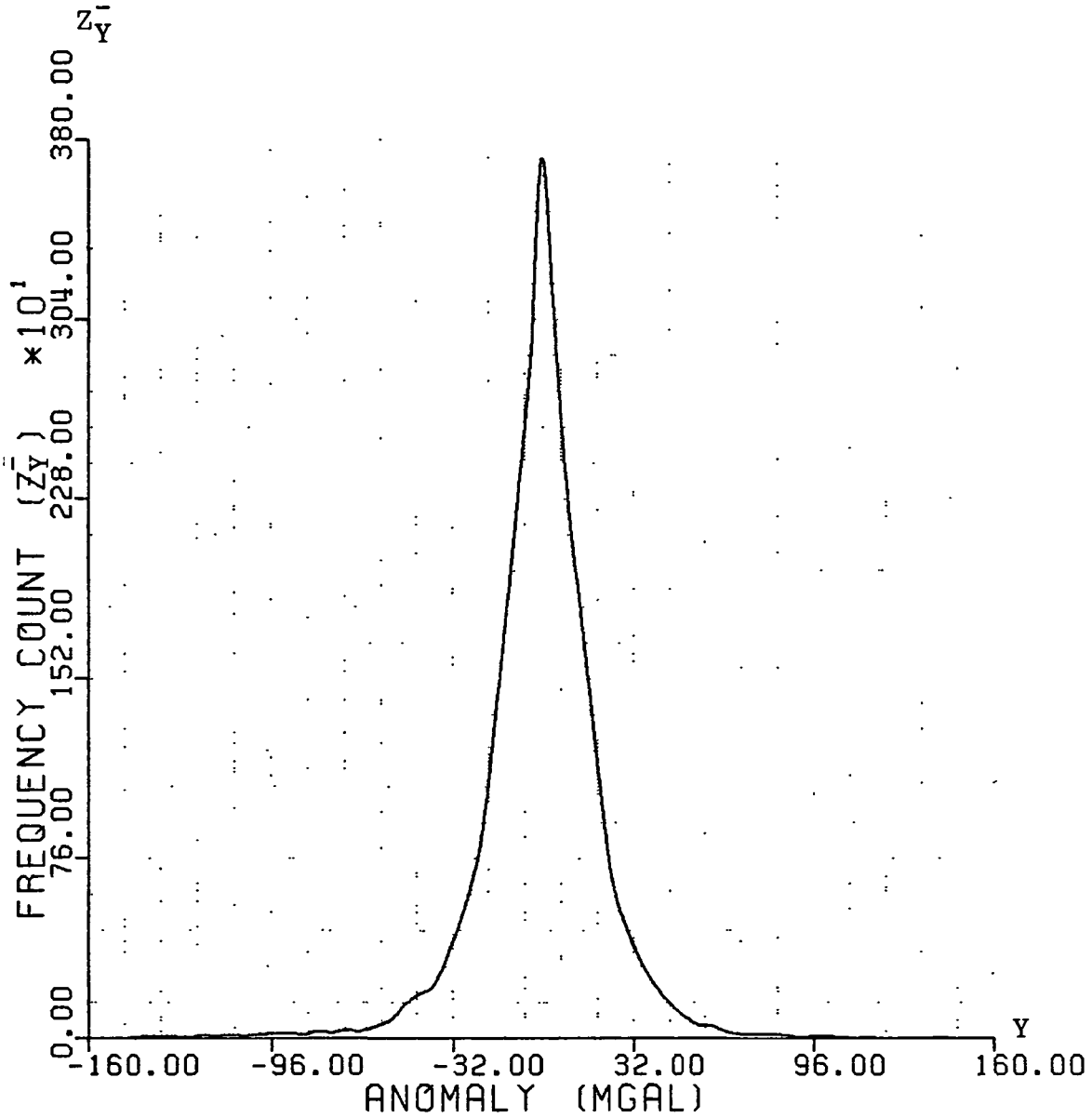

Figure 9: Number of Observed 60nm Blocks in the World With 60nm Anomalies Falling Within A Specified 5-mgal Interval, Considering Only 60nm Blocks with 60nm Elevations Less than -1200m.

where X_0 is kept constant while Y is allowed to vary. Z°_{Y} may be obtained as a profile of Z_{XY} (see Figure 6):

$$Z^{\circ}_{Y}(X_0,Y) = Z_{XY}(X_0,Y) \ . \qquad (64)$$

Several different plots of Z°_{Y} vs. Y may be constructed given different X_0-values. It is found from actual plots that the plot Z°_{Y} vs. Y always tends to be bell-shaped as in Figures 8 and 9. This fact will be the starting point of discussions in the next section.

12.2 Global Trend Between 60nm Anomalies and Elevations

12.2.1 Correlation Slope by Line Fitting

In the last section it was indicated that plots of Z°_{Y} vs. Y, which are profiles of Z_{XY} (see Figure 6 and equation (64)), always tend to be bell-shaped. This means that 60nm anomalies Δg_p occuring within a given 100-meter elevation interval

$$X-50 \leq h_p < X+50 \text{ (meters)}$$

tend to cluster around some average 60nm anomaly value. This average 60nm anomaly value can be expressed as (see Figure 6):

$$\bar{\Delta g}(X) = \frac{\int_Y Z_{XY}(X,Y) \cdot (Y)}{\int_Y Z_{XY}(X,Y)} \text{ (mgal)} \qquad (65)$$

A plot of $\bar{\Delta g}$ vs. X is given in Figure 10, obtained from the Z_{XY} shown in Figure 6. Figure 10 becomes a portrayal of the global trend that exists between 60nm anomalies and elevations.

Figures 7 and 10 should be compared with each other. For convenience, the graph of the elevation counts shown in Figure 7 was superimposed on the graph of average anomalies shown in Figure 10, with the resulting graph shown in Figure 11. In elevation ranges where there are large samples of cases occuring (see major peaks of elevation count graph) the average 60nm anomaly tends to zero (see horizontal intercepts of average anomaly graph). This corresponds to the tendency of positive and negative anomalies to cancel each other when a large sample of anomalies is considered.

As smaller samples are considered a weak correlation between 60nm anomalies and elevations tends to show up. Figure 11 shows

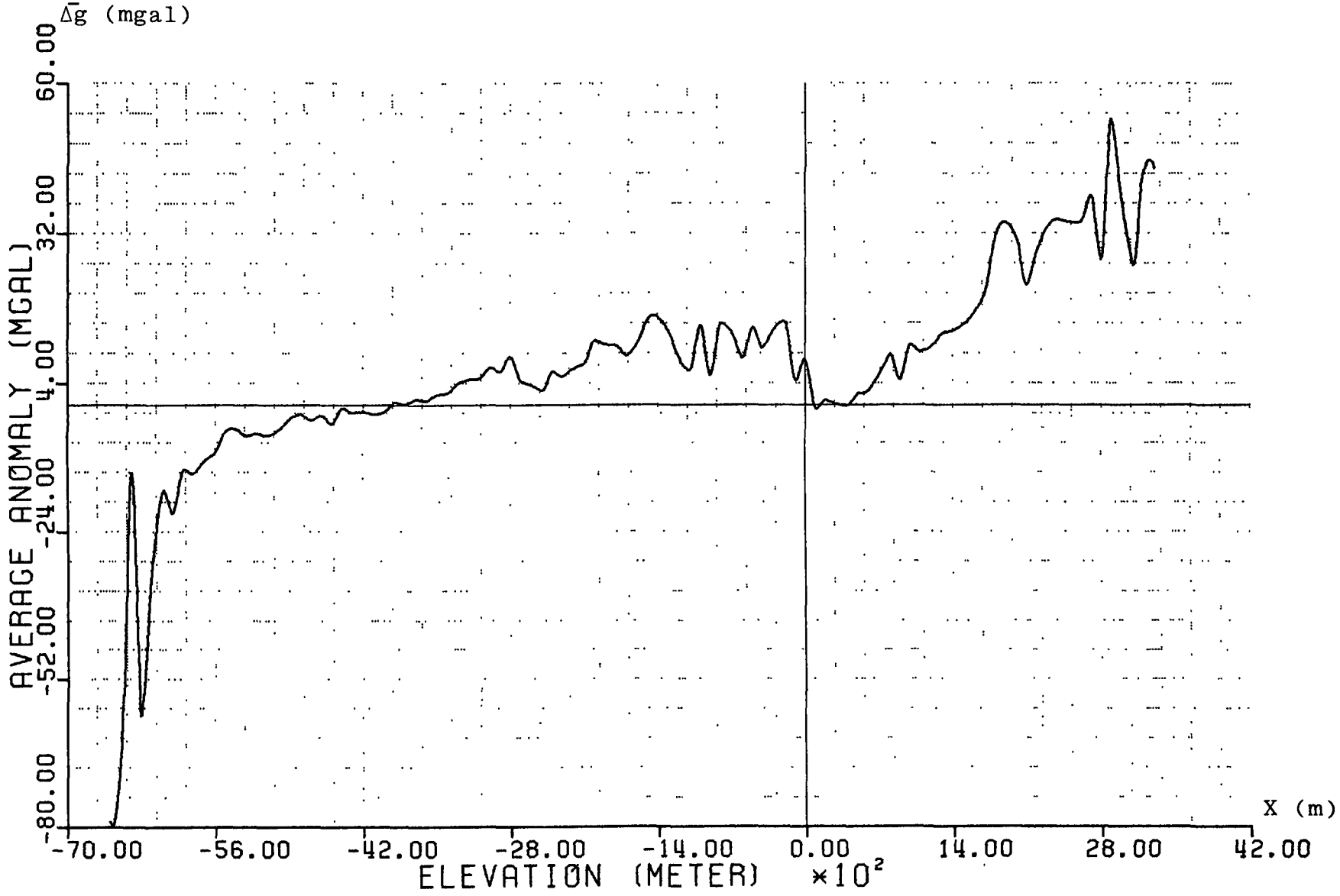

Figure 10: Average of 60nm Anomalies Occuring Within A Specified 100-meter Elevation Interval.

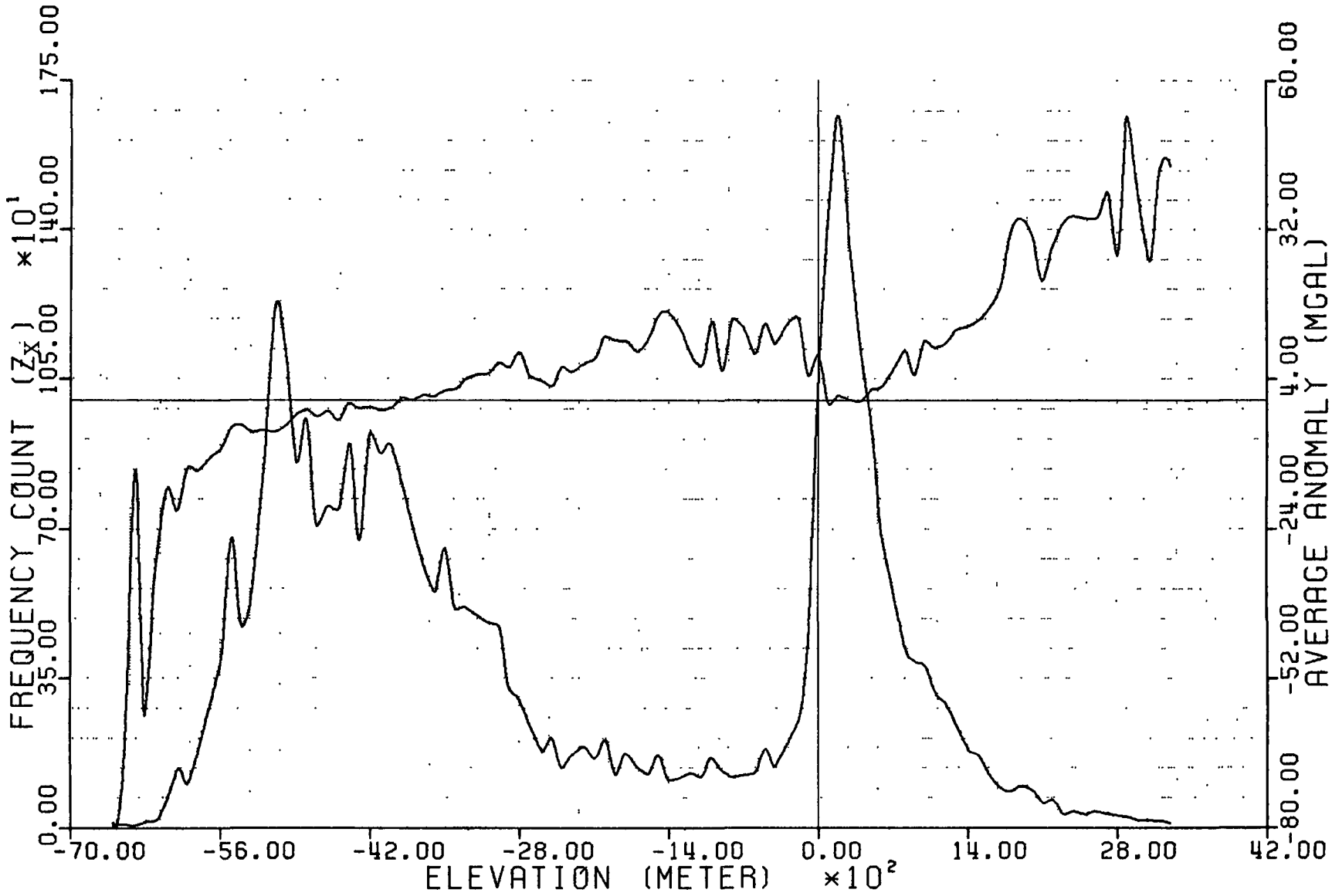

Figure 11: Superimposed Plot of the Elevation Count Graph Shown in Figure 7 And of the Average Anomaly Graph Shown in Figure 10.

that as elevation goes away from the central value -4200m towards higher values up to about -1200m, anomaly tends to go away from the central value zero towards larger values up to about +15mgals on the average. As elevation gets lower and lower than -4200m the anomaly tends to get smaller and smaller than zero. This is just exactly the definition of positive correlation, which is the mutual tendency of two quantities which are random around their respective central values to be both larger or both smaller than their central values at the same time. It can be said that 60nm elevations which are less than about -1400m (see left peak in Figure 7) correlate positively with their corresponding 60nm anomalies (see peak in Figure 9). This correlation is expressible as the slope of a line that fits the left branch of the graph in Figure 10 up to an elevation of about -1200m.

Similarly, it can be said that the right peak in Figure 7 correlates with the peak in Figure 8. Figure 11 shows that as the 60nm elevation becomes higher and higher than +300m, the 60nm anomaly tends to be larger and larger than zero. This corresponds to positive correlation between 60nm elevations greater than about +300m and their corresponding 60nm anomalies. This correlation is expressible as the slope of a line that fits the right branch of the graph in Figure 10 down to an elevation of about +300m. At elevations between roughly -1200m to +300m, Figure 10 exhibits a transition between the left and the right slopes of the total graph.

Based on the slope of the graph in Figure 10 it seems sufficient to consider two correlation slopes, one for negative elevations and the other for positive elevations. A slope of +0.0024 mgal/m was found to fit the negative branch of the graph in Figure 10, and this slope then expresses the very weak positive correlation that globally exists between negative 60nm elevations and their corresponding 60nm anomalies. A slope of +0.0141mgal/m was found to fit the positive branch of the graph in Figure 10, and this slope expresses a larger correlation between the positive 60nm elevations and their corresponding 60nm anomalies. In other words, in a global average sense, an increase of 1000 meters in a negative 60nm elevation corresponds to an increase of about 2 mgals in the 60nm anomaly and an increase of 1000 meters in a positive 60nm elevation corresponds to an increase of about 14 mgals in the 60nm anomaly.

12.2.2 Correlation Slope by Ratio of Covariance Functions

Correlation Slopes may also be computed, not by straight line fitting to graphs such as the one in Figure 10, but by taking the ratio of two covariance functions.

Following section 5.1, numerical mean anomaly-elevation cross-covariances can be computed as follows:

$$\mathrm{cov}(\Delta g,\Delta h) = \frac{\sum A_j\, A_k\, \Delta g_j\, \Delta h_k}{\sum\, A_j\, A_k} \qquad (66)$$

Similarly, numerical mean elevation covariances can be computed as follows:

$$\mathrm{cov}(\Delta g,\Delta g) = \frac{\sum A_j\, A_k\, \Delta h_j \Delta h_k}{\sum A_j\, A_k} \qquad (67)$$

Here, Δh is the mean elevation of the block, centered to the average of all mean elevations being considered.

Now assume that

$$\Delta g_j = b\, \Delta h_j \qquad (68)$$

where b is some constant that represents the correlation slope between Δg and Δh. Then, equation (66) may be written as:

$$\mathrm{cov}(\Delta g,\Delta h) = \frac{\sum A_j\, A_k\, b\, \Delta h_j\, \Delta h_k}{\sum A_j\, A_k}$$

$$= b\, \frac{\sum A_j\, A_k\, \Delta h_j\, \Delta h_k}{\sum A_j\, A_k}$$

$$\mathrm{cov}(\Delta g,\Delta h) = b\, \mathrm{cov}(\Delta h,\Delta h)\ . \qquad (69)$$

Equation (69) more readily follows from formulas for propagation of covariance functions through linear transformations such as equation (68) (see Moritz (1980), pp.86-87). From equation (69) the correlation slope may be computed as the ratio:

$$b = \frac{\mathrm{cov}(\Delta g,\Delta h)}{\mathrm{cov}(\Delta h,\Delta h)} \qquad (70)$$

In section 12.2.1 it was pointed out that negative 60nm elevations are correlated with their 60nm anomalies, with a global correlation slope of 0.0024 mgal/m. This correlation slope is the b-value that can also be computed from equation (70), if only those 60nm blocks with negative elevations are considered in the computation of the numerical covariance functions $\mathrm{cov}(\Delta g,\Delta h)$ and $\mathrm{cov}(\Delta h,\Delta h)$.

Using equations (66) and (67), along with conditions (14), (15), and (16), 60nm numerical covariance functions $\mathrm{cov}(\Delta g,\Delta h)$ and $\mathrm{cov}(\Delta h,\Delta h)$ were computed from the altimeter/terrestrial data set (Section 5.1). Only those 60nm blocks with negative 60nm

Table 11

Covariance Functions $cov(\Delta g, \Delta h)$ and $cov(\Delta h, \Delta h)$ as Computed Based on Equations (66) and (67), Using only 60nm Blocks with Negative Elevation.

Elevations are centered to their computed mean value -4120m; Anomalies are centered to zero.

deg.	rad.	$cov(\Delta g, \Delta h)$ mgal-meter	$cov(\Delta h, \Delta h)$ $meter^2$
0.0000	0.0000	8560	3576553
0.9803	0.0171	5782	2041906
1.6214	0.0283	4543	1840109
2.5079	0.0438	3623	1556291
3.4644	0.0605	3388	1367771
4.3780	0.0764	2953	1217362
5.3677	0.0937	2467	1124613
6.2205	0.1086	3434	1117875

Table 11A

$cov(\Delta g, \Delta h)/cov(\Delta h, \Delta h)$ (mgal/m)
0.0033
0.0029
0.0025
0.0023
0.0025
0.0024
0.0022
0.0031

mean ratio: 0.00264 mgal/m

std. dev. : 0.00039 mgal/m

elevations and known 60nm anomalies were considered in the computations, with the 60nm elevations centered to their computed mean value value of -4120m. The results are shown in Table 11.

In terms of the numerical functions, equation (70) means that b can be computed as the ratio of corresponding pairs of values from columns 3 and 4 of Table 11. The results of dividing the values in Table 11, Column 3 with the corresponding values from Table 11, Column 4 are shown in Table 11A. It is to be noted that the ratios are about the same, as they should be if Equation (68) is more or less correct. The mean ratio of +0.0026mgal/m agrees well with the correlation slope of +0.0024 mgal/m obtained by fitting a straight line to the negative branch of the graph in Figure 10. Tables similar to Tables 11 and 12 may be generated for the case of positive elevations and the resulting mean ratio compared with the value +0.0141 mgal/m obtained in Section 12.2.1 from line fitting.

12.2.3 Anomaly Field Roughness vs. Terrain Roughness

Since 60nm anomalies and elevations are correlated, though weakly in a global average sense, it would be expected that 300nm blocks with a smoother anomaly field would tend to have a smoother terrain and those with rougher anomaly field would tend to have rougher terrain.

Figure 12 shows the frequency count of 300nm blocks falling within the terrain roughness category of SMOOTH, MEDIUM ROUGH, ROUGH, and VERY ROUGH (see Table 4). Each bar is subdivided to show the distribution of 300nm blocks falling within the anomaly field roughness category of SMOOTH, MILD, ROUGH, and VERY ROUGH (Table 4). The bar chart indeed shows a weak global tendency for smoother anomaly field to be associated with smoother terrain and for rougher anomaly field to be associated with rougher terrain.

Figure 13 shows the mean RMSCA for each terrain roughness category. Recall from Table 4 that RMSCA (RMS Centered Anomaly) is the root mean square of 60nm anomalies inside the 300nm block after the mean 60nm anomaly for the 300nm block has been subtracted from each 60nm anomaly. RMSCA being a measure of roughness of the local anomaly field inside the 300m block, shows that smoother anomaly field is associated with smoother terrain and rougher anomaly field is associated with rougher terrain.

Figure 14 shows the mean RMSA for each terrain roughness category. Recall from Table 4 that RMSA (RMS Anomaly) is the root mean square of 60nm anomalies inside the 300nm block without removing the mean 60nm anomaly for she 300nm block. Figure 14 shows the same conclusions as Figure 13, only this time the bars are about 5 mgals taller.

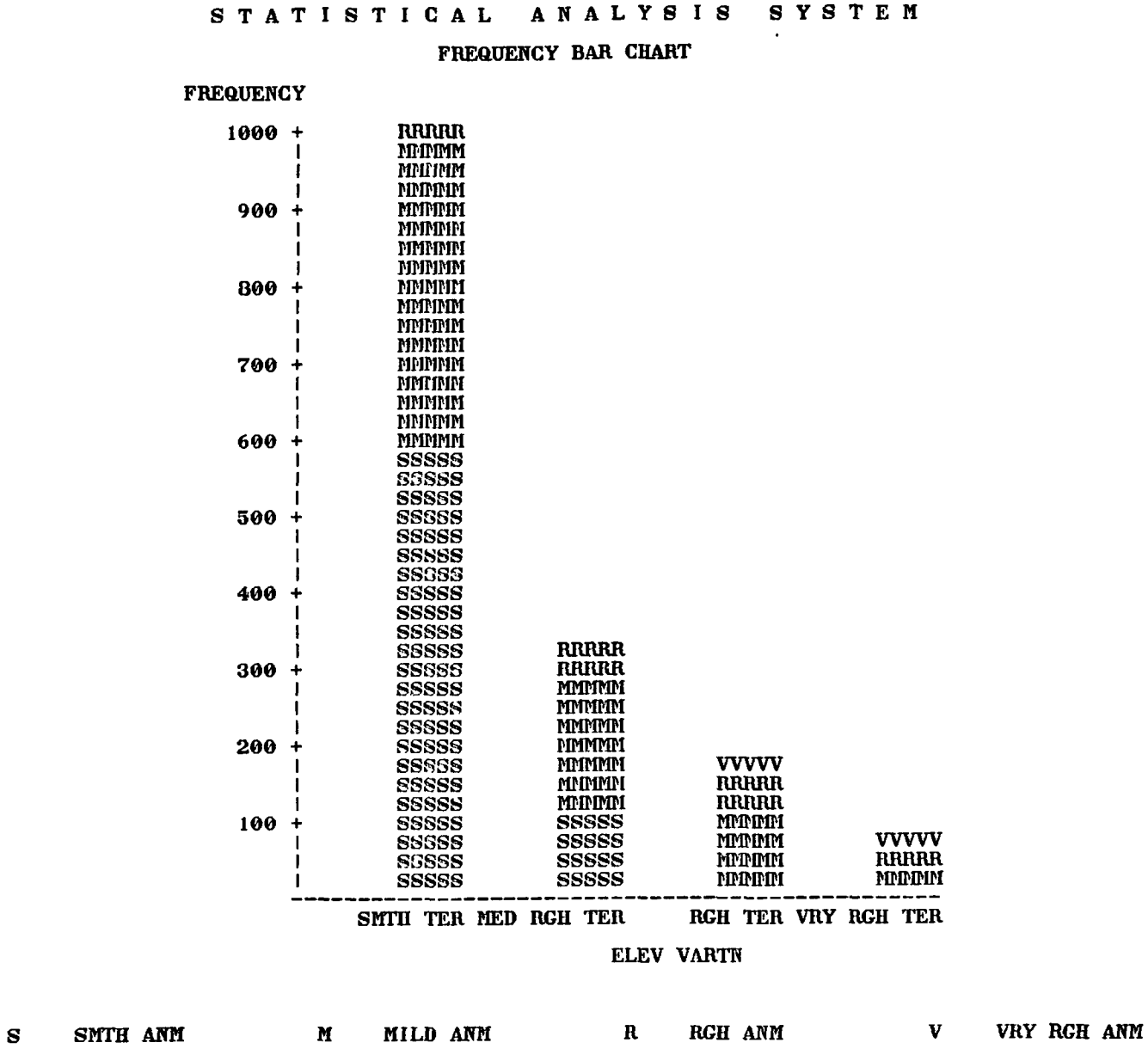

Figure 12: Bar Chart Showing a) the Number of Observed 300nm Blocks in the World with Terrain Roughness Falling into a Specified Category, and b) the Distribution of Anomaly Roughness Categories Occuring Within a Given Terrain Roughness Category.

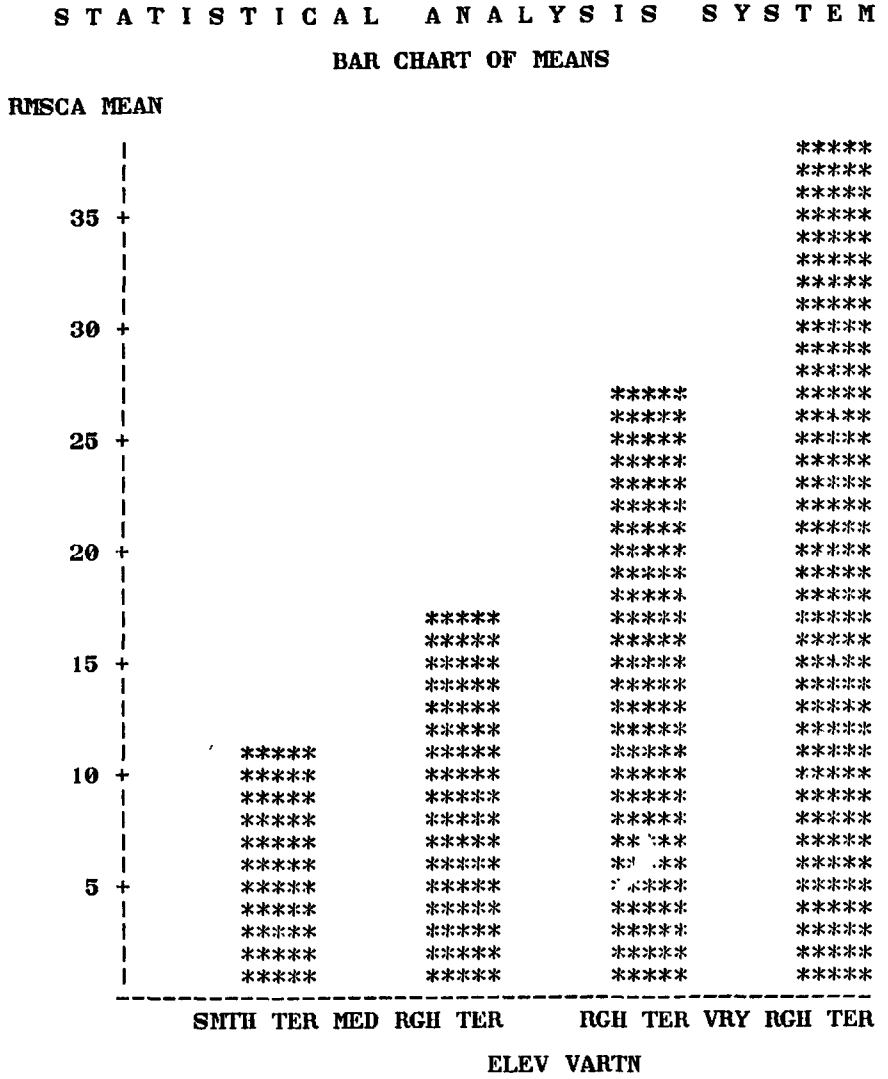

Figure 13: Average Value of RMS Centered 60nm Anomaly For a Specified Terrain Roughness Category.

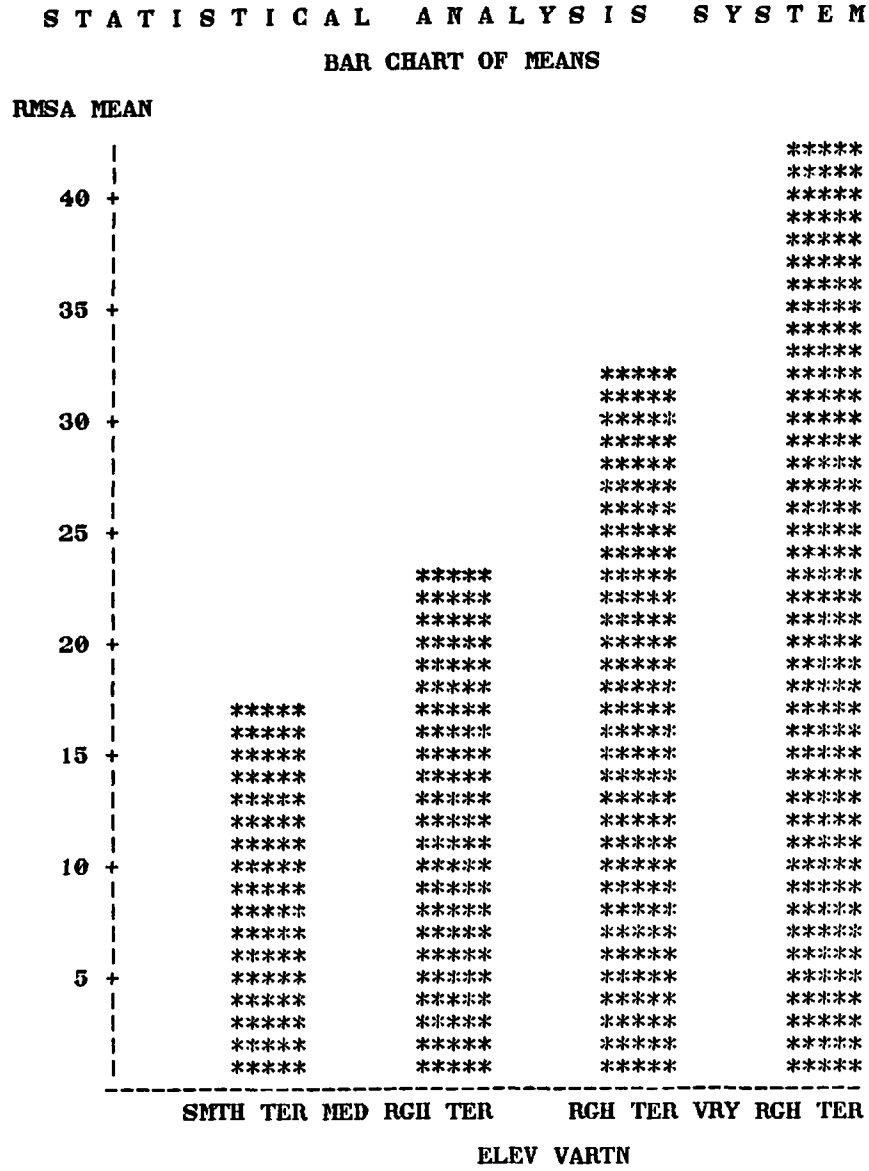

Figure 14: Average Value of RMS 60nm Anomaly For a Specified Terrain Roughness Category.

13. Removal of Local Trend Between 60nm Anomalies and Elevations

It was shown in the last section that the correlation between 60nm anomalies and elevations is weak in a global average sense. However, when local areas are considered, much larger correlations can be found. In particular, 300nm blocks with rough anomaly field, say RMSCA $\geq$ 45mgals (see Table 4), exhibit much larger correlation slopes than the global values found in the last section. These correlation slopes are a form of local systematic effects on 60nm anomalies caused by local variations in 60nm elevations. It is therefore natural to investigate improvements of 300nm anomaly prediction through the use of the model of Least Squares Collocation with systematic parameters.

Following equation (1), the vector of "observed" 60nm anomalies inside a 300nm block can be modeled as:

$$\Delta g^* = b\,\Delta h^* + \Delta g_s^* + n \qquad (71)$$

where

- b : local correlation slope between 60nm anomalies and elevations inside the 300nm block
- Δh^*: vector of 60nm elevations corresponding to Δg^*, centered to the area-weighted average of the 25 60nm elevations inside the 300nm block; subset of the Δh in equation (74).
- $b\Delta h^*$: systematic part of Δg^*.
- Δg_s^*: signal part of Δg^*.
- n: noise part of Δg^*.

The vector of 25 predicted 60nm anomalies would be (see equation (6)):

$$\Delta g = b\,\Delta h + \Delta g_s \,. \qquad (72)$$

Various methods that can be used to estimate the parameter b will be described in Sections 14, 15, and 16. Assuming an estimate of b has been obtained, the signals Δg_s can be solved using equations (4) and (5), which with changed notations become:

$$\Delta g_s = C_{\Delta g_s \Delta g_s^*}(C_{\Delta g_s^* \Delta g_s^*} + C_{nn})^{-1}\,(\Delta g^* - b\Delta h^*)\,. \qquad (73)$$

The vector of 25 60nm elevation differences can be computed from:

$$\Delta h = h - \bar{h} \cdot \bar{1} \qquad (74)$$

where

$\underline{h}$: vector of 25 60nm elevations
$\bar{h}$: area-weighted average of the 25 60nm elevations
$\bar{1}$: column vector of 25 1's .

The quantity $\bar{h}$ can be computed as:

$$\bar{h} = L\underline{h} \tag{75}$$

where L is the area-weighted averaging operator given in equation (34):

$$L = L_{\Delta\bar{g}\Delta g} \cdot \tag{76}$$

Once the 25 60nm anomalies inside the 300nm block have been predicted through equation (72), the 300nm anomaly can be computed as (see equations (33) and (34):

$$\Delta\bar{g} = L_{\Delta\bar{g}\Delta g}\, \Delta g \ .$$

Substituting equation (72) into the last equation:

$$\Delta\bar{g} = L_{\Delta\bar{g}\Delta g}(b\Delta h + \Delta g_s)$$

$$= L_{\Delta\bar{g}\Delta g}\, b\Delta h + L_{\Delta\bar{g}\Delta g}\, \Delta g_s \ .$$

$$\Delta\bar{g} = bL\Delta h + L_{\Delta\bar{g}\Delta g}\, \Delta g_s \tag{77}$$

The first term on the right-hand side of equation (77) can be shown to equal zero:

$$bL\Delta h = bL(\underline{h} - \bar{h}\,\bar{1})$$

$$= bL\underline{h} - bL\bar{h}\bar{1}$$

$$= b\bar{h} - b\bar{h}L\bar{1}$$

$$= b\bar{h} - b\bar{h} \cdot 1$$

$$= 0 \ .$$

Therefore, equation (77) reduces to:

$$\Delta\bar{g} = L_{\Delta\bar{g}\Delta g}\, \Delta g_s \ . \tag{78}$$

Equations (73) and (78) constitute the 300nm anomaly prediction equations under the model expressed by equation (71).

As mentioned in section 11, in order to make the error of prediction smaller, steps have to be taken to smooth out a rough anomaly field in some way in order to obtain an anomaly field which has a smaller variance and a larger correlation length.

Using the model expressed by equation (71) is a step in this direction. In equation (73), the data vector is the smoothed $(\Delta g^* - b\Delta h^*)$ instead of the original vector Δg^* used in the model Least Squares Collocation without systematic parameters (equation (54)). The smaller the value of b, the less becomes the difference between the use of $(\Delta g^* - b\Delta h^*)$ compared with the use of Δg^* as data vector in the prediction. As it will turn out in the next sections, the value of b for very rough blocks is large enough so that significant improvement in the prediction over rough blocks can be achieved by modeling b and using $(\Delta g^* - b\Delta h^*)$ instead of Δg^* as data vector.

14. Local Trend Removal by Least Squares Slope

As shown in Figure 4, the test area over the Tonga Trench had good data coverage in the altimeter/terrestrial data set. Using this data set, Least Squares straight lines were fitted to plots of 60nm elevation vs. 60nm anomaly inside the 300nm test blocks. Equal weights were given to the known 60nm values. The slopes of the regression lines, which are actually the b-values, are given in Table 12. Also given are the characteristics of the 300nm blocks as to roughness of anomaly field as copied from Table 3.

The rough 300nm blocks (marked with astrisk in Table 12) tend to exhibit much larger b-values than the smoother blocks. Since all the 60nm blocks of the test area have negative mean elevations, the b-values should be compared with the global average of 0.0024mgal/m found in Section 12.2. It is seen that the local b-values in Table 12 tend to be larger than the global average.

Questions about the statistical significance of the determined values of b will be dealt with later, in Section 16. In the meantime, it is felt that the b-values in Table 12 are well determined because of the good coverage of the data set used, and it will be interesting at this point to go ahead and show prediction results using the computed b-values.

Using equations (73) and (78), the altimeter/terrestrial subset described in Section 9, the global covariance function shown in Table 1, and the b-values from Table 12, predictions were done, with the results shown in Table 13. This method, which was Least Squares Collocation with the systematic parameter b obtained from Least Squares, will be called Method B. Only those 300nm test blocks which showed significant prediction differences are shown in Table 13. The other 300nm blocks had practically the same predicted results as compared with the predicted results from Method A (Section 10). Method A was

Table 12

Slope b From Least Squares Using
The Altimeter/Terrestrial Set

Block	Slope b mgal/meter	CHAR
1005	0.02375	MLD
1006	0.01252	MLD
1007	0.01464	MLD
1008	0.01141	MLD
1075	0.00616	SMTH
1076*	0.03406	VRY RGH
1077	0.03204	MLD
1078	0.01432	SMTH
1142	0.02444	MLD
1143	0.01267	MLD
1144*	0.03328	VRY RGH
1145	-0.00689	SMTH
1208	0.00194	SMTH
1209*	0.02376	VRY RGH
1210	-0.01507	MLD
1211	0.01535	SMTH
1270	0.00565	SMTH
1271*	0.04299	VRY RGH
1272*	0.04578	RGH
1273	0.00027	SMTH
1329	0.00429	MLD
1330*	0.00163	RGH
1331	-0.00971	SMTH
1332	-0.00353	SMTH

*rough and very rough blocks

Table 13

Comparison of Predictions Without the Use of the b-Parameter (Method A) against Predictions With the use of the b-Parameter from Least Squares (Method B).

Altimeter/Terrestrial Subset Used.

Block	'true' anom alt/ter set (mgals)	No.of known 60nm blocks used	anom/$m_{\bar{\Delta g}}$ (mgals) Method A alt/ter subset	anom/$m_{\bar{\Delta g}}$ (mgals) Method B alt/ter subset	Anom Difference Method B-Method A (mgals)
1076	21.7	13	-4.1/5.5	8.7/5.5	12.8
1144	10.3	22	6.0/2.0	9.1/2.0	3.1
1209	16.0	14	-11.9/3.7	-0.2/3.7	11.7
1271	17.0	12	7.3/5.7	20.6/5.7	13.3
1272	13.4	5	-2.7/9.7	10.4/9.7	13.1

Table 14

Comparison of Predictions Without the Use of the b-Parameter (Method A) against Predictions With the use of the b-parameter from Least Squares (Method B).

Terrestrial Data Set Used.

Block	No.of known 60nm blocks used	anom/$m_{\bar{\Delta g}}$ (mgals) Method A Oct 79 Terr Set	anom/$m_{\bar{\Delta g}}$ (mgals) Method B Oct 79 Terr Set	Anom Difference Method B-Method A (mgals)
1076	13	11.8/7.5	5.6/7.5	-6.2
1144	22	1.6/4.5	6.9/4.5	5.3
1209	14	-6.6/7.8	-2.5/7.8	4.1
1271	12	0.4/7.5	17.8/7.5	17.4
1272	5	-13.5/11.4	-3.8/11.4	9.7

used for comparison since it is the most improved version of current prediction procedures at this point of the investigation.

To be noted from Table 13 is the large improvement in the predicted values through the use of Method B. As compared with predicted values from Method A, the values from Method B are much closer to "true" values by the amounts given in the last column ("true" values come from Table 5). The values in the last column are all greater than the values of standard errors of predictions $m_{\Delta g}$, indicating that the difference between Method A and Method B is significant. There was no attempt to propagate the error of Least Squares estimation of b into the predicted values, hence the error of prediction for Method B was computed by the same formula used in Method A.

Method B, together with the global covariance function in Table 1, was again applied to predict the 300nm test block anomalies, this time using the terrestrial data set. Results are given in Table 14. Again, it is indicated from Table 14 that there could be significant differences between the use of Method A and Method B.

The conclusion from this section is that it is promising to base the idea of improving 300nm anomaly predictions over rough areas on the use of the model Least Squares Collocation with the b-parameter. It is very encouraging that the blocks that had unreasonable predictions under current procedures (Table 5) are the same blocks that had large improvements under Method B. The next section will give an idea of how much improvement could be attained through the use of a b-value that closely represents the true correlation between 60nm anomalies and elevations inside the 300nm block.

15. Local Trend Removal by Empirical Slope

In the last section, a statistical determination of the b-value was performed inside the 300nm block. In actual production applications, there may not be enough known 60nm blocks inside the 300nm block from which to statistically determine the b-value. An alternative is to use a b-value that is known to reasonably represent the gradient of 60nm anomaly as a function of elevation in the area of interest. A possible source of such b-values would be any empirically derived regional averages of b-values.

Woollard and Daugherty (1970) conducted extensive empirical studies of the magnitude of free air anomaly gradients that exist over various typical topographic forms in the oceans:

continental shelves, continental border trenches, island arcs and trenches, rises and ridges. The data analyzed were in the form of a voluminous amount of oceanic gravity traverse data across the various topographic forms. A complex situation was found that precluded the establishment of consolidated models that can define gravity gradients, given characteristic topographic forms. However, a large number of empirically determined gradients were given, covering a wide sample of the world's oceanic areas. A general conclusion was reached that oceanic free air anomaly gradients as a function of elevation might be expected to vary between zero and 0.069mgals/m, although frequent exceptions can be encountered (Woolard and Daugherty (1970), p.218). An overall value that was found for the Tonga Trench area was 0.06mgal/m (ibid., p.248).

The studies of Woollard and Daugherty involved data spacings that are consistent with those of the present investigation, namely angular distances of about 1°. It is thus reasonable to use the value 0.06mgal/m as b-value in 300nm anomaly predictions over the Tonga Trench area. Prediction results, using this b-value in equations (73) and (78) and using the global covariance function from Table 1, are as shown in Table 15, Column 5. The data set used was the altimeter/terrestrial subset (Section 9). The method will be called Method C. Again, there was no propagation of an error in b into the predicted values, hence predicted accuracies are the same as in Method A and Method B (Table 13).

For comparison, predictions were repeated using an arbitrary b-value of 0.04 mgal/m, with the results shown in Table 15, Column 4. Also given, in the last column of Table 15, are the prediction results and b-values from Method B of the last section.

The empirically based b-value of 0.06 mgal/m yielded prediction results which are very close to "true" values. An exception to this is block 1271 for which a b-value of about 0.04 mgal/m seems to be the best one to use. It is seen from a comparison of predicted values associated with the different b-values of 0.04 mgal/m, 0.06 mgal/m, and the Least Squares b-values, that the prediction is sensitive to the b-value used. This sensitivity of predictions to b-values indicates that it will be preferable to obtain the b-value using some uniform set of procedures that will yield a unique b-value; this will be the subject of next sections.

The conclusion from this section is that, if no reliable statistical estimate of b-value can be made, then a b-value that is empirically known to apply over the topographic area of interest may be used for the removal of local trend between 60nm anomalies and elevations.

Table 15

Comparison of Prediction Results from the Use of an Empirical b-value Against Prediction Results from the Use of the Least Squares b-value (Anom and $m_{\bar{\Delta g}}$ in mgals; b in mgal/m).

Block	"True" Anom	No.of known 60nm Blocks	anom/$m_{\bar{\Delta g}}$ b=0.04 alt/ter subset	anom/$m_{\bar{\Delta g}}$ b=0.06 Method C alt/ter subset	anom/$m_{\bar{\Delta g}}$ Least Squares b Method B alt/ter subset
1076	21.7	13	12.2/5.5	18.4/5.5	8.7/5.5 , b=0.03406
1144	10.3	22	10.0/2.0	11.7/2.0	9.1/2.0 , b=0.03328
1209	16.0	14	8.3/3.7	17.6/3.7	-0/2/3.7 , b=0.02376
1271	17.0	12	21.2/5.7	25.9/5.7	20.6/5.7 , b=0.04299
1272	13.4	5	12.7/9.7	14.5/9.7	10.4/9.7 , b=0.04578

16. Local Trend Removal by Collocation Parameters

16.1 Significance of Parameters

It will be shown in this section that in the use of the model Least Squares Collocation with systematic parameters, the only parameter that should be modeled is the parameter b , and only when the parameter b satisfies some strict significance test should it be used in the actual prediction.

First, consider the modeling of two systematic parameters. The vector of known 60nm anomalies, Δg^* , is modeled as:

$$\Delta g^* = AX + \Delta g^*_s + n \qquad (79)$$

where now,

$$A = [\bar{1}\ \Delta h^*] \quad \text{and} \quad X^T = [\Delta g_0\ b] \qquad (80)$$

$\bar{1}$: column vector containing all 1's.
Δh^* : vector of 60nm elevations corresponding to Δg^* , centered to the area-weighted average of 60nm elevations inside the 300nm block.
Δg_0 : a constant shift of the 60nm anomaly values inside the 300nm block
b : correlation slope between 60nm anomalies and elevations inside the 300nm block
n : noise part of observations

Applying equation (2), the parameters Δg_0 and b can be computed from:

$$X = (A^T(C_{\Delta g_s^* \Delta g_s^*} + C_{nn})^{-1} A)^{-1} A^T (C_{\Delta g_s^* \Delta g_s^*} + C_{nn})^{-1} \Delta g^* \quad (81)$$

The error covariance of the estimated parameters can be computed by applying equation (3):

$$E_{XX} = (A^T(C_{\Delta g_s^* \Delta g_s^*} + C_{nn})^{-1} A)^{-1} \quad (82)$$

The variance of the predicted value of Δg_0 is the element of E_{XX} in the (1,1) position:

$$\sigma^2_{\Delta g_0} = E_{XX}(1,1) \ . \quad (83)$$

Similarly, the variance of the predicted value of b is:

$$\sigma_b^2 = E_{XX}(2,2) \ . \quad (84)$$

Now, the t-test can be applied to measure the significance of the estimated parameters Δg_0 and b. This procedure involves the assumption of normally distributed residuals, but as Uotila (1967) pointed out the t-test is rather insensitive to moderate deviations from such an assumption. Moreover, it will be shown in the next section that the t-test indeed works as a device that can be used in a prediction program for the purpose of automatically deciding whether or not to use the parameter b in a certain 300nm anomaly prediction.

The null hypotheses to be tested are:

$$H_{01} : \Delta g_0 = 0 \quad (85)$$

$$H_{02} : b = 0 \quad (86)$$

It is to be recalled that the null hypothesis in statistical testing is a statement that is assumed to be true unless proven to be false beyond any "reasonable doubt." The amount of doubt that remains after the rejection of the null hypothesis is the type I error: the type I error is the probability that the rejected null hypothesis is in fact true. The user of a particular statistical test decides on the size of the type I error that can be tolerated. The size of the type I error is normally kept very small, since it is normally dangerous to reject a null hypothesis that is in fact true.

In the case of the present report, it has already been shown that Method A, an improved version of current procedures, works satisfactorily over a great majority of 300nm blocks

of the world, and improvement is being sought only for rough blocks. Thus, in introducing improvements to Method A, it is necessary to disturb Method A as little as possible. Since Method A assumes $\Delta g_0 = 0$ and $b = 0$, therefore in order not to disturb Method A unnecessarily, the null hypotheses are chosen as they are in equations (85) and (86).

The results of applying equation (81) to compute Δg_0 and b for the 300nm test blocks over the Tonga Trench Area (Section 8) are shown in Table 16. The data set used was the altimeter/terrestrial subset (obtained by considering only those altimeter/terrestrial anomalies for which there was a corresponding known anomaly in the terrestrial data set; see Section 9), and the covariance function was the global covariance function given in Table 1. Also shown in Table 16 are the quantities $|\Delta g_0/\sigma_{\Delta g_0}|$ and $|b/\sigma_b|$, where $\sigma_{\Delta g_0}$ and σ_b were computed using equations (82), (83), and (84). Under the null hypothesis the quantities $|\Delta g_0/\sigma_{\Delta g_0}|$ and $|b/\sigma_b|$ are the quantities used in the t-test:

$$t_{\Delta g_0}(\underline{\alpha},m) = |\Delta g_0/\sigma_{\Delta g_0}| \qquad (87)$$

$$t_b(\underline{\alpha},m) = |b/\sigma_b| . \qquad (88)$$

where

$\underline{\alpha}$ = probability

m = degree of freedom

(see, for example, Mikhail (1976), p.477). The degree of freedom m was taken to be

$$m = \text{no. of known 60nm blocks} - 2 , \qquad (89)$$

since there were two parameters being determined.

Given $t_{\Delta g_0}(\underline{\alpha},m)$ and the value of m, the probility $\underline{\alpha}$ can be obtained from a t-table. The quantity $\underline{\alpha}$ is the type I error if the null hypotehsis $H_{01} : \Delta g_0 = 0$ is rejected in favor of the predicted Δg_0. Similarly, given the value of $t_b(\underline{\alpha},m)$ and the degree of freedom, the value of $\underline{\alpha}$ obtained from a t-table is the type I error if the null hypothesis $H_{02} : b=0$ is rejected in favor of the predicted value of b. The type I errors associated with the Δg_0 and b in columns 3 and 4 of Table 16 are shown in columns 7 and 8.

As seen in column 7, the type I error associated with rejecting the null hypothesis $\Delta g_0=0$ in favor of the predicted Δg_0 in column 3 are all large. In other words, there is no reason to reject the null hypotehsis, namely $\Delta g_0 = 0$. Indeed, there is no need to model a shift Δg_0: the approach being taken to improve predictions over rough areas is to smooth out the local anomaly field and the use

Table 16

Testing for the Significance of b and Δg_0
in $\Delta g = \Delta g_0 + b\Delta h + s + n$
(Least Squares Collocation Solution for b and Δg_0 ;
t-test to test Significance;
Altimeter/Terrestrial subset used.)

No.of Known 60nm Blocks	Block	Δg_0 (mgal)	b (mgal/m)	$\lvert \Delta g_0 / \sigma_{\Delta g_0} \rvert$	$\lvert b / \sigma_b \rvert$	t-test $\alpha_{\Delta g_0}$	t-test α_b
16	1005	8.3	0.02070	0.514	2.314	>25%	1%
16	1006	6.3	0.00749	0.394	0.967	>25%	20%
22	1007	2.2	0.02013	0.143	3.675	>>25%	.05%
16	1008	-2.5	0.01985	0.155	1.985	>>25%	2.5%
23	1075	22.4	0.00664	1.416	1.212	10%	10%
13	1076*	8.5	0.03586	0.505	8.019	>25%	<<.05%
20	1077	3.2	0.04676	0.201	2.225	>>25%	20%
13	1078	-3.7	0.01303	0.221	0.608	>>25%	25%
11	1142	17.9	0.03805	1.051	3.337	15%	.5%
3	1143	21.4	0.00675	0.680	0.216	>>25%	>>25%
22	1144*	10.3	0.04093	0.654	12.943	25%	<<.05%
8	1145	8.0	-0.00415	0.461	0.084	> 25%	>>25%
3	1208	8.2	0.00642	0.236	0.252	>>25%	>>25%
14	1209*	15.7	0.03179	0.970	10.053	20%	<<.05%
10	1210	11.3	-0.04796	0.659	0.396	25%	>25%
0	1211	#	#	#	#		#
2	1270	-3.5	0.02000	0.031	0.396	>>25%	>>25%
12	1271*	32.1	0.05083	1.835	16.074	5%	<<.05%
5	1272	41.2	0.10485	1.833	6.054	5%	.5%
7	1273	-0.1	-0.00702	0.005	0.136	>>25%	>>25%
19	1329	23.5	0.00385	1.458	0.460	10%	>25%
21	1330	2.0	0.00703	0.127	1.572	>>25%	5%
0	1331	#	#	#	#	#	#
8	1332	5.7	-0.03408	0.314	1.130	>25%	15%

of a Δg_0 will not contribute to such smoothing; in fact the use of Δg_0 burdens the solution for the parameter b because of the reduced degree of freedom.

Column 8 of Table 16 shows that the type I errors associated with accepting the predicted b-values for very rough blocks (marked with asterisks) are very much smaller than the type I errors associated with accepting the predicted b-values for the other blocks. This suggests the possibility of using the t-test to automatically point to 300nm blocks where the parameter b needs to be modeled during predictions. For example, if the maximum type I error that can be tolerated is set to 0.05%, then only the b-values for very rough blocks will be found significant; for the smoother blocks, the b-value will continue to be taken as zero, since the null hypothesis H_{02} : b=0 cannot be rejected for those blocks.

To test the effect of not modeling Δg_0 , estimations were repeated, this time using:

$$A = \Delta h^* \quad \text{and} \quad X = b \tag{90}$$

in equations (79), (81), and (82). In this case, $\sigma_b^2 = E_{XX}$. The computed value of b and the t-test ratio $|b/\sigma_b|$ are shown in Table 17. Knowing $t_b(\underline{\alpha},m)=|b/\Delta_b|$ and the degree of freedom m , the size of type I error $\underline{\alpha}$ can be looked up from the t-table; $\underline{\alpha}$-values are shown in the last column of Table 17.

The b-values from Table 17 are very similar to the b-values from Table 16, except for those blocks with very few known 60nm blocks. The conclusions about which b-values are significant are unchanged in going from Table 16 to Table 17.

In conclusions, only the parameter b should be modeled to improve predictions over rough areas; the shift Δg_0 should continue to be modeled as $\Delta g_0=0$. During the actual prediction, the estimated b-value should be used only when the type I error committed by using this b-value instead of b=0 is less than some very small tolerance. The next section will indicate the danger of using a b-value that is not highly significant, and will suggest a significance level for use in a production type of work.

16.2 Recommended Significance Level

For convenience, the equations for 300nm anomaly predictions using Least Squares Collocation with the systematic parameter b are summarized here. From equation (73), the observation vector is modeled as:

$$\Delta g^* = b\Delta h^* + \Delta g_s^* + n \ . \tag{91}$$

Table 17

Testing for the Significance of b in $\Delta g = b\Delta h+s+n$;
Least Squares Collocation to get b , t-test to test significance;
Altimeter/Terrestrial Subset from Section 9 used.

Block	No.of Known 60nm Blocks	slope b mgal/m	$\lvert b/\sigma_b \rvert$	t-test α
1005	16	0.02049	2.291	2.5%
1006	16	0.00747	0.964	15%
1007	22	0.02012	3.673	0.1%
1008	16	0.01968	1.968	2.5%
1075	23	0.00603	1.101	15%
1076*	13	0.03557	11.248	<<0.05%
1077	20	0.04673	2.254	2.5%
1078	13	0.01294	0.603	25%
1142	11	0.03995	3.647	0.4%
1143	3	0.02255	1.075	25%
1144*	22	0.04100	12.965	<<0.05%
1145	8	-0.00400	0.081	>>25%
1208	3	0.01119	0.722	>25%
1209*	14	0.03158	9.986	<<0.05%
1210	10	-0.04143	0.343	>25%
1211	0	#	#	#
1270	2	0.01847	1.847	>>25%
1271*	12	0.04938	15.615	<<0.05%
1272	5	0.08960	5.908	0.5%
1273	7	-0.00701	0.136	>>25%
1329	19	0.00332	0.397	>25%
1330	21	0.00704	1.574	7.5%
1331	0	#	#	#
1332	8	-0.03219	1.085	20%

#No October 1979 terrestrial data exist for these blocks

*blocks with very significant b-values; very rough blocks

Applying equation (2), the parameter b can be estimated from (see also equation (81)):

$$b = (\Delta h^{*T} (C_{\Delta g^* \Delta g^*} + C_{nn})^{-1} \Delta h^*)^{-1} \Delta h^* (C_{\Delta g_S^* \Delta g_S^*} + C_{nn})^{-1} \Delta g^* \tag{92}$$

Applying equation (3), the variance of the estimated parameter is (see also equation (82)):

$$\sigma_b^2 = (\Delta h^{*T} (C_{\Delta g_S^* \Delta g_S^*} + C_{nn})^{-1} \Delta h^*)^{-1} . \tag{93}$$

The signals at computation points can be solved using equation (73):

$$\Delta g_S = C_{\Delta g_S \Delta g_S^*} (C_{\Delta g_S^* \Delta g_S^*} + C_{nn})^{-1} (\Delta g^* - b \Delta h^*) . \tag{94}$$

The vector of 25 predicted 60nm anomalies is given by equation (72):

$$\Delta g = b \Delta h + \Delta g_S . \tag{95}$$

Finally, the 300nm anomaly can be computed using equation (78):

$$\Delta \bar{g} = L_{\Delta \bar{g} \Delta g} \Delta g_S . \tag{96}$$

The variance of the predicted 300nm anomaly can be derived as follows:

First, applying equation (7) and (8), the error covariance of the 25 predicted 60nm anomalies is:

$$E_{\Delta g \Delta g} = C_{\Delta g_S \Delta g_S} - C_{\Delta g_S \Delta g_S^*} (C_{\Delta g_S^* \Delta g_S^*} + C_{nn})^{-1} C_{\Delta g_S \Delta g_S^*}^T + (H \Delta h^* - \Delta h) \sigma_b^2 (\Delta h^{*T} H^T - \Delta h^T) , \tag{97}$$

where

$$H = C_{\Delta g_S \Delta g_S^*} (C_{\Delta g_S^* \Delta g_S^*} + C_{nn})^{-1} . \tag{98}$$

Now apply equation (50):

$$E_{\Delta \bar{g} \Delta \bar{g}} = L_{\Delta \bar{g} \Delta g} E_{\Delta g \Delta g} L_{\Delta \bar{g} \Delta g}^T . \tag{99}$$

The quantity $E_{\Delta \bar{g} \Delta \bar{g}}$ is the same as $m_{\Delta g}^2$, the variance of the predicted 300nm anomaly. Substituting equation (97) into (99) and freely employing propagation of covariance matrices result in:

$$m_{\bar{\Delta g}}^2 = C_{\bar{\Delta g}\bar{\Delta g}} - C_{\bar{\Delta g}\Delta g_s^*}(C_{\Delta g_s^*\Delta g_s^*} + C_{nn})^{-1} C_{\bar{\Delta g}\Delta g_s^*}^T + \\ + \bar{H}\, \Delta h^*\, \sigma_b^2\, \Delta h^{*T}\, \bar{H}^T \qquad (100)$$

where

$$\bar{H} = C_{\bar{\Delta g}\Delta g_s^*}(C_{\Delta g_s^*\Delta g_s^*} + C_{nn})^{-1} \ . \qquad (101)$$

The linear transformation expressed by equation (96), together with the relations $L_{\bar{\Delta g}\Delta g} = L$ and $L\Delta h = 0$ from section 13 have been used in obtaining equations (100) and (101). Equation (100) allows for the propagation of the error of parameter estimation into the prediction results, through the presence of the third term on its right-hand side.

A 300nm anomaly prediction procedure which will be called Method D is defined as follows: for each 300nm block, the following steps are done:

1. First compute b and σ_b using equations (92) and (93).
2. Form the ratio:

   $$t(\alpha,m) = \frac{b}{\sigma_b} \ .$$

3. Compute the degree of freedom:

   m = number of known 60nm blocks - 1 .

4. Given m and a pre-selected value $\underline{\alpha}$ (significance level, e.g., 0.005) look up the critical t-test variable $t_0(\underline{\alpha},m)$ from the t-table.
5. If $t(\alpha,m) < t_0(\underline{\alpha},m)$ set $b = 0$ and $\sigma_b = 0$; otherwise, ignore this step.
6. Predict the 300nm anomaly using equations (94) and (96).
7. Compute the variance of the predicted 300nm anomaly using equations (100) and (101).

The presence of step 5 in Method D in effect causes Method D to reduce to Method A when the computed parameter b is not found to be significant at the selected significance level $\underline{\alpha}$. It is important to choose a proper value for $\underline{\alpha}$, in order to ensure that the already satisfactory performance of Method A over certain blocks will not be unnecessarily disturbed. The next two sets of predictions will point out a proper $\underline{\alpha}$ to use.

First, Method D was used to predict 300nm anomalies for the Tonga Trench area (Section 8) using a significance level of $\underline{\alpha} = 0.005$. The data set used was the altimeter/terrestrial subset from Section 9, and the covariance function was the global function in Table 1. Prediction results are shown in Table 18.

Table 18

Comparison of Prediction Results from Method D (i.e., Least Squares Colocation with the b-parameter Tested by t-test at 0.5% Significance Level) and from Method A (i.e., Least Squares Collocation Without Systematic Parameter)

Block	'True' Anom(mgal) Alt/Ter Subset	Anom/$m_{\bar{\Delta g}}$ (mgal) Method A Alt/Ter Subset	Anom/$m_{\bar{\Delta g}}$ (mgal) Method D Alt/Ter Subset	Anom Difference Method D- Method A	Slope b (mgal/m)
1005	11.1	8.7/3.5	8.7/3.5	0.0	0.0
1006	9.2	6.5/3.2	6.5/3.2	0.0	0.0
1007	2.4	0.1/2.0	0.0/2.0	-0.1	0.00142
1008	-2.9	-2.3/3.1	-2.3/3.1	0.0	0.0
1075	19.4	19.0/1.6	19.0/1.6	0.0	0.0
1076*	21.7	-4.1/5.5	9.2/5.7	13.3	0.03557
1077	5.3	7.0/2.5	7.0/2.5	0.0	0.0
1078	-4.3	-4.0/3.9	-4.0/3.9	0.0	0.0
1142	23.4	21.3/5.4	12.6/6.0	-8.7	0.03995
1143	21.6	13.3/11.0	13.3/11.0	0.0	0.0
1144*	10.3	6.0/2.0	9.9/2.1	3.9	0.04100
1145	4.1	6.0/6.1	6.0/6.1	0.0	0.0
1208	16.5	8.2/11.3	8.2/11.3	0.0	0.0
1209*	16.0	-11.9/3.7	3.6/4.0	15.5	0.3158
1210	17.9	10.0/6.3	10.0/6.3	0.0	0.0
1211	-0.5	#	#	#	#
1270	22.2	19.0/11.8	19.0/11.8	0.0	0.0
1271*	17.0	7.3/5.7	22.6/5.8	15.3	0.04938
1272*	13.4	-2.7/9.7	23.0/10.7	25.7	0.08960
1273	0.7	-0.2/8.0	-0.2/8.0	0.0	0.0
1329	27.1	27.9/2.7	27.9/2.7	0.0	0.0
1330*	2.4	-4.3/2.1	-4.3/2.1	0.0	0.0
1331	7.7	#	#	#	#
1332	6.2	-0.2/8.1	-0.2/8.1	0.0	0.0

#No October 1979 terrestrial data exists for these blocks

*Rough and very rough blocks.

For comparison, "true" values from Table 5 and the prediction results from Method A are also shown in Table 18. It is seen that over rough areas (marked with asterisk), Method D took effect, yielding predicted values that are much closer to "true" values than the predicted values from Method A. Over the other blocks, it is desirable that Method D reduce to Method A since Method A already performs satisfactorily over those areas. Block 1142 points up the danger of unnecessarily changing over from Method A to Method D: Method A already had a good prediction for block 1142, and a switch over to Method D gave a worse prediction.

To avoid an unnecessary switch over from Method A to Method D, a smaller value of the significance level was used: $\underline{\alpha} = 0.0005$. The application of Method D was repeated, and the new results are shown in Table 19. This time, Method D took effect only on those blocks where Method A yields unreasonable predictions. For comparison of Method A and Method D ($\underline{\alpha} = 0.0005$), the errors of the two methods (predicted value minus true value from Table 5) are the values given in Table 19. The errors should be viewed with proper regard to the corresponding standard errors of predictions. At this point of the investigations, the most improved prediction procedure, which is Method D, seems to be performing very well.

Table 19

Comparison of Prediction Results from Method D
(i.e., Least Squares Collocation with
the b-parameter tested by t-test
at 0.05% significance level)
and from Method A
(i.e., Least Squares Collocation
without systematic parameter).

Block	Error/$m_{\Delta\bar{g}}$ (mgal) Method A alt/ter subset	Error/$m_{\Delta\bar{g}}$ (mgal) Method D alt/ter subset	No. of known 60nm blocks, N	Slope b (mgal/m)
1005	-2.4/3.5	-2.4/3.5	16	0.0
1006	-2.7/3.2	-2.7/3.2	16	0.0
1007	-2.3/2.0	-2.3/2.0	22	0.0
1008	0.6/3.1	0.6/3.1	16	0.0
1075	-0.4/1.6	-0.4/1.6	23	0.0
1076*	-25.8/5.5	-12.5/5.7	13	0.03557
1077	1.7/2.5	1.7/2.5	20	0.0
1078	0.3/3.9	0.3/3.9	13	0.0
1142	-2.1/5.4	-2.1/5.4	11	0.0
1143	-8.3/11.0	-8.3/11.0	3	0.0
1144*	-4.3/2.0	-0.4/2.1	22	0.04100
1145	1.9/6.1	1.9/6.1	8	0.0
1208	-8.3/11.3	-8.3/11.3	3	0.0
1209*	-27.9/3.7	-12.4/4.0	14	0.03158
1210	-7.9/6.3	-7.9/6.3	10	0.0
1211	#	#	0	#
1270	-3.2/11.8	-3.2/11.8	2	0.0
1271*	-9.7/5.7	5.6/5.8	12	0.04938
1272*	-16.1/9.7	-16.1/9.7	5	0.0
1273	-0.9/8.0	-0.9/8.0	7	0.0
1329	0.8/2.7	0.8/2.7	19	0.0
1330*	-6.7/2.1	-6.7/2.1	21	0.0
1331	#	#	0	#
1332	-6.4/8.1	-6.4/8.1	8	0.0

#No October 1979 terrestrial data exist for these blocks.

*rough and very rough blocks.

17. Comparison of Methods of Trend Removal

Table 20 is a compilation of important prediction results from Sections 14, 15 and 16. The blocks shown are typical blocks over which predictions with the parameter b should be applied. The different sets of prediction were all derived from the same altimeter/terrestrial subset defined in Section 9. For easier inter-comparison the values shown are errors of predictions (error=predicted value - "true" value from Section 9), along with the standard errors of predictions, $m_{\Delta\bar{g}}$.

The values of $m_{\Delta\bar{g}}$ from Method B and Method C are the same. These standard errors were computed using the same equation used by Method A (Section 10), and consequently, there was no propagation made of any error in the b-value into the value of $m_{\Delta\bar{g}}$. In contrast, the value of $m_{\Delta\bar{g}}$ from Method D includes the propagated σ_b , the standard error of Least Squares Collocation estimation of b . It is seen that the effect of σ_b on $m_{\Delta\bar{g}}$ is very small for the typical blocks shown.

From an examination of the different sets of errors predictions, it is seen that the prediction is sensitive to the b-value used. It is therefore important to have a well-defined set of procedures for computing the b-value that will be used in the prediction. The recommended procedure here is Method D with a significance level of 0.05% To increase the reliability of b-values, it is proposed not to compute b-values for blocks with fewer than 4 known 60nm anomalies, the number 4 being a somewhat arbitrary number that we recommend based on experience with further numerical tests. In those blocks with at least 4 known 60nm anomalies, the computed b-value should be tested for significance only when the b-value falls within reasonable limits; it is proposed to use $|b| < 0.2$mgal/m , since out of a total of 245 significant b-values that we have found in a global analysis of the OSU July 1981 terrestrial data set (Rapp, private communication) the b-values are mostly on the order of 0.04mgal/m , with very few b-values reaching 0.08 to 0.09mgal/m , and only one value reaching the maximum value 0.1mgal/m . For those blocks where the parameter b will not be used in the prediction, the following should be set: $b = 0$ and $\sigma_b = 0$, in order that the equations of Method D reduce to the equations of Method A. The main advantage of the procedures just described is that they can be used in a production type of work in order to reliably decide on which of Method A and Method B should be used for a particular situation.

The b-values from Least Squares were obtained by straight line fitting to conceptual plots of the 25 known 60nm altimeter/terrestrial anomalies vs. elevations inside the 300nm blocks. Since the Least Squares method is a very common method

Table 20

Error of Predicted Anomaly and Standard Error of Prediction for Various Methods of Establishing the b-value. (Error and $m_{\bar{\Delta g}}$ in mgals; b in mgal/m .)

Block	N/CHAR	b from Least Squares (Method B) Error	$m_{\bar{\Delta g}}$	b	Empirical b (Method C) b = 0.06 Error	$m_{\bar{\Delta g}}$	b = 0.04 Error	$m_{\bar{\Delta g}}$	b from Least Squares Collocation (Method D) Error	$m_{\bar{\Delta g}}$	b
1076	13/VRY RGH	-13.0	5.5	0.03406	-3.3	5.5	-9.5	5.5	-12.5	5.7	0.03557
1144	22/VRY RGH	-1.2	2.0	0.03328	1.4	2.0	-0.3	2.0	-0.4	2.1	0.04100
1209	14/VRY RGH	-16.2	3.7	0.02376	1.6	3.7	-7.7	3.7	-12.4	4.0	0.03158
1271	12/VRY RGH	3.6	5.7	0.04299	8.9	5.7	4.2	5.7	5.6	5.8	0.04938

used for line fitting, the Least Squares b-value and the corresponding predictions serve as reference values with which to compare the values from Method C and Method D. It is seen that Method D and Method B produce very similar b-values and prediction results. Method C and Method B have very different prediction results because of the difference in b-balues used; the b-value of 0.06mgal/m in Method C was empirically derived from gravity traverses across the Tonga Trench area, and have no direct connection with the altimeter/terrestrial data values inside the individual 300nm blocks.

It is seen that the use of the empirical b-value 0.06mgal/m which applies over the Tonga Trench area produced very small errors of prediction. The predictions using the b-value of 0.04mgal/m were included to further illustrate the sensitivity of predictions to the b-value (compare the b-values and predictions from columns 3 and 4, for example). An empirical b-value, if available for the characteristic topography of the 300nm block, can be used over rough 300nm blocks where no reasonable and statistically significant b-value can be found by Method D. The disadvantage of the empirical method is that the b-value is not unique, since there are no consolidated models that can uniquely define the gravity gradient given the character of the topography.

18. Prediction Using Both Known Anomalies and Elevations As Observed Quantities

In the previous sections, elevation data were used, considering them as error-free quantities. The b-parameter was computed under this assumption, and so 60nm elevations enter only in the design matrix A while the 60nm anomalies are the observed quantities (see Section 16). An alternative is to consider both 60nm anomalies and elevations as observed quantities, with their associated standard errors known from the data set being used. Anomaly predictions can then be done using standard Least Squares Collocation formulas. In this case, aside from the usual autocovariance matrix of 60nm anomalies, there will be a need for an autocovariance matrix of the signal part of 60nm elevations and also a crosscovariance matrix between the signal parts of 60nm anomalies and elevations.

18.1 Prediction Equations

Let

Δg^* : N X 1 vector of observed 60nm anomalies inside the 300nm block

Δh : 25 X 1 vector of observed 60nm elevations inside the 300nm block, centered to some mean elevation.

The observation vectors Δh and Δg^* can be modeled as:

$$\Delta g^* = \Delta g^*_s + n_{\Delta g} \tag{102}$$

$$\Delta h = \Delta h_s + n_{\Delta h} \ , \tag{103}$$

which follow the form of equation (9), with:

$$x = \begin{bmatrix} \Delta g^* \\ \Delta h \end{bmatrix} \ ; \ s' = \begin{bmatrix} \Delta g^*_s \\ \Delta h_s \end{bmatrix} \ ; \ n = \begin{bmatrix} n_{\Delta g} \\ n_{\Delta h} \end{bmatrix} . \tag{104}$$

Equations (102) and (103) are in accordance with the model of Least Squares Collocation without systematic parameters. The vector of 25 predicted 60nm anomalies can be modeled as:

$$\Delta g = \Delta g_s \ , \tag{105}$$

where Δg_s is obtained by applying equation (10):

$$\Delta g = \Delta g_s = C_{\Delta g_s s'} \ (C_{s's'} + C_{nn})^{-1} \ x \ . \tag{106}$$

Substituting equations (104) into equation (106):

$$\Delta g = \underset{25 \times (N+25)}{[C_{\Delta g_s \Delta g^*_s}; C_{\Delta g_s \Delta h_s}]} \ \underset{(N+25) \times (N+25)}{\begin{bmatrix} C_{\Delta g^*_s \Delta g^*_s} + C_{n_{\Delta g} n_{\Delta g}}; C_{\Delta g^*_s \Delta h_s} \\ C^T_{\Delta g^*_s \Delta h_s}; C_{\Delta h_s \Delta h_s} + C_{n_{\Delta h} n_{\Delta h}} \end{bmatrix}^{-1}} \ \underset{(N+25) \times 1}{\begin{bmatrix} \Delta g^* \\ \Delta h \end{bmatrix}} \tag{107}$$

The above equation, which predicts the 25 60nm anomalies inside the 300nm block using the models expressed by equations (102) and (103), will be referred to as Method E.

The 300nm anomaly can now be computed using equations (33) and (34):

$$\Delta\bar{g} = L_{\Delta\bar{g}\Delta g} \ \Delta g \ . \tag{108}$$

The variance of the predicted $\Delta\bar{g}$ can be computed from the error covariance of Δg (see equation (49)):

$$m^2_{\Delta\bar{g}} = L_{\Delta\bar{g}\Delta g} \ E_{\Delta g \Delta g} \ L^T_{\Delta\bar{g}\Delta g} \ . \tag{109}$$

Applying equation (11) to express $E_{\Delta g \Delta g}$, and employing propagation of covariance matrices, equation (109) becomes:

$$m^2_{\bar{\Delta g}} = C_{\bar{\Delta g}\bar{\Delta g}} - [C_{\bar{\Delta g}\Delta g^*_S} \; C_{\bar{\Delta g}\Delta h_S}] \begin{bmatrix} C_{\Delta g^*_S \Delta g^*_S} + C_{n_{\Delta g} n_{\Delta g}} ; & C_{\Delta g^*_S \Delta h_S} \\ C_{\Delta g^*_S \Delta h_S}^T ; & C_{\Delta h_S \Delta h_S} + C_{n_{\Delta h} n_{\Delta h}} \end{bmatrix}^{-1} \begin{bmatrix} C_{\bar{\Delta g}\Delta g^*_S}^T \\ C_{\bar{\Delta g}\Delta h_S}^T \end{bmatrix} \quad (110)$$

18.2 Covariance and Crosscovariance Functions and Matrices

The computation of a numerical 60nm anomaly covariance function $cov(\Delta g,\Delta g)$ is described in Section 5.1. The computation of a numerical 60nm elevation covariance function $cov(\Delta h,\Delta h)$ and the computation of a numerical 60nm anomaly-elevation crosscovariance function $cov(\Delta g,\Delta h)$ follow similar procedures as described in Section 5.1, and are explicitly given in Section 12.2.2. An example of $cov(\Delta g,\Delta g)$ is given in Table 1, while examples for $cov(\Delta h,\Delta h)$ and $cov(\Delta g,\Delta h)$ are given in Table 11. Following exactly the same procedures described in Section 5.2 for the generation of the basic anomaly covariance matrix $C_{\Delta g \Delta g}$ from $cov(\Delta g,\Delta g)$, basic covariance matrices $C_{\Delta h,\Delta h}$ and $C_{\Delta g \Delta h}$ may also be generated from $cov(\Delta h,\Delta h)$ and $cov(\Delta g,\Delta h)$. Then, following Section 5.3, other needed covariance matrices in equations (107) and (110) can be derived by covariance propagation from the basic covariance matrices. For example, the $C_{\bar{\Delta g}\Delta h_S}$ appearing in equation (110) can be computed by area-weighted averaging columns of $C_{\Delta g \Delta h}$.

18.3 Prediction Results

Equations (107), (108), and (110) were used to predict 300nm anomalies for the 300nm test blocks. The method is called Method E. The first set of predictions are given in Table 21. The data set used was the altimeter/terrestrial subset. The covariance and crosscovariance functions used were those given in Tables 1 and 11. (The 60nm elevations in the test area are all negative, hence it is reasonable to use $cov(\Delta g,\Delta h)$ and $cov(\Delta h,\Delta h)$ from Table 11). In accordance with Table 11, the given 60nm anomalies were centered to the mean value for negative elevations: -4120m.

Table 21 shows the difference between Method E and Method A. The values for Method A were copied from Table 8, column 4. It is seen that Method E yields practically the same predicted anomalies and standard errors of prediction as Method A. This

Table 21

Comparison of Prediction Results from the Use of Both Known Anomalies and Elevations as Observed Quantities (Method E, equation (102) and (105)) Against Prediction Results from the Use of only the Known Anomalies (Method A, Section 10). $cov(\Delta g,\Delta g)$ from Table 1; $cov(\Delta g,\Delta h)$ and $cov(\Delta h,\Delta h)$ from Table 11; altimeter/terrestrial subset (Section 9) Used. (units: mgals).

Block	"True" Anom Alt/Ter Set	Anom/$m_{\bar{\Delta g}}$ Method A	Anom/$m_{\bar{\Delta g}}$ Method E	Difference Method E- Method A
1005	11.1	8.7/3.5	8.8/3.4	0.1
1006	9.2	6.5/3.2	6.8/3.1	0.3
1007	2.4	0.1/2.0	0.1/2.0	0.0
1008	-2.9	-2.3/3.1	-2.3/3.1	0.0
1075	19.4	19.0/1.6	19.0/1.6	0.0
1076*	21.7	-4.1/5.5	-2.1/5.4	2.0
1077	5.3	7.0/2.5	6.9/2.5	-0.1
1078	-4.3	-4.0/3.9	-4.2/3.8	-0.2
1142	23.4	21.3/5.4	20.6/5.3	-0.7
1143	21.6	13.3/11.0	13.8/10.8	0.5
1144*	10.3	6.0/2.0	6.2/2.0	0.2
1145	4.1	6.0/6.1	5.4/5.9	-0.6
1208	16.5	8.2/11.3	6.0/11.1	-2.2
1209*	16.0	-11.9/3.7	-10.4/3.6	1.5
1210	17.9	10.0/6.3	9.5/6.2	-0.5
1211	-0.5	#	0.0/15.7	#
1270	22.2	19.0/11.8	17.1/11.5	-1.9
1271*	17.0	7.3/5.7	8.6/5.6	1.3
1272*	13.4	-2.7/9.7	-3.2/9.5	-0.5
1273	0.7	-0.2/8.0	-0.9/7.8	-0.7
1329	27.1	27.9/2.7	28.2/2.7	0.3
1330*	2.4	-4.3/2.1	-4.2/2.1	0.1
1331	7.7	#	-0.1/15.7	#
1332	6.2	-0.2/8.1	-1.2/7.9	-1.0

#No October 1979 terrestrial anomaly data exist for these blocks.

*rough and very rough blocks.

is understandable because as shown in Table 11A, the functions cov(Δg,Δh) and cov(Δh,Δh) used in the predictions imply a very small anomaly-elevation correlation of 0.026mgal/m.

A second set of predictions was obtained by repeating the first predictions, this time using the terrestrial data set. The results are shown in Table 22. For comparison, the results for Method A applied to the terrestrial data set are also shown. Again, there is essentially no difference between the results of Method A and Method E.

To test the effect of using a drastically different set of covariance functions, cov(Δg,Δh) and cov(Δh,Δh) were first computed by equations (66) and (67) using Δg centered to zero (i.e., Δg used as they are) and Δh centered to the mean 60nm elevation of individual 300nm blocks. The computed functions are shown in Table 23. Note the big difference between these functions and the corresponding functions in Table 11.

A third set of predictions was done, differing from the first set only in that the covariance functions from Table 23 were used instead of those from Table 11. The 60nm elevations were centered to the mean 60nm elevation inside the 300nm block, to obtain the Δh which was used as part of the data vector. Prediction results are shown in Table 24. Again, the results are to be compared with corresponding values from Method A. It is seen from Table 24 that, again, there is no substantial difference between Method A and Method E, even with the use of very different covariance functions from those used in Table 21.

The conclusion from this section is that Method E, which uses both 60nm anomalies and elevations as observed quantities (see equation (102), does not seem to be able to extract a significant amount of information about the 60nm anomaly from the known values of 60nm elevations. The effect is that equations (107) and (110) of Method E produce essentially the same results as equation (54) and (53) of Method A.

Table 22

Comparison of Prediction Results from the Use of Both known Anomalies and Elevations as Observed Quantities (Method E, equations (107) and (110)) Against Prediction Results from the Use of Only the Known Anomalies (Method A, Section 10). $cov(\Delta g,\Delta g)$ from Table 1; $cov(\Delta g,\Delta h)$ and $cov(\Delta h,\Delta h)$ from Table 11; terrestrial data set (Section 8) used. (units: mgals).

Block	anom/$m_{\Delta g}$ Method A Oct 79 Terr Set	Anom/$m_{\Delta g}$ Method E Oct 79 Terr Set	Difference Method E- Method A
1005	4.8/5.5	5.3/5.4	0.5
1006	12.3/5.3	12.7/5.3	0.4
1007	8.3/3.8	8.1/3.8	-0.2
1008	5.5/5.3	5.3/5.3	-0.2
1075	18.6/3.7	18.9/3.7	0.3
1076*	11.8/7.5	12.2/7.4	0.4
1077	3.7/4.5	3.5/4.5	-0.2
1078	-4.6/5.6	-5.0/5.6	-0.4
1142	32.4/7.4	31.8/7.3	-0.6
1143	13.5/12.4	14.4/12.2	0.9
1144*	1.6/4.5	2.0/4.5	0.4
1145	-14.1/8.5	-14.9/8.4	-0.8
1208	0.5/12.8	-0.9/12.6	-1.4
1209*	-6.6/7.8	-5.6/7.7	1.0
1210	-10.1/8.0	-10.8/7.9	-0.7
1211	#	-3.1/15.7	#
1270	23.5/13.4	22.7/13.1	-0.8
1271*	0.4/7.5	2.2/7.4	1.8
1272*	-13.5/11.4	-14.8/11.2	-1.3
1273	-15.4/9.0	-16.4/8.8	-1.0
1329	27.4/5.2	29.1/5.0	1.7
1330*	-15.1/4.8	-15.2/4.7	-0.1
1331	#	-3.1/15.7	#
1332	-20.9/10.7	-22.5/10.5	-1.6

#No October 1979 terrestrial anomaly data exist for these blocks

*rough and very rough blocks.

Table 23

cov(Δg,Δh) and cov(Δh,Δh). h centered to 300nm block. Δg centered to zero.

ψ Deg.	Rad.	cov(Δh,Δh) meter**2	No. of product pairs used
0.0000	0.0000	535581	41350
0.9795	0.0171	346666	55716
1.6192	0.0283	174593	104078
2.5080	0.0438	-25945	143208
3.4656	0.0605	-185872	113752
4.3763	0.0764	-310360	69580
5.3610	0.0936	-421861	9568
5.2456	0.1090	-474506	298

ψ Deg.	Rad.	cov(Δg,Δh) mgal-meter	No. of product pairs used
0.0000	0.0000	6714	37814
0.9795	0.0171	3596	101875
1.6204	0.0283	1499	189887
2.5084	0.0438	-596	261425
3.4662	0.0605	-1782	208486
4.3770	0.0764	-2424	127758
5.3625	0.0936	-3037	17865
6.2476	0.1090	-3842	614

Table 24

Comparison of Prediction Results from the Use of Both Known Anomalies and Elevations as Observed Quantities (Method E, equations (107) and (110)) Against Prediction Results from the Use of Only the Known Anomalies (Method A, Section 10). cov(Δg,Δg) from Table 1; cov(Δg,Δh) and cov(Δh,Δh) from Table 23; altimeter/terrestrial subset (Section 9) Used. (units: mgals).

Block	"True" Anom alt/ter set	Anom/$m_{\Delta g}$ Method A	Anom/$m_{\Delta g}$ Method E	Difference Method E-Method A
1005	11.1	8.7/3.5	8.6/3.3	-0.1
1006	9.2	6.5/3.2	6.9/3.0	0.4
1007	2.4	0.1/2.0	0.1/2.0	0.0
1008	-2.9	-2.3/3.1	-2.1/3.0	0.2
1075	19.4	19.0/1.6	19.0/1.6	0.0
1076*	21.7	-4.1/5.5	-0.5/5.1	3.6
1077	5.3	7.0/2.5	7.1/2.4	0.1
1078	-4.3	-4.0/3.9	-3.9/3.7	0.1
1142	23.4	21.3/5.4	19.8/5.0	-1.5
1143	21.6	13.3/11.0	11.9/10.2	-1.4
1144*	10.3	6.0/2.0	6.7/2.0	0.7
1145	4.1	6.0/6.1	6.2/5.7	0.2
1208	16.5	8.2/11.3	2.5/10.5	-5.7
1209*	16.0	-11.9/3.7	-8.6/3.5	3.3
1210	17.9	10.0/6.3	10.0/5.7	0.0
1211	-0.5	#	0.0/16.0	#
1270	22.2	19.0/11.8	11.2/11.1	-7.8
1271*	17.0	7.3/5.7	7.7/5.2	0.4
1272*	13.4	-2.7/9.7	-2.4/9.0	0.3
1273	0.7	-0.2/8.0	0.2/7.4	0.4
1329	27.1	27.9/2.7	28.0/2.7	0.1
1330*	2.4	-4.3/2.1	-4.5/2.1	-0.2
1331	7.7	#	0.0/16.0	#
1332	6.2	-0.2/8.1	-1.1/7.3	-0.9

#No October 1979 terrestrial anomaly data exist for these blocks.

*rough and very rough blocks.

19. Computer Implementation of Improved 300nm Anomaly Prediction Procedures

As stated in the Introduction, the computer program supplied by Kaula (1966), which have had additions to it introduced by Rapp (1972), is the current operational program being used for the global prediction of 300nm anomalies from known values of 1°x 1° mean free air anomalies inside the individual 300nm blocks. This program is called program F234. In order to implement the recommended improved procedures developed in this report, we have introduced modifications and additional coding to program F234. Call the improved program as program F234A.

Program F234A retains the procedures of F234 regarding the computation of a global numerical covariance function of 60nm anomalies. This function is computed from a preliminary analysis of the entire global data set being used (Section 5.1). The formation of the basic covariance matrix $C_{\Delta g \Delta g}$ (Section 5.2) is also retained. The difference is in the manner of propagation of $C_{\Delta g \Delta g}$ to obtain $C_{\Delta \bar{g} \Delta g}$ and $C_{\Delta \bar{g} \Delta \bar{g}}$ needed in the computation of the standard error of prediction: whereas F234 uses straight averaging, program F234A uses area-weighted averaging from the elements of $C_{\Delta g \Delta g}$ (Section 5.3). As such, F234A computes a new set of $C_{\Delta \bar{g} \Delta \bar{g}}$ and $C_{\Delta \bar{g} \Delta g}$ for each 300nm block encountered in order to account for the specific 60nm areas occuring in that 300nm block. This area-weighted averaging is a consequence of the assumption that the 300nm anomaly should be computed as the area-weighted average of the 25 predicted 60nm anomalies inside the 300nm block (see Section 5.3).

The prediction procedures implemented in F234A are those of Method D as summarized in Section 16.2. The prediction technique used is therefore that of Least Squares Collocation with the systematic parameter b, where b is the correlation slope between 60nm anomalies and their corresponding elevations inside the 300nm block. The parameter b is analyzed for each 300nm block to be predicted. In order to control the conceivable occurrence of an unreasonable b-value that can pass the t-test (although we have not found this to be a problem even in a global prediction that we have conducted) it was decided to compute the b-value for the block only if there are at least 4 known 60nm anomalies inside the block, and moreover, to consider only b-values that satisfy $|b| < 0.2$mgal/m . A considered b-value is tested for significance using the t-test at 0.05% level of significance. The critical values t_0 used for conducting the t-test at this significance level (Mikhail, 1976, p. 477) are input into the program through a DATA statement. The argument used to obtain the proper t_0 - value is the degree of freedom, which is taken to be the number of known 60nm anomalies minus one. For a 300nm block in which no reasonable and significant b-value is found by the described procedures, the b-value and its standard error are set to zero and the computations continued.

Program F234A reads 1°x 1° mean elevations as input data in addition to the usual 1°x 1° mean anomalies and their standard errors. These 1°x 1° elevations are formed into 60nm elevations just like the 1°x 1° anomalies and their standard errors are formed into 60nm anomalies and propagated standard errors (see Section 4 for the data structure used in the prediction). The 60nm elevations enter the computations for b and σ_b , and the subsequent prediction equations.

The original data vector Δg^* is reduced to the mean elevation of the 300nm block, as in $(\Delta g^* - b\Delta h^*)$, for use in the prediction. All the 25 60nm anomalies of the 300nm block are predicted using the reduced data vector (see equation (94)). The 300nm anomaly is taken as the area-weighted average (equation (96)) of the 25 predicted 60nm anomalies, using as weights the computed areas of the 60nm blocks. The predicted accuracy of the 300nm anomaly is computed using equations (100) and (101).

As the 300nm blocks of the world are processed one after another, a record is kept of 300nm blocks which cannot be predicted because they do not have any 1°x 1° anomaly data. These 300nm blocks are output at the end of all processing, in the format needed for direct input into the separate program of Rapp (Section 7) which handles the prediction of 300nm blocks containing no 1°x 1° anomaly data. It is proposed to retain Rapp's procedures for predicting 300nm blocks containing no 1°x 1° anomaly data, namely, the prediction of the unknown 300nm anomaly from the 10 closest 300nm anomalies which have been predicted beforehand (this time, these prior predictions can be done using the procedures of this report). The prediction from the 10 closest previously predicted 300nm anomalies involve much larger areas than a 300nm area that we have considered in this report, and therefore the use of the b-value (which applies to local areas like a 300nm block) has no direct applicability in this case.

20. Prediction of Two New Sets of 1654 300nm Anomalies

20.1 Generation of the Two 1654 Sets

In this section we will describe the different operational steps that were recently taken to predict two complete sets of 1654 300nm anomalies. The starting data set was the OSU terrestrial data set of December 1981, which contained 42,585 1°x 1° mean free air anomalies (see Figure A.1 of the Appendix) referred to the gravity formula of the Geodetic Reference System 1967. Out of the 42,585 anomalies, there were 6,413 (see Figure A.2 of the Appendix) which were coded as having been predicted by geophysical correlation techniques, and were therefore not based on actual gravity measurements. In accordance with Rapp (1972) these geophysical anomalies were given special consideration. That is, two sets of 1654 300nm anomalies were generated, one based on the original 42,585 1°x 1° anomaly data set, and the other based on the lesser 36,172 1°x 1° anomaly data set obtained after removing the 6,413 geophysically correlated anomalies from the original "42,585" data set.

As a first step, the most recent OSU 1°x 1° mean elevation data set was merged into the "42,585" data set. For the purposes of the new prediction program (program F234A of Section 19), 1°x 1° elevations were merged into the data set even in the case of those 1°x 1° squares which did not have the 1°x 1° anomaly known (in this case, the 1°x 1° anomaly was coded as 999 to denote it as being unknown). Since 1°x 1° elevations are fully known globally, there were a total of 64,800 1°x 1° mean elevations that were merged into the fundamental data set. The use of 1°x 1° mean elevation information is a feature of the improved procedures as implemented in program F234A.

The "42,585" data set was actually a data base that contained much more information about each 1°x 1° square than were needed in the predictions of this section; these extra information persisted in the merger data set of the last paragraph. The next step was therefore to pull out from the merger data set, only four pieces of needed information about each 1°x 1° square of the world:

1. the 1°x 1° mean elevation
2. the 1°x 1° mean anomaly (if unknown, the anomaly was coded as 999)
3. the standard deviation of the 1°x 1° elevation
4. the standard deviation of the 1°x 1° anomaly (for an unknown anomaly, the standard deviation was coded as 99).

In accordance with the housekeeping procedures of program F234A, each of the four sets of information given above was arranged

into 15°-latitude belts for input into F234A. Two separate input data sets (each arranged into 15°-latitude belts) were created for use in F234A. The first set (DEC81WGP) contained the complete 42,585 1°x 1° anomalies which included 6,413 geophysical anomalies, and the second set (DEC81NGP) contained the lesser 32,172 1°x 1° anomalies which excluded the 6,413 geophysical anomalies.

Two separate sets of predictions using F234A were done, corresponding to the two input data sets. The two numerical 60nm covariance functions that were generated at the start of each prediction set and were used in the predictions are given in Tables A.1 and A.2 of the Appendix.

For DEC81WGP (with geophysical anomalies), 300nm anomaly predictions using F234A yielded predicted mean anomalies for 1,542 300nm blocks. The remaining 112 300nm blocks which did not contain any 1°x 1° anomaly data could not be predicted by F234A. However, the standard sequence numbers (see Section 3), and the latitudes and longitudes of the centers of the 112 unknown blocks, were output by F234A in a format consistent for input into the follow-up prediction programs which would be used to complete the prediction of the 1654 set. Predictions using DEC81NGP (no geophysical anomalies) yielded mean anomalies for 1,484 300nm blocks, and the sequence numbers and latitudes and longitudes of centers of the remaining 170 unknown 300nm blocks.

The follow-up procedures used for completing each of the two sets of 1654 300nm anomalies were identical. Follow-up procedures were started by computing a numerical 300nm anomaly covariance function based on the partial set of predicted 300nm anomalies from program F234A. The method of generation of the covariances followed the global averaging procedures described in Section 5.1, this time using 300nm anomalies and areas instead of 60nm anomalies and areas. Using these global averaging procedures, covariances for ψ-values from 0° to 180° in ψ-steps of about 2° (= $\Delta\psi$ of Section 5.1) were generated. The covariances were then interpolated using the International Mathematical and Scientific Library (IMSL) routines IQHSCU and ICSEVU to form a regular table giving covariances for ψ-values from 0° to 180° in uniform ψ-steps of 0°.5 (see Table A.3 and Figure A.3 of the Appendix). During actual predictions for the unknown 300nm anomalies, covariances for other ψ-values not in the table were linearly interpolated from the values in the table. The ψ-values were referred to the centers of the 300nm blocks.

A program (program F342 of the OSU Department of Geodetic Science and Surveying) was used to predict the remaining unknown 300nm anomalies using the following as input:

1. table giving 300nm anomaly covariances for ψ-values from 0° to 180° in ψ-steps of 0°5

2. the predicted 300nm anomalies and related information (latitude and longitude of block center and accuracy of predicted 300nm anomaly) as output by program F234A.

3. the sequence numbers, and the center latitudes and longitudes of the unknown 300nm blocks.

The unknown 300nm anomalies were individually predicted from the 10 closest known 300nm anomalies, using Least Squares Collocation with the numerical 300nm covariance function (Rapp, 1977). Prediction results were output in a format identical with the output of F234A, and as a final step these prediction results were merged with the predicted 300nm anomalies from F234A, forming a complete set of 1654 predicted 300nm anomalies.

20.2 Comparison of 300nm Anomaly Sets

Performing the above described follow-up procedures for both DEC81WGP (with geophysical anomalies) and DEC81NGP (no geophysical anomalies) predictions, the results were two complete sets of 1654 300nm anomalies (the listing of the two sets are available upon request from The Ohio State University Department of Geodetic Science and Surveying). As part of operational procedures, comparisons were made involving these two 1654 sets and other previously existing 300nm anomaly sets. Table 25 gives the description and selected statistics of the considered sets.

Since the altimeter anomalies and the combination solution anomalies refer to the gravity formula of the Geodetic Reference System 1980, while the terrestrial anomalies refer to the gravity formula of the Geodetic Reference System 1967, the following transformation should be considered:

$$\Delta g_{1967} = \Delta g_{1980} + 0.83 + 0.08 \sin^2\phi \text{(mgals)}.$$

In addition, an atmospheric mass correction δg_A should be considered, so that the final altimeter or combination solution anomaly that should be compared with the corresponding terrestrial anomaly would be:

$$\Delta g' = \Delta g_{1980} + 0.83 + 0.08 \sin^2\phi - \delta g_A \text{(mgals)} .$$

In the last equation, the total correction to Δg_{1980} turns out to be small (not more than 0.04mgal for an altimeter anomaly and often less than 0.5mgal for a combination solution anomaly) for all values of the latitude ϕ , and this correction was neglected in subsequent comparisons.

Table 25

Description and Statistics of Various 300nm Anomaly Sets
(Statistics in mgals)

Designation Here	DEC81WGP*	DEC81NGP*	OCT79WGP*	NOV81ALT	DEC81COMB
Data Current as of	Dec. 1981	Dec. 1981	Oct. 1979	Nov. 1981	Dec. 1981
Anomaly Data Type	1°x 1° Terr. w/Geophys. Anom.	1°x 1° Terr. w/o Geophys. Anom.	1°x 1° Terr. w/Geophys. Anom.	300nm Seasat Altimeter Derived (Rapp,1982)	64,800 1°x 1° Values from Combination Solution (Rapp,1981)
Reference Gravity Formula	GRS67	GRS67	GRS67	GRS80	GRS80
Method of 300nm Anomaly Generation	Procedures of this Report	Procedures of this Report	Old Procedures (See Section 7)	Already 300nm Anomalies	Area-Weighted Averaging
Minimum Anomaly	-49.7	-56.9	-54.1	-55.2	-55.2
Maximum Anomaly	75.9	76.6	71.0	44.2	68.2
Root Mean Sq. Anom.	15.3	15.1	15.4	14.9	14.8
Min. Std. Deviation	0.2	0.2	0.2	0.4	0.9
Max. Std. Deviation	16.3	16.4	16.1	19.5	4.0
Root Mean Sq. Std. Dev.	6.5	7.6	6.7	2.5	3.6
No. of 300nm Anom.	1654	1654	1654	1179	1654

*(WGP means "with Geophysical", NGP "no geophysical" anomalies.)

Table 26 shows some comparisons that may indicate the effect of including or not including 1°x 1° geophysical anomalies in the generation of a 300nm anomaly set. There is an RMS difference of 3.9mgals between the set that includes geophysical anomalies (DEC81WGP) and the set that does not include geophysical anomalies (DEC81NGP), and this RMS difference is within the RMS standard deviation of the anomalies used in the comparison as given at the bottom of the table. A comparison of DEC81WGP and DEC81NGP with DEC81COMB, also given in Table 26, shows that the set with geophysical anomalies has a smaller RMS difference with the combination solution than does the set with no geophysical anomalies (this is expected since the Combination Solution included geophysical anomalies as data--see Rapp, 1981). Overall, Table 26 indicates that DEC81WGP and DEC81NGP are consistent with each other and with DEC81 COMB to within the RMS standard deviations of the anomalies compared, and that the DEC81WGP is nearer DEC81COMB than is DEC81NGP.

Table 27 shows other comparisons of interest between various 300nm anomaly sets. The December 1981 and the October 1979 terrestrial sets, which differ because of the incorporation of new 1°x 1° data and the use of modified prediction procedures in the December 1981 set, have an RMS difference of 2.9mgals which is well within the RMS standard deviation of about 6.5mgals (see Table 25) for each of the two sets. The other columns of Table 27 show that the December 1981 predictions compare slightly better with the November 1981 Seasat Altimeter set, than does the October 1979 predictions. Both the December 1981 and the October 1979 sets are consistent with the altimeter set to within the RMS standard deviations of the anomaly sets compared.

Table 26

Intercomparison of 300nm Anomaly Sets, Using Only those 300nm Anomalies such that the Standard Deviation is Less Than or Equal to 10mgals, and that the Corresponding Predicted 300nm Anomaly Values in DEC81WGP and DEC81NGP Actually Differ With Each Other. (See Table 25 for a Description of the 300nm Anomaly Sets.)

	DEC81WGP -DEC81NGP (mgals)	DEC81COMB -DEC81WGP (mgals)	DEC81COMB -DEC81NGP (mgals)
Min. Difference	-27.5	-21.7	-24.0
Ave. Difference	0.4	-0.3	0.1
Max. Difference	40.8	27.0	44.7
RMS Difference	3.9	6.2	7.2
No. of Diff. >±3mgals	1	0	1
No. of Anom. Compared	510	510	510

RMS Std. Dev. of 300nm Anomalies used in:

DEC81WGP - 4.7mgals
DEC81NGP - 5.6mgals
DEC81COMB - 3.6mgals

Table 27

Statistics of the Difference Between Various 300nm Anomaly Sets Described in Table 25 (mgals)

	DEC81WGP -OCT79WGP all data	DEC81WGP - NOV81ALT		OCT79WGP - NOV81ALT	
		all data	data with $m_{\Delta g} \leq 10$mgals	all data	data with $m_{\Delta g} \leq 10$mgals
Min. Difference	-18.9	-28.3	-28.3	-39.1	-39.1
Ave. Difference.	0.1	0.6	0.5	0.4	0.5
Max. Difference.	36.3	43.2	27.8	44.2	28.0
RMS Difference	2.9	7.1	6.5	7.3	6.7
No. of Diff. $>\pm$30mgals	1	1	0	2	1
No. of Anom. Compared	1654	1179	956	1179	944

21. Summary and Conclusions

In summarizing the studies conducted in this report, it is convenient to carry out the discussion in terms of three general types of anomaly field inside the 300nm block:

Type I field: field which does not cause any roughness-related prediction problem;
Type II field: field which causes prediction problems because of its roughness;
Type III field: field obtained after removing from a type II field the linear effect of 60nm elevations on 60nm anomalies.

The main purpose of this report has been to improve the performance of current 300nm anomaly prediction procedures over a type II field, while at the same time not disturbing the satisfactory performance of current procedures over a type I field. 300nm blocks which have a rough anomaly field (see Table 4) and which contain relatively few observed 60nm blocks are the blocks with a type II field.

Improvements which were not necessarily designed for type II fields were first introduced into the prediction procedures (Section 10). These were: (a) the prediction of all the 25 60nm anomalies, unknown or known, inside the 300nm block; and (b) the use of area-weighted averaging as opposed to unweighted averaging of the 25 60nm anomalies to obtain the 300nm anomaly.

The use of a covariance function that is representative of the variance and correlation length of the anomaly field of interest will result in a better estimation of the absolute accuracy of prediction. Whether this absolute accuracy of prediction will be high or low depends on the character of the field as to its variance and correlation length. To increase the absolute accuracy of prediction, a type II field must be smoothed in some way in order to obtain an anomaly field with lower variance and longer correlation length (see Sunkel (1981a)). Prediction should then be carried out from the smoothed field, then whatever systematic influences were removed prior to the prediction must be put back into the predicted value to obtain the final predicted value.

With a view towards smoothing a type II field by removing the linear effect of 60nm anomalies on 60nm elevations, the correlation between 60nm anomalies and their elevations was first investigated in a global average sense. Two methods for computing an average correlation slope, one using line fitting to a graph of mean 60nm anomaly vs. 60nm elevation interval, and the other

using the ratio of two covariance function, were presented (Section 12). Weak correlation slopes (b-values) of 0.0024mgal/m for negative 60nm elevations and 0.0141mgal/m for positive 60nm elevations were found. Charts showing the global association between anomaly field roughness and terrain roughness were given in Section 12.2.3.

In order to improve 300nm anomaly prediction over a type II field, it is proposed that the model of Least Squares Collocation with systematic parameters be used, the parameter being the correlation slobe b between 60nm anomalies and their 60nm elevations. Three possible sources of the value of the b-parameter were discussed. The b-value from Least Squares served as reference value, since Least Squares line fitting to data values is a very common method of computing regression slopes. The use of an existing empirical b-value, one that applies to the characteristic topography of the 300nm block, can be resorted to if there is an insufficient number of known 60nm blocks inside the 300nm block to determine a reasonable and significant b-value. Finally, the b-value computed by Least Squares Collocation equation is the recommended b-value to use if it turns out to be reasonable and significant.

To eliminate a priori unreliable b-values, it is proposed to compute the b-value only for blocks with at least 4 known 60nm anomalies. Also, it is proposed to consider only b-values which have $|b| < 0.2$mgal/m as reasonable b-values. Of the b-values considered, only those b-values which are statistically significant under a t-test at 0.05% level of significance should be actually used in the prediction. These requirements appear satisfactory in practice, because the b-values that pass these requirements and are thus actually used in the prediction turn out to be the b-values of 300nm blocks with type II field.

Some numerical results were also presented on the prediction of 300nm anomaly using both anomalies and elevations as observed quantities. It appears that no additional information about the 300nm anomaly being predicted can be extracted using such prediction procedure.

Remarks about other study areas connected with this report should be made at this point. This report considered the removal of local linear trend between 60nm anomalies and their 60nm elevations, essentially producing a type III field from a type II field. A type III field is not necessarily a type I field, although a type III field is closer to a type I field than does a type II field. The reason for this is that there are factors other than the linear trend between 60nm anomalies and elevations that make a type II field different from a type I field. Therefore, although the type III field is a significant step in the conversion from a type II field to a type I field, other data reduction steps can be studied. For example, Woollard and Daugherty (1970,p.21)

state that there are geologic effects on the anomaly at sea on the order of 10 to 60mgals that are not related to topography. An overview of the effects on anomaly at sea caused by elevation and other geophysical phenomena may be found in Kearsley (1977), for example.

As seen in Table 11, the improvement of 300nm anomaly prediction over a type II field could be a factor of two, through the use of the b-parameter. It will be of interest to study the feasibility of further improving the prediction through the use of the terrain correction. A recent report dealing with terrain correction computations has been published by Sunkel (1981b).

The computer program developed for the operational implementation of the recommended prediction procedures in this report is described in Section 19. Operational predictions were actually performed as described in Section 20, in order to generate two new sets of 1654 300nm anomalies, one involving 1°x 1° geophysical anomalies and the other involving no geophysical anomalies. The two new sets incorporate the effect of new and updated anomalies in the starting 1°x 1° data set, and the effect of modifications to prediction procedures as introduced in this report. Statistical comparisons show that the two sets (called the December 1981 terrestrial sets) are consistent with each other and with the November 1981 Altimeter set and the December 1981 Combination Solution set. The December 1981 terrestrial set with geophysical anomalies agree better with the combination solution, than does the set without geophysical anomalies (this is expected since the combination solution included geophysical anomalies as data--see Rapp, 1981). Also the December 1981 terrestrial set with geophysical anomalies agree better with the altimeter derived set, than does the older October 1979 terrestrial data set with geophysical anomalies.

References

Hajela, D.P. "Equal Area Blocks for the Representation of the Global Mean Gravity Anomaly Field," Report No. 224, Department of Geodetic Science, The Ohio State University, June 1975.

Kaula, W.M., W.H.K. Lee, P.T. Taylor, and H.S. Lee, "Orbital Perturbations from Terrestrial Gravity Data," final report, Institute of Geophysics and Planetary Physics, University of California, Los Angeles, March 1966.

Kearsley, W., "The Estimation of Mean Gravity Anomalies at Sea from Other Geophysical Phenomena," Report No. 270, Department of Geodetic Science, The Ohio Sate University, December 1977.

Mikhail, E.M., Observations and Least Squares, Harper & Row, Publishers, Inc., New York, 1976.

Moritz, H., "Advanced Least Squares Methods," Report No. 175, Department of Geodetic Science, The Ohio State University, June 1972.

Rapp, R.H., "The Formation and Analysis of a 5° Equal Area Block Terrestrial Gravity Field," Report No. 178, Department of Geodetic Science, The Ohio State University, June 1972.

Rapp, R.H., "Potential Coefficient Determinations from 5° Terrestrial Gravity Data," Report No. 251, Department of Geodetic Science, The Ohio State University, January 1977.

Rapp, R.H., "The Earth's Gravity Field to Degree and Order 180 Using Seasat Altimeter Data, Terrestrial Gravity Data, and Other Data," Report No. 322, Department of Geodetic Science and Surveying, The Ohio State University, December 1981.

Rapp, R.H.,"The determination of geoid undulations and gravity anomalies from Seasat altimeter data," J. Geophys. Res., 1982, (in press).

Sunkel, H., "Cardinal Interpolation," Report No. 312, Department of Geodetic Science, The Ohio State University, March 1981a.

Sunkel, H., "The Estimation of Free-Air Anomalies," Report No. 315, Department of Geodetic Science and Surveying, The Ohio State University, September 1981b.

Uotila, Urho A., "Analysis of Correlation Between Free-Air Anomalies and Elevations," Report No. 94, Department of Geodetic Science, The Ohio State University, November 1967.

Woollard, G. P., and K. I. Daughterty, "Collocation, Processing, and Geophysical Analysis of Gravity and Magnetic Data: Gravity Gradients Associated with Sea-Floor Topography," final report 1969-1970 (two volumes), Hawaii Institue of Geophysics, University of Hawaii, September 1970.

Appendix

This appendix contains figures and tables referred to in Section 20, in relation to the prediction of complete 1654 sets of 300nm anomalies.

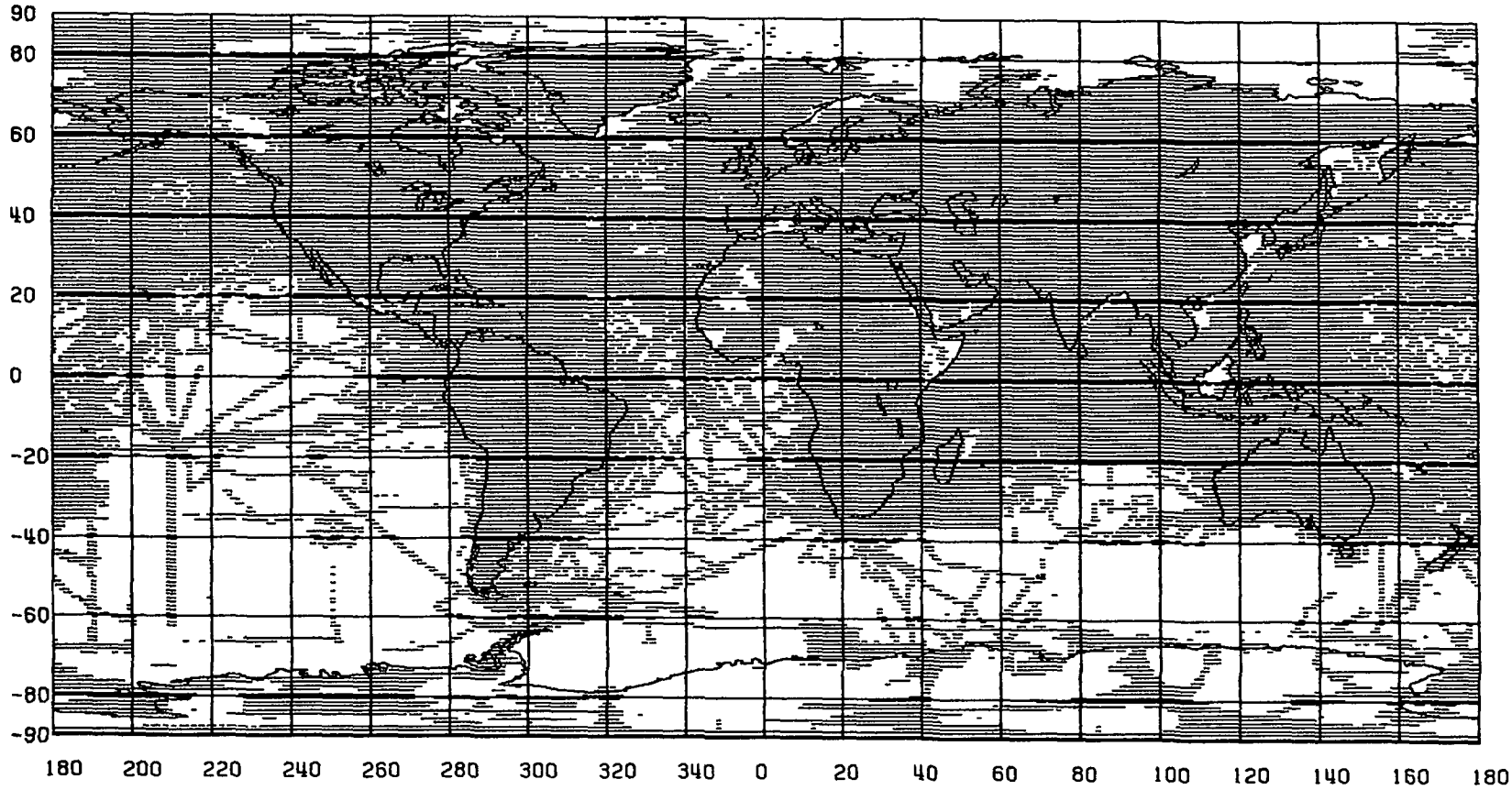

Figure A.1 Location of 42,585 1°x1° Anomalies of December 1981 Terrestrial Data Set

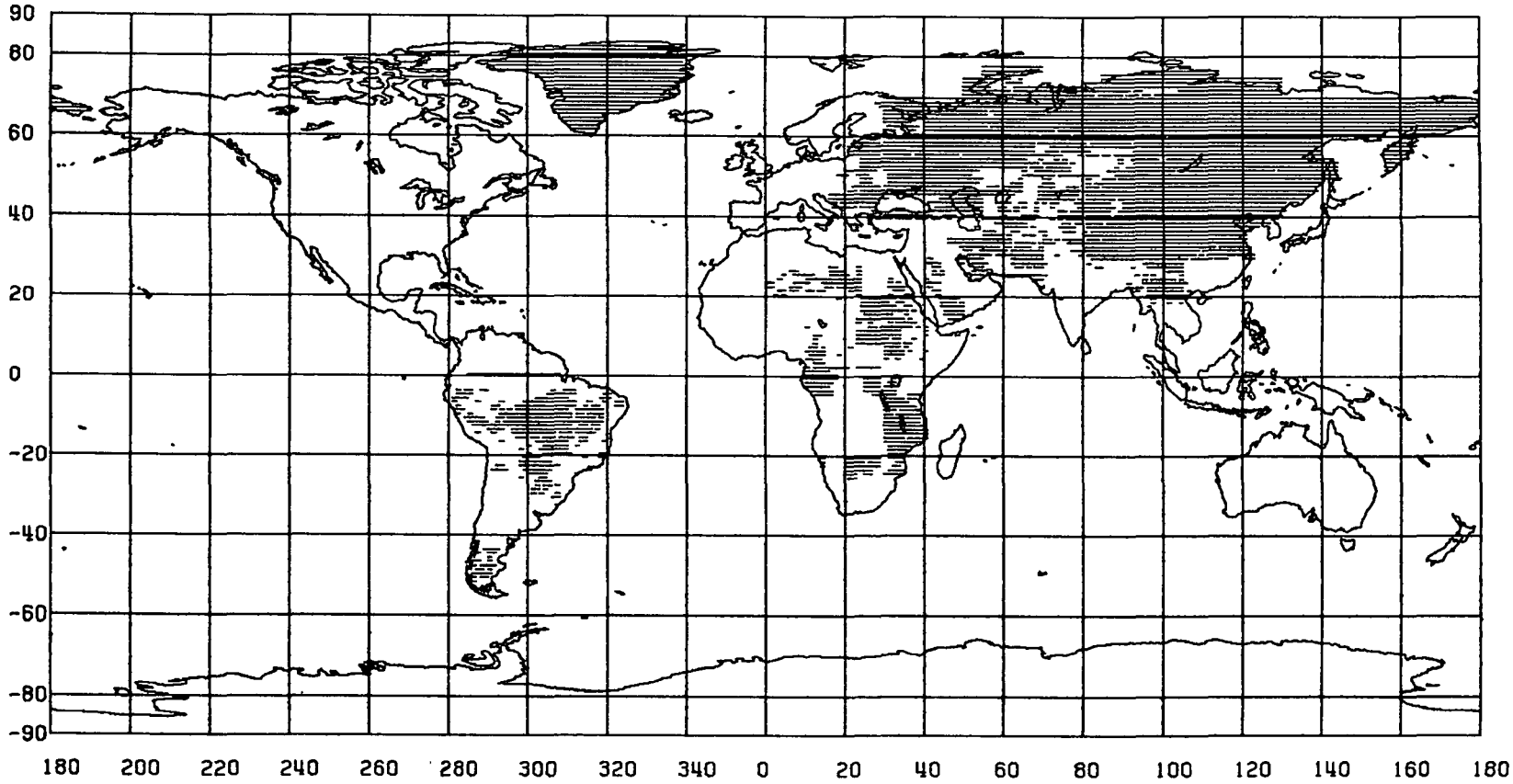

Figure A.2 Location of 6,413 Geophysically Predicted 1°x1° Anomalies Of December 1981 Terrestrial Data Set

Table A.1

60nm Covariance Function $cov(\Delta g,\Delta g)$, Computed as Described in Section 5.1 Based on the December 1981 1°x 1° Terrestrial Data Set that Includes Geophysical Anomalies. Anomalies Refer to the Geodetic Reference System 1967.

ψ DEG	ψ RAD	$cov(\Delta g,\Delta g)=C(\psi)$ $(mgal^2)$	No.of Product Pairs Used
0.0000	0.0000	824.56	30395
0.9798	0.0171	478.39	38394
1.6232	0.0283	342.35	68836
2.5085	0.0438	251.40	93364
3.4657	0.0605	219.84	73430
4.3780	0.0764	205.80	44933
5.3729	0.0938	175.86	5999
6.2380	0.1089	155.43	201

Table A.2

60nm Covariance Function $cov(\Delta g,\Delta g)$, Computed as Described in Section 5.1 Based on the December 1981 1°x 1° Terrestrial Data Set with Geophysical Anomalies Removed. Anomalies Refer to the Geodetic Reference System 1967.

ψ DEG	ψ RAD	$cov(\Delta g,\Delta g)=C(\psi)$ $(mgal^2)$	No.of Product Pairs Used
0.0000	0.0000	860.80	26600
0.9802	0.0171	488.58	32831
1.6266	0.0284	336.09	57724
2.5091	0.0438	247.99	77347
3.4649	0.0605	221.59	60515
4.3796	0.0764	213.33	36829
5.3815	0.0939	162.94	4792
6.2427	0.1090	167.64	177

Table A.3

300nm Anomaly Covariance Functions as Computed (see Section 20)
Based on the "known" December 1981 300nm Anomalies.
Anomalies Refer to the Geodetic Reference System 1967.

ψ (DEG.)	Covariance ($mgal^2$) Geophysical Anomalies Included	Geophysical Anomalies Removed	ψ (DEG.)	Covariance ($mgal^2$) Geophysical Anomalies Included	Geophysical Anomalies Removed
0.0	252.13	251.10	15.0	62.29	62.50
0.5	240.52	237.88	15.5	61.62	62.81
1.0	229.08	225.04	16.0	59.89	61.55
1.5	217.94	212.70	16.5	57.78	59.72
2.0	207.20	200.94	17.0	55.34	57.33
2.5	196.98	189.89	17.5	52.10	53.95
3.0	187.41	179.64	18.0	45.00	47.03
3.5	178.59	170.30	18.5	36.12	38.55
4.0	170.64	161.98	19.0	28.65	31.42
4.5	163.67	154.77	19.5	26.58	29.35
5.0	157.81	148.80	20.0	32.03	34.81
5.5	152.98	144.60	20.5	27.19	50.02
6.0	148.16	141.40	21.0	34.90	37.74
6.5	143.14	136.84	21.5	28.62	31.39
7.0	137.96	131.03	22.0	21.51	24.18
7.5	132.77	125.07	22.5	15.99	18.66
8.0	127.61	119.73	23.0	13.72	16.47
8.5	122.53	115.44	23.5	12.17	14.94
9.0	117.54	111.64	24.0	10.94	13.67
9.5	112.56	107.99	24.5	10.08	12.76
10.0	107.54	104.18	25.0	9.76	12.35
10.5	102.32	99.96	25.5	10.25	12.61
11.0	96.75	95.38	26.0	10.71	12.75
11.5	91.04	90.58	26.5	9.92	11.80
12.0	85.25	85.25	27.0	6.14	8.97
12.5	78.56	76.98	27.5	1.19	5.40
13.0	71.70	67.84	28.0	-2.42	2.48
13.5	65.71	60.77	28.5	02.87	1.17
14.0	62.09	58.44	29.0	-1.81	0.39
14.5	61.68	60.04	29.5	-0.42	-0.12
			30.0	0.30	-0.43

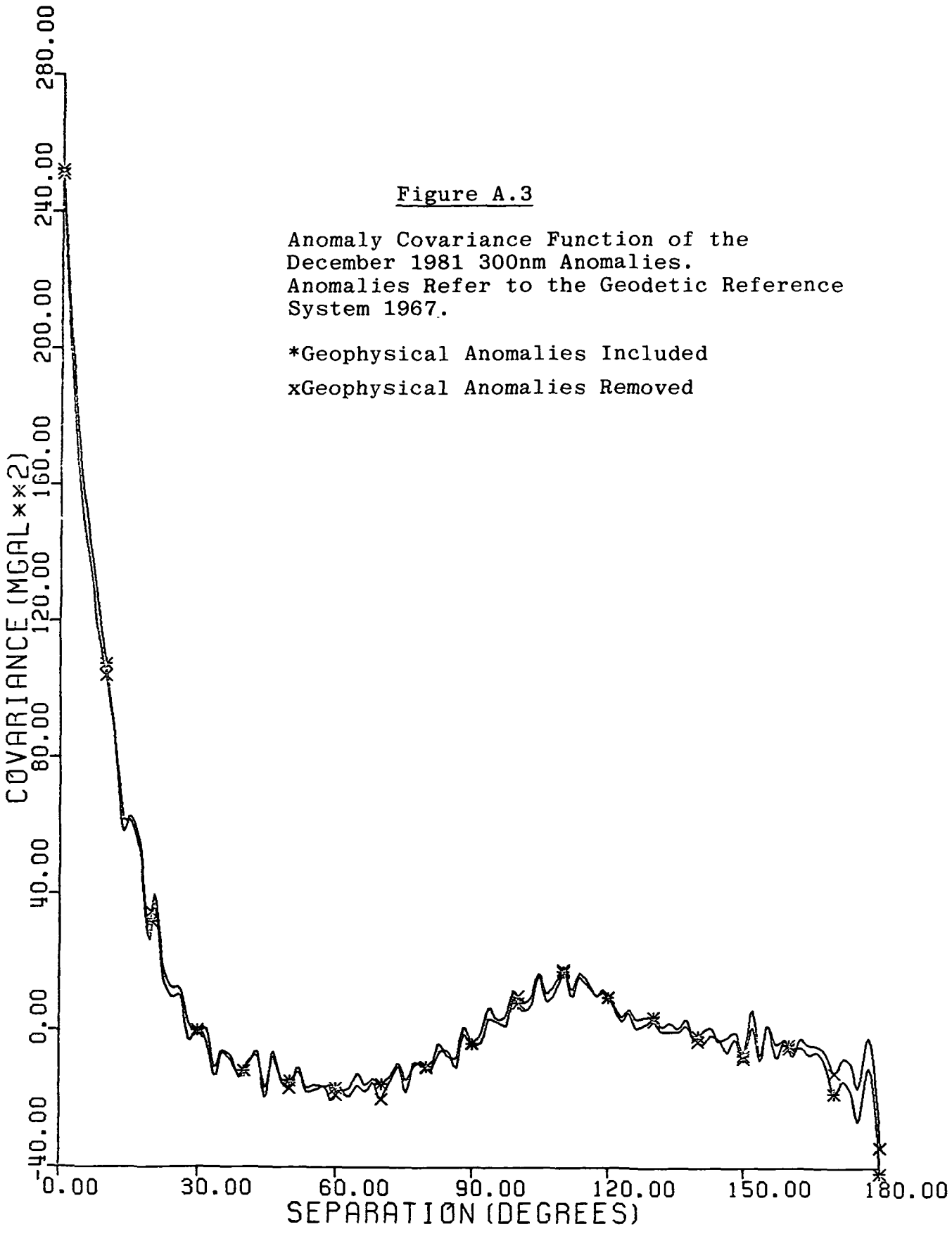

Figure A.3

Anomaly Covariance Function of the December 1981 300nm Anomalies. Anomalies Refer to the Geodetic Reference System 1967.

*Geophysical Anomalies Included

xGeophysical Anomalies Removed